MASTERARBEIT | MASTER'S THESIS

Titel | Title

Phytochemical Analysis of Lipophilic and Hydrophilic Fractions of *Brassica oleracea* (Brassicaceae)

verfasst von | submitted by

Lukas Robert Nagl BSc

angestrebter akademischer Grad | in partial fulfilment of the requirements for the degree of

Magister pharmaciae (Mag. pharm.)

Wien | Vienna, 2025

Studienkennzahl lt. Studienblatt | Degree programme code as it appears on the student record sheet:	UA 066 605
Studienrichtung lt. Studienblatt | Degree programme as it appears on the student record sheet:	Masterstudium Pharmazie
Betreut von | Supervisor:	ao. Univ.-Prof. Mag. Dr. Sabine Glasl-Tazreiter

Acknowledgement

First of all, I would like to thank my parents. Their support in every aspect of my life has made this journey possible. Without their belief in me, my studies would not have been achievable. I would also like to express my gratitude to my girlfriend, Lisa, whose encouragement has been a constant source of motivation throughout this journey.

I am thankful to ao. Univ. Prof. Mag. Dr. Sabine Glasl-Tazreiter for giving me the opportunity to write my master thesis under her guidance and for providing me the workplace at the Division of Pharmacognosy.

My sincere thanks also go to Mag. Dr. Elisabeth Eichenauer for her support and for helping me with every question I had. As well as for selecting me for this research topic and for introducing this project to me.

I would also like to thank Ass. Prof. DI Dr. Karin Ortmayr for performing the LC-MS analyses. As well as PD Mag. Dr. Ulrike Grienke for supplying the thiocyanate pure substances necessary for the GC-MS analysis, Mag. Christina Sykora for her training on the GC-MS, and Mag. Alina Marcher for her training on the FC.

Lastly, I would like to thank the entire Division of Pharmacognosy for the wonderful company, the coffee breaks, and the unforgettable time spent together.

Table of contents

1 Introduction 1

1.1 Human skin and wound healing 1

1.2 *Brassica oleracea* var. *capitata* f. *alba* in wound healing 2

2 Aim of the work 4

3 Materials and methods 5

3.1 Plant material 5

3.1.1 Aqueous extract 5

3.1.2 Dichloromethane extract 5

3.2 Chromatography 6

3.2.1 Flash chromatography (FC) 6

3.2.2 Thin layer chromatography (TLC) 7

3.2.3 High performance liquid chromatography (HPLC) 8

3.2.4 Gas chromatography (GC) 10

3.3 Mass spectrometry (MS) 11

3.4 List of used solvents and substances 12

4 Results 14

4.1 Fractionation and analysis of the aqueous extract 14

4.1.1 Fractionation via flash chromatography 14

4.1.2 Phytochemical characterization of fraction BraOleWFC3 16

4.2 Phytochemical analysis of the most active dichloromethane fractions 21

4.2.1 Extract BraOleD 21

4.2.2 Fraction BraOleD15 24

4.2.3 Fraction BraOleD40 27

4.2.4 Fraction BraOleD70 30

4.3 GC-MS analysis of volatile components in the dichloromethane extract 33

4.3.1 Comparison of German and Austrian cabbage 34

4.3.2 Identification of substances in the DCM extract from the Austrian cabbage 34

5 Discussion and conclusion 37

6 Abstract 42

7 Zusammenfassung 43

8 References.....44

9 List of abbreviations.....50

10 Appendix.....51

1 Introduction

1.1 Human skin and wound healing

The human skin is the body's largest organ and consists of two layers: the epidermis and the dermis. The epidermis, which is the outermost layer, is composed of five sub-layers: the stratum corneum, stratum lucidum, stratum granulosum, stratum spinosum, and stratum basale. The structure of the human skin can be seen in Figure 1 below. Our skin is responsible for many vital tasks. Some of these are: Protecting us from noxious environmental influences, playing a crucial role in sensing our surroundings, or regulating the body temperature (1). Due to the importance of these tasks, it is not surprising that they must be maintained at all costs. For this reason, the skin has the ability to heal itself after various kinds of injuries, such as burns, cuts, trauma, or even surgical interventions. This healing process consists of four phases: the coagulation and hemostasis phase, the inflammatory phase, the proliferative phase, and the remodeling phase (2). When it comes to renewing the epidermal layer in the proliferative phase, keratinocytes play a huge role in closing the wound as fast as possible (3). Although our skin can heal itself, wound treatment is crucial and remains a clinical problem. Wound management is a practice which has been done by human mankind for ages. Those who do not have access to modern medicine depend on traditional remedies such as soil, animal products, or plants (4).

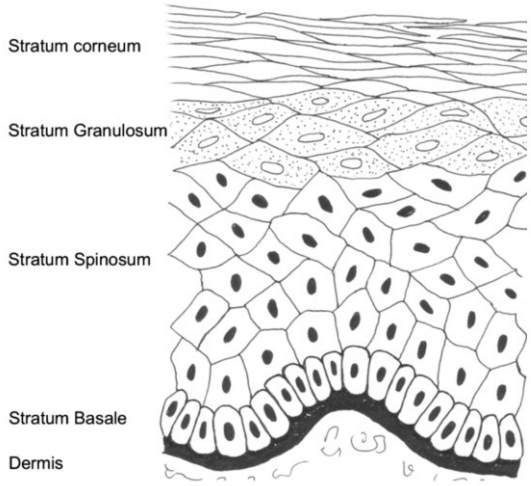

Figure 1: Structure of the human skin. Stratum lucidum (which only occurs in very thick layers of the skin) is not shown here (1)

1.2 *Brassica oleracea* var. *capitata* f. *alba* in wound healing

White cabbage (*Brassica oleracea* var. *capitata* f. *alba*), which belongs to the Brassicaceae family, is a vegetable that has been consumed and raised by humans worldwide for centuries. It can be found nearly all over the world except Antarctica (5). Since cabbage can be found worldwide, it is no surprise that it is very important not only as a food but also as traditional medicine. Its medicinal use can be traced back to the ancient Greeks, Romans, and Egyptians (5). The area of its application in medicine is very broad. Cabbage is used to treat inflammation, gastrointestinal problems, or rheumatism (5-8). Furthermore, it is believed that the Romans used cabbage as poultices to treat wounds of their legionnaires (9). To treat wounds, fresh cabbage leaves are mostly crushed with a rolling pin and then applied to the injured body part (8, 9). The positive effect of cabbage on wound healing has been shown in studies. In these studies, rats were treated with cabbage extract. The results showed improvements in wound healing, such as a reduction in wound size and a higher number of fibroblasts in rats with wounds or burns. Fibroblasts are involved in the formation of granulation tissue. They play a key role in synthesizing collagen (types I and III) and other components of the extracellular matrix that are essential for wound healing (10-13). It is possible that the effect of cabbage on wound healing is due to lysophosphatidic acid (LPA). LPA is produced through the hydrolysis of phosphatidic acid, which is found in cabbage, by phospholipase A2 in the gastrointestinal tract. While this effect has only been demonstrated in the gastrointestinal tract, it is possible that this process could also occur in the human skin (8, 14). Additionally, pectin-type polysaccharides could have a supportive effect on wound healing due to their complement-fixing effects (8, 15, 16).

More constituents found in cabbage are glucosinolates, polyphenols, vitamins, and carotenoids. These substances are antioxidative and show anti-inflammatory as well as anti-cancer activity (5). Furthermore, the antioxidative and anti-inflammatory properties have a positive effect on wound healing (8, 17). Glucosinolates, which are secondary metabolites, can be differentiated in aliphatic, aromatic, and indolic structures (6). The most common glucosinolates in cabbage are sinigrin, glucoiberin, and glucobrassicin. When it comes to the synthesis of breakdown products of glucosinolates, an enzyme called myrosinase is needed. This enzyme needs to be released from the compartiment in the cell where it is stored to exert its

activity. If the cabbage is treated with a rolling pin, the tissue gets destroyed, myrosinase is set free and hydrolyzes these glucosinolates (5). Some of these hydrolysis products are epithionitriles, nitriles, thiocyanates, isothiocyanates like allyl isothiocyanate, or indolic structures like indol-3-carbinol. The most common glucosinolates and their breakdown products are shown in Figure 2 below. Glucosinolates as well as their hydrolysis products have several health benefits and show anti-cancer, antioxidative, and antibacterial activity (18).

Furthermore, polyphenoles are of great interest because of their antioxidative effect. Due to their antioxidative activity, these substances are considered for treating chronic diseases caused by oxidative stress which include cancer, cardiovascular or neurodegenerative diseases (6). A few of the polyphenols found in white cabbage are flavonoids and hydroxycinnamic acids (5, 18). The most common flavonoids are quercetin and kaempferol. Typical hydroxycinnamic acids are caffeic acid, p-coumaric acid, ferulic acid, and sinapic acid (19).

More substances described in cabbage are carotenoids, tocopherols, and vitamins like vitamin C, vitamin K, or vitamin B6. Vitamins and carotenoids play a huge role in the immune system as well as the metabolism and show antioxidative activity (5, 18).

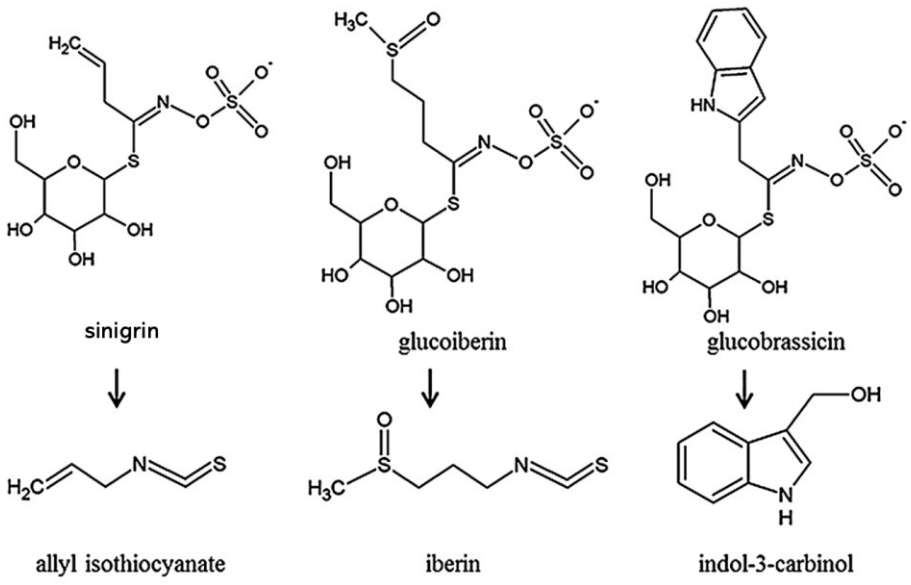

Figure 2: Glucosinolates and their breakdown products (5)

2 Aim of the work

Over many years, cabbage traditionally has been used to treat wounds (5, 8, 9). Despite its long history there is still more information needed about all the constituents and their effects on wound healing.

Initially, for this master thesis, two different extracts of *Brassica oleracea* var. *capitata* f. *alba* were available: an aqueous extract and a dichloromethane (DCM) extract. Both were obtained from a previous master thesis and a previous bachelor thesis (20, 21). The DCM extract demonstrated antioxidative and anti-inflammatory activities (22) and had already been fractionated by using solid-phase extraction (21). These fractions were investigated in bioactivity tests to examine their ability to activate Nrf2 and inhibit NF-κB (22). This work aimed to investigate the phytochemical composition of the most bioactive fraction and identify the bioactive compounds. The second aim was to produce more of the DCM extract and search for volatile components, such as isothiocyanates, by using gas chromatography (GC). Furthermore, the aqueous extract, which has already been fractionated to a small extent via solid-phase extraction (SPE), had shown activity in a wound healing assay on keratinocytes (22). Therefore, the third aim was to further fractionate the aqueous extract using flash chromatography (FC) to achieve a higher yield of the respective fractions including their phytochemical analysis.

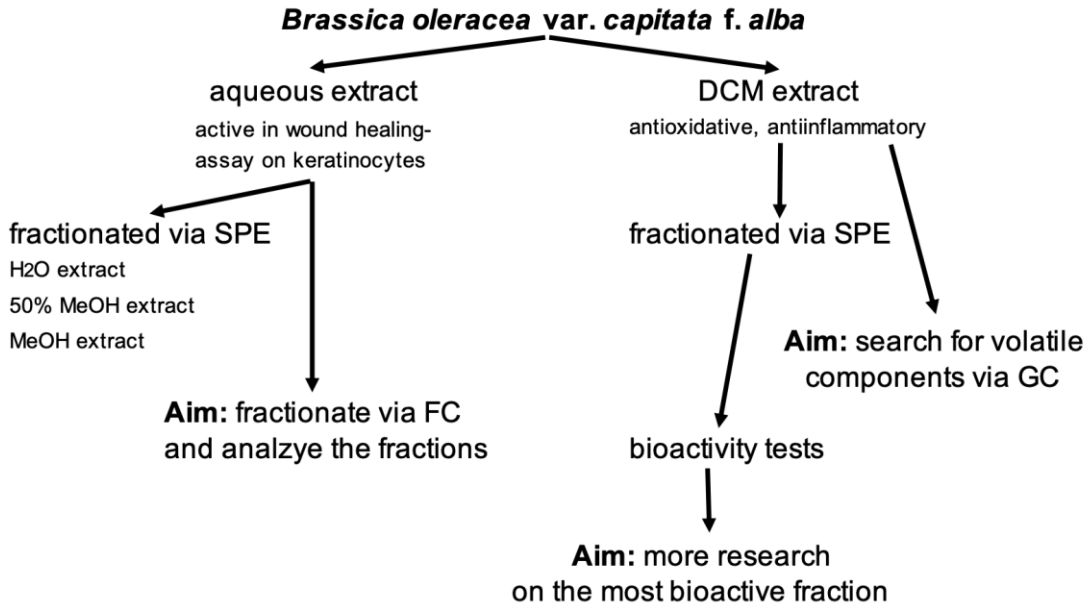

Figure 3: Aim of the work

3 Materials and methods

3.1 Plant material

This chapter presents the plant materials used in this master thesis and describes their preparation for the production of the respective extracts

3.1.1 Aqueous extract

The aqueous extracts used were obtained from a previous master thesis (21). The cabbage used in the extracts was harvested in Austria and bought from local stores. However, the cabbages were purchased from different local stores for each of the three available extracts. A cabbage from Denns BioMarkt® was used for extract 1 (BraOleW1), a cabbage from Billa® for extract 2 (BraOleW2) and a cabbage from Spar® for extract 3 (BraOleW3). To obtain the aqueous extract, fresh cabbage leaves were crushed using a rolling pin. The crushed leaves then were stored in a closed container overnight at a temperature between 32°C and 35°C using the Lucky Reptile Thermoelectric Cooler & Warmer. To remove lipophilic compounds, the leaves were defatted in a hexane bath for about two minutes and then cut into small pieces of approximately 1 × 1 cm. Afterwards the extraction was carried out using distilled water at a ratio of 1:5 on an orbital shaker for two hours. The resulting extract was filtered through a Büchner funnel, afterwards the aqueous phase was removed by lyophilization (22).

3.1.2 Dichloromethane extract

The DCM extract used for the GC-MS analysis was prepared from cabbage originating from Austria as well as Germany. Both cabbages were purchased from local stores: The German cabbage from Denns BioMarkt® and the Austrian cabbage from Spar®. The extracts were prepared as follows: To destroy the tissue and release myrosinase from the vacuoles, 20 g of cabbage were crushed using a rolling pin. Then, 200 mL of DCM was added to the crushed cabbage. The mixture was shaken for about 60 minutes in an Erlenmeyer flask, filtered over vacuum, and dried over anhydrous sodium sulfate. Finally, the solvent was evaporated using a Heidolph Hei-VAP rotary evaporator at 40°C and 850 mbar.

Another DCM extract used was obtained from a previous bachelor thesis (20). Here again the cabbages used for the extracts had been harvested in Austria and bought

from various local stores. The extract had already been fractionated via SPE and the obtained fractions had underwent bioactivity tests to assess their ability to activate Nrf2 and inhibit NF-κB (22). These tests suggested that the most bioactive fractions are the 15% (BraOleD15) and 40% (BraOleD40) methanolic fraction in case of inhibiting NF-κB, and the 70% (BraOleD70) methanolic fraction in case of activating Nrf2 (22). For this reason, all three fractions were examined in more detail.

3.2 Chromatography

Chromatography is an analytical separation method in which analytes interact with a mobile phase and a stationary phase. The stationary phase is at rest, while the mobile phase flows past it. Depending on the chemical and physical characteristics of the analytes, each analyte interacts differently with the stationary phase and the mobile phase. This leads to various retention times so that the analytes are registered as different peaks (23). The different methods used in this master thesis are discussed below.

3.2.1 Flash chromatography (FC)

Flash chromatography is used for the separation of mixtures into their distinct components. In this separation method, small silica gel particles are used as a stationary phase. Due to these small particles, the flow of the mobile phase is very limited. Hence, pressurized gas (e.g. nitrogen) is used to carry the solvent through the stationary phase (24). For this master thesis a Puriflash 4250 with a photodiode array (PDA) and an evaporative light scattering detector (ELSD) were used. The Interchim® software was utilized. The divided fractions were collected automatically based on the ELSD signal. To inject the sample, a dry load was prepared as follows. The aqueous extract was dissolved in water and mixed with about twice the amount of silica gel 60 (particle size 0.063-0.200 mm) in a round bottom flask. Afterwards the solvent was removed by using a rotary rotavapor. Then, this silica-gel sample mixture was filled into the cartridge column and topped up with pure silica gel 60. After both columns (separation column and cartridge filled with analyte) were mounted, the separation was carried out. All used columns and the different gradients of the mobile phase (solvent A and solvent B) are shown below in Table 1 and Table 2. The flow rate was 5 mL/min for each run.

Table 1: Used solvents and columns for the flash chromatography. Fractionation is described in chapter 4.1.1.

Run	Column	Solvent A	Solvent B
FC01	Part number: PF-15C18HP/6G length: 62 mm, ID: 12 mm, C18 column	H_2O	Methanol
FC02-15	Part number: PF-15PHC4/6G length: 62mm, ID: 12mm, phenyl-butyl column	H_2O	Methanol

Table 2: Solvent gradients used for the flash chromatography runs. Fractionation is described in chapter 4.1.1. The exact partitioning of the fractions is shown in Figure 6. All other chromatograms can be found in the Appendix (Figures A1-A18 on the pages 51-66).

Minute	Solvent B concentration in %	
	FC01-FC02	FC03-FC15
0	5%	0%
15	5%	0%
60	95%	95%
70	95%	95%

3.2.2 Thin layer chromatography (TLC)

In TLC, the stationary phase is on a plate and not inside a column. In this master thesis, silica gel 60 F_{254} on an aluminum sheet was used as a stationary phase. The samples were dissolved in the appropriate solvent and carefully applied to the stationary phase using a glass capillary. Then the mobile phase was prepared and filled into the TLC chamber. The mobile phases and derivatization reagents used are shown in Table 3 below. Once the chamber saturation was reached, the stationary phase was put into the chamber and closed to start development. The mobile phase flows from the starting zone towards the end zone and transports the analytes, depending on their interaction with the stationary and mobile phases (23). The TLC was documented by using the Camag® TLC visualizer and the visionCATS Camag® HPTLC Software, both before and after derivatization. The evaluation was carried out by using 254 nm and 366 nm UV light, as well as visible light.

Table 3: Used mobile phase and derivatization reagents for the TLC

Mobile phases and mixing ratio	**Derivatization reagent**	**Analyzed fractions**
System 1: DCM + MeOH +1% formic acid (6+5+1)	anisaldehyde sulfuric acid	**TLC1:** 6 obtained fractions from run FC02 **TLC2:** 6 obtained fractions from run FC03 **TLC5:** BraOleW + 4 obtained fractions received from all FC runs combined
System 2: DCM + MeOH (9+1)	anisaldehyde sulfuric acid	**TLC3:** 6 obtained fractions from run FC03 **TLC4:** BraOleW + 4 obtained fractions received from all FC runs combined
System 3: DCM + cyclohexane + formic acid + ethyl formate (30 + 35 + 5 + 30)	natural product reagent	**TLC6:** BraOleD, cyanidin, quercetin, kaempferol, caffeic acid, p-coumaric acid, ferulic acid, sinapic acid **TLC7:** BraOleWFC3, quercetin-3-4-dimethylether, quercetin-3-7-dimethylether

3.2.3 High performance liquid chromatography (HPLC)

In HPLC, the mobile phase is transported to the sample injector by a high-pressure pump, where the sample is supplied. In addition to the main column, a pre-column is often used. The pre-column protects the main column from impurities. In the main column, the separation from the samples is carried out by interactions between the mobile and stationary phase (23). A common detector is the PDA detector. In this detector, light passing through the sample is separated into different wavelengths, typically using a grating or prism. These wavelengths are then directed to photosensitive diodes for detection (25). Another detector is the ELSD which provides quantitative information through measuring the light scattered by non-volatile particles. The intensity of the scattered light is proportional to the concentration of the analyte (26, 27). Reversed phase (RP) columns are commonly used as the stationary phase, primarily because polar solvents such as methanol or water are used as mobile phases (23, 28). The used HPLC instrumentation as well as the used solvents and the associated solvent gradients can be found in Table 4, Table 5, and Figure 4 below.

Table 4: HPLC instrumentation

Instrumentation	SHIMADZU Degasser DGU-20A5
	SHIMADZU Auto Sampler SIL-20AC HAT
	SHIMADZU Communications Bus Module CBM-20A
	SHIMADZU Liquid Chromatograph LC-20AD
	SHIMADZU Column Oven CTO-20AC
	SHIMADZU Diode Array Detector SPD-M20A
	SHIMADZU Low temperature-evaporative light scattering detector ELSD-LT
Software	SHIMADZU Lab solutions
Stationary phase	Acclaim™ 120 RP C18 3 µm, Part No.: 059130; ID: 2.1mm, length: 150mm

Table 5: Used solvents and analyzed fractions

Used solvents	
Mobile phase	solvent A: water + 0.1% formic acid
	solvent B: acetonitrile + 0.1% formic acid
Flow rate	0.3 mL/min
Dilution	5 mg/mL
Analyzed fractions	
HPLC run 1	BraOleD15, 40, 70 and BraOleWFC3
HPLC run 2	cyanidin, ferulic acid, sinapic acid, caffeic acid, p-coumaric acid, kaempferol, and quercetin
HPLC run 3 and 4	caftaric acid
HPLC run 5	ferulic acid, quinic acid, BraOleD70 (after acid hydrolysis)
HPLC run 6	ferulic acid mixed with BraOleD70 (after acid hydrolysis), BraOleD15, acacetin

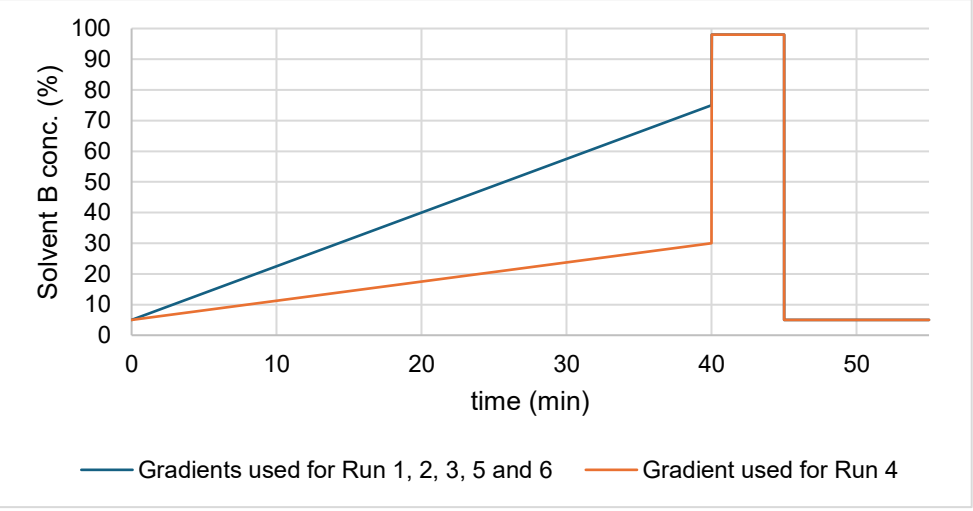

Figure 4: Gradients used for HPLC Run 1 - 6

3.2.4 Gas chromatography (GC)

Gas chromatography is a separation method where carrier gases are used as mobile phases to transport the gaseous analytes. A capillary column or a packed column serve as the stationary phase. In case of the capillary GC, quartz glass is used as column material and the stationary phase is immobilized on the inner wall of the capillary (23). The instrumentation used in this work was the GCMS QP 2010 with a Shimadzu auto injector AOC-20i. The initial temperature of the GC oven was 50°C and increased to 270°C with an increase of 6°C/min. To identify the different substances, an electron ionization quadrupole (EI-QP) mass spectrometer was used. In mass spectrometry, the analyzed substances are transformed into positively or negatively charged particles with an ion source. These ions are then sorted based on their mass-to-charge ratio. A detector captures these signals and shows the relative intensity of the ions against their mass-to-charge ratio (23). The used column, the GC-MS settings, as well as the single runs and the respective analysis dilutions are listed below in Table 6 and Table 7.

Table 6: GC-MS instrumentation and parameter

Column	DP-5 capillary column, MN OPTIMA-5, ID: 0.25 mm, thickness: 0.5 µm, length: 50 m
Temperature	Initial 50°C, increased to 270°C with an increase of 6°C/min, hold at 270°C for 10 min
Injection mode	splitless
Mobile phase	helium (quality 5.0)
Flow rate	1.14 mL/min
Interface temperature	270°C
Ion source temperature	250°C
Ionization mode	electron ionization (EI), 70 eV
Scan area (MS)	40-500 m/z

Table 7: GC-MS analyses with corresponding analysis solutions and dilutions

Run	**Extract**	**Dilution**	**Injected volume**
1	fresh DCM extract (Austrian cabbage)	1:100	2 µl
2	fresh DCM extract (German cabbage)	1:100	2 µl
3	Allyl isothiocyanate	1:25.000	1 µl
4	3-Butenyl isothiocyanate	1:25.000	1 µl
5	1 week old DCM extract (Austrian cabbage)	1:50	1 µl
6	Allyl isothiocyanate	1:100.000	1 µl

7	3-Butenyl isothiocyanate	1:1.000.000	1 µl
8	1 week old DCM extract from run 5 combined with allyl isothiocyanate and 3-butenyl isothiocyanate from run 6 and 7	-	3 µl

3.3 Mass spectrometry (MS)

In mass spectrometry, the substances being analyzed are transformed into positive or negative charged particles with an ion source (23), like in case of this master thesis with electron-spray ionization. Afterwards, these charged analytes are accelerated towards a separation system. The separation system is used to sort these ions based on their mass-to-charge ratio with for example a magnetic field like a quadrupole. Furthermore, mass spectrometry is often combined with separation methods like liquid chromatography (23). In the case of this master thesis an ultra-performance liquid chromatography-mass spectrometry (UPLC-MS) with an ion trap was used. Hereby the ions from the ion source enter a trap where these are trapped in a quadrupole field and later enter the detector. A detector registers the separated ions and shows the relative intensity of the ions against their mass-to-charge ratio (23). This method mentioned above is also called MS1 and was used for the first MS run. In this first run, the following fractions were analyzed: BraOleD15, 40, 70 and BraOleWFC3. For more detailed information about the structure of the original molecules, MS2 is used. In this method, ions from the first MS run are further fragmented. This happens in a collision cell where the ions from the first run collide with a gas and break into smaller fragments. The fragments of the precursor ions are once again separated and detected according to their m/z ratio (23). MS2 was used in the second MS run. Here again the above-mentioned fractions were analyzed. The used instrumentation, software, mobile and stationary phases can be seen in Table 8 below. In case of this master thesis, the positive as well as the negative ions were measured.

Table 8: HPLC-MS instrumentation, software, used mobile and stationary phases

HPLC Instrumentation	UltiMate 3000 RS pump
	UltiMate 3000 RS Autosampler
	UltiMate 3000 RS Column Compartment
	UltiMate 3000 RS Diode Array Detector (DAD)
	Corona Ultra RS (CAD)
MS Instrumentation	Thermo Scientific™ LTQ XL™ Linear Ion Trap Mass Spectrometer
	Sciex X500$_R$ QTOF LC-MS/MS
Ionization source	Electrospray Ionization (ESI)
Ionization parameters	Sheath gas: 40 arb. units, Auxiliary gas: 10 arb. units, Sweep gas: 1 arb. unit, Heater temperature: 300 °C, Capillary temperature: 275 °C, Spray voltage: 3.5 kV
Scan range	Positive mode: m/z 100–1500, Negative mode: m/z 110–2000
Software	Thermo Xcalibur Roadmap
	Chromeleon Xpress
	Thermo Tune Plus
	GA2 – Real Time Plot
Stationary phase used for HPLC	Acclaim™ 120 RP C18 3 µm; ID: 2.1 mm, length: 150mm Part No.: 059130
Mobile phase used for HPLC	solvent A: water + 0.1% formic acid
	solvent B: acetonitrile + 0.1% formic acid
Flow rate	0.3 mL/min

3.4 List of used solvents and substances

This chapter consists of two tables. Table 9 lists all solvents and substances used in this thesis, and Table 10 summarizes the composition of the derivatization reagent “anisaldehyde sulfuric reagent” used for visualization in TLC.

Table 9: List of the used solvents and substances

Solvent	**Lot**	**Producer**
Acacetin	-	Carl Roth GmbH + Co. KG
Acetic acid 96%	191308335	Carl Roth GmbH + Co. KG
Acetonitrile (chromanorm)	23G244009	VWR International®
Allyl isothiocyanate	-	Abcam®
Anhydrous sodium sulfate	9Q010313	AppliChem GmbH®
Anisaldehyde	STBJ4172	Sigma-Aldrich®
Anisaldehyde sulfuric reagent	-	-
3-Butenyl isothiocyanate	-	Sigma Aldrich®

Caftaric acid	-	Phytolab 89170
Caffeic acid	-	Sigma-Aldrich®
p-Coumaric acid	-	Honeywell Fluka™
Cyanidin	-	Honeywell Fluka™
Cyclohexane	K40565666 010	E. Merck KG
Dichloromethane	19G234019	VWR International®
Ethyl formate	S6619591 527	E. Merck KG
Formic acid 98%	112165431	Carl Roth GmbH + Co. KG
Ferulic acid	-	Honeywell Fluka™
Kaempferol	-	Carl Roth GmbH + Co. KG
Methanol (chromanorm)	231023C005	VWR International®
Natural product reagent	018263638	Carl Roth GmbH + Co. KG
Quercetin	-	Carl Roth GmbH + Co. KG
Quercetin-3-4-dimethylether	-	Inst. F. Botanik, Univ. Darmstadt
Quercetin-3-7-trimethylether	-	Inst. F. Botanik, Univ. Darmstadt
Quinic acid	-	Heilmittelstelle
Silica gel 60	TA637234 448	E. Merck KG
Sinapic acid	-	Honeywell Fluka™
Sulphuric acid 96%	027250286	Carl Roth GmbH + Co. KG
Water	-	double distilled with Satorius® Arium Pro

Table 10: Composition of anisaldehyde sulfuric reagent

Component	**Portion**
Anisaldehyde	5 parts
Acetic acid	100 parts
Methanol	845 parts
Sulphuric acid	50 parts

4 Results

The following chapter shows the results of this master thesis. These include the fractionation and phytochemical analysis of the aqueous extract (see chapter 3.1.1, p5), as well as the analysis of the dichloromethane extract (see chapter 3.1.2, p5).

4.1 Fractionation and analysis of the aqueous extract

This chapter presents the fractionation of the aqueous extract (see chapter 3.1.1, p5) using flash chromatography, as well as the following analysis of these fractions by TLC, HPLC, and MS.

4.1.1 Fractionation via flash chromatography

The used extract (BraOleW1, see chapter 3.1.1, p5) was obtained from a previous master thesis (21), originating from cabbage harvested in Austria and purchased from Denns BioMarkt®. Previous TLC analyses revealed a high content of sugars (22). To separate the sugars from the other substances, about 100 mg of the aqueous extract were fractionated via flash chromatography. A C18 column was used for the first run but did not lead to a sufficient separation of substances (see Figure A 1, p51), so a more polar column with phenyl-butyl as stationary phase was chosen. Using this column, the peaks were separated more clearly (see Figure A 2, p52). To determine if the sugars were separated from the other compounds, the individual fractions were combined according to the ELSD signal, concentrated using a rotary evaporator, and analyzed using TLC. However, this TLC analysis, which can be found in the appendix section on page 54 showed that the sugars were not separated clearly from the other substances. For this reason, the solvent B gradient was adjusted from 5%-95% to 0%-95% (see Table 2, p7) to remove the sugars. Afterwards, the different fractions were analyzed again using TLC (see Figure 5, p15). The substances applied to the stationary phase were the original cabbage extract (BraOleW1, see chapter 3.1.1, page 5), as well as the four fractions resulting from FC (see Figure 6, p16).

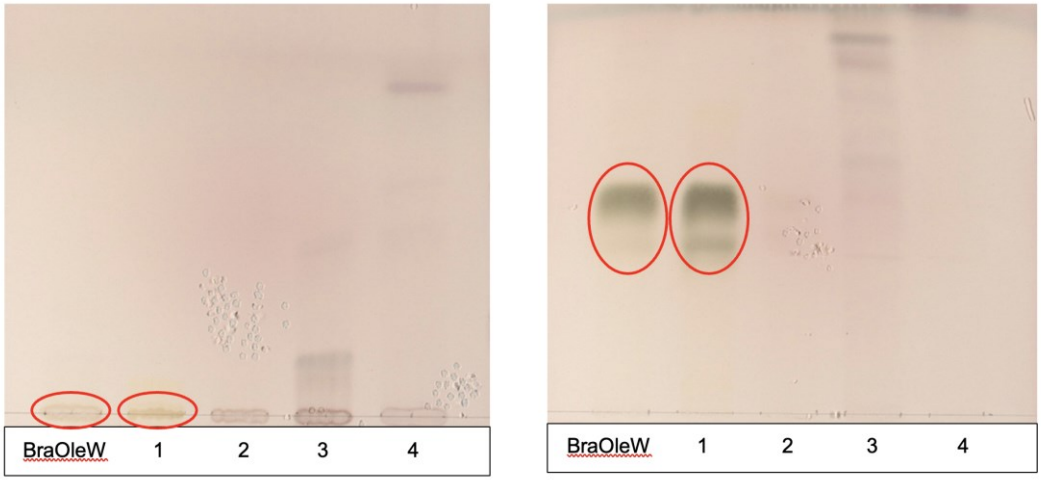

Figure 5: Results of BraOleW1 (see chapter 3.1.1, p5) and the four fractions 1-4 obtained from FC run 3 (system: see Table 1 and Table 2, p7). Left (TLC5): system 2 (DCM + MeOH +1% formic acid (6+5+1)). Right (TLC4): system 1 (DCM + MeOH (9+1)); detection: anisaldehyde sulfuric reagent (see Table 10, p13); sugars are marked red.

The TLC analysis suggested that fraction 1 contains all the sugars that were in the aqueous extract BraOleW1 and were separated from the other substances. Furthermore, it can be assumed that fractions 3 and 4 are the most interesting because, according to the TLC analysis, these contain the most substances other than saccharides. Therefore, all three extracts, BraOleW1-3 were separated in 12 semi-preparative runs (FC04-FC15) employing phenyl-butyl as stationary phase (see Table 1, p7) and methanol - water as mobile phase with a gradient of 2%/min (see Table 1 and Table 2, p7). For each run, about 250 mg of the aqueous extract were applied to flash chromatography. All resulting FC fractions were unified to 4 fractions as shown in Figure 6 and Table 11 below. Chromatograms of the single FC runs can be found in the appendix section on the pages 51-66. Table 11 summarizes the yields of fractions BraOleWFC1-4 in mg and %. All together 3 g of the extracts BraOleW1-3 (see chapter 3.1.1, p5) were fractionated by FC.

Table 11: Yields of fractions BraOleWFC1-4 (see Figure 6, p16) resulting from 3 g of the extracts BraOleW1-3 see (chapter 3.1.1, p5) fractionated by FC

Fraction	**Yield [mg]**	**Yield [%]**
BraOleWFC1 (blue)	2543.7 mg	94.4%
BraOleWFC2 (red)	102.4 mg	3.8%
BraOleWFC3 (green)	36.9 mg	1.4%
BraOleWFC4 (yellow)	11.5 mg	0.4%

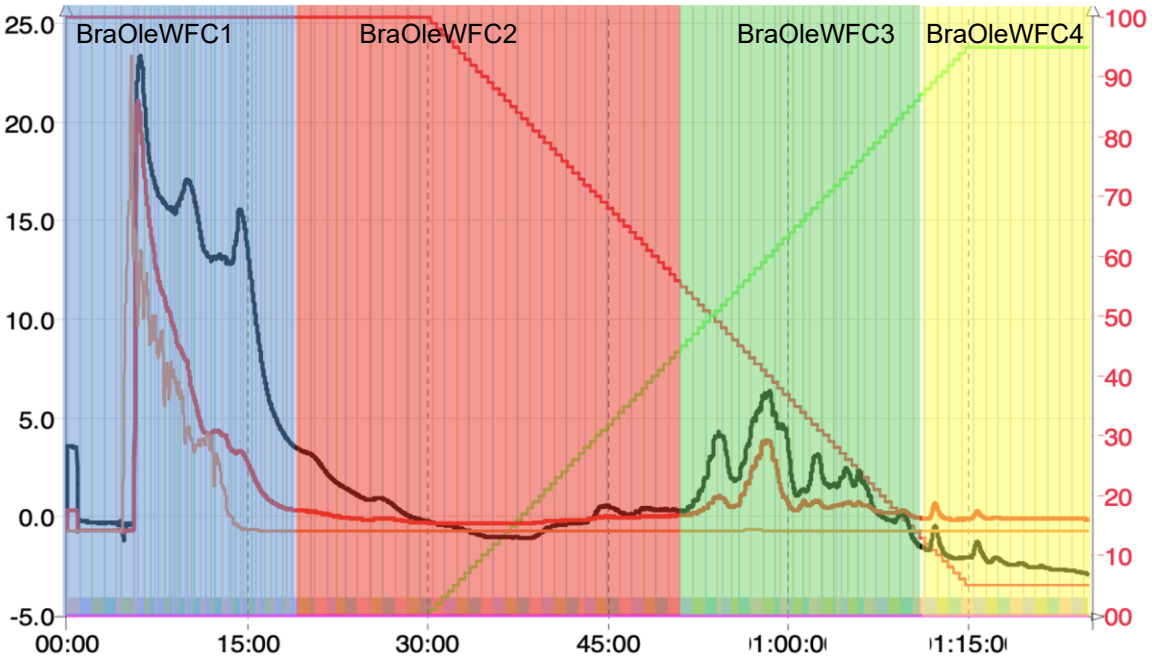

Figure 6: Analysis of BraOleW1 (see chapter 3.1.1, p5) by FC (system see Table 1 and Table 2, p7) resulting in fractions BraOleWFC1-4 (BraOleWFC1 = blue, BraOleWFC2 = red, BraOleWFC3 = green, BraOleWFC4 = yellow)

4.1.2 Phytochemical characterization of fraction BraOleWFC3

To determine the composition of the constituents in fraction BraOleWFC3 (see Figure 6, p16), an HPLC analysis was carried out (HPLC run 1 and 2, see Table 5 and Figure 4, p9). The pure substances cyanidin, quercetin, kaempferol, caffeic acid, p-coumaric acid, ferulic acid, and sinapic acid were chosen to be analyzed as reference substances, since they are well-known constituents occurring in cabbage (5, 19, 29). The retention times and the UV spectra of the pure substances were compared with those from fraction BraOleWFC3. According to the retention times, none of the above-mentioned substances were detected in this fraction. However, the UV spectra from the analyzed hydroxycinnamic acids like caffeic acid, ferulic acid and sinapic acid showed a minimum at 260 nm and a maximum at about 320 nm (see Figure 7). Comparing the spectrum from sinapic acid with the spectrum of the compound eluting at 23.950 min (see Figure 8), similarities were observed. Therefore, different hydroxycinnamic acids or derivates from the abovementioned substances were expected in BraOleWFC3.

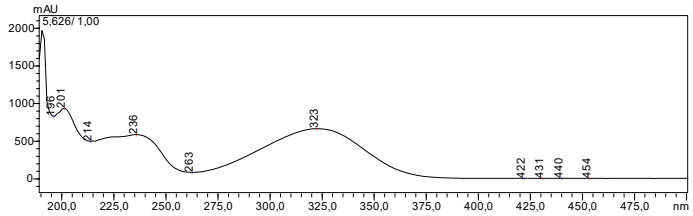

Figure 7: UV spectrum of sinapic acid

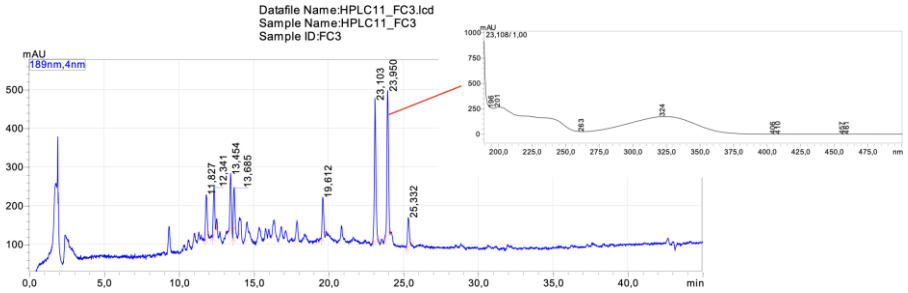

Figure 8: Analysis of fraction BraOleWFC3 (see Figure 6, p16) by HPLC-UV-DAD (system see Table 5, p9) and UV spectrum of the substance eluting at the retention time 23.950 min

For further identification an HPLC analysis hyphenated to CAD, PDA, and MS was carried out. Figure 9 shows the MS data from BraOleWFC3 (see Figure 6, p16). The positive ion mode is represented by the black chromatogram, while the negative ion mode is shown in brown. The CAD signal is depicted in green, and the PDA signal in blue. Peaks 1-4 in the CAD-detected chromatogram (Figure 9, green) were assigned to the corresponding peaks in the MS-ion chromatograms. The MS data recorded in the positive and negative mode suggested the molecular weights m/z = 456 g/mol, 206 g/mol, 328 g/mol, and 330 g/mol for peaks 1, 2, 3, and 4, respectively. These molecular weights were compared with the database from CAS SciFinder®. Additionally, MS-DIAL® from CompMS® was used to analyze the MS data. The analysis of the different peaks is described in more detail below.

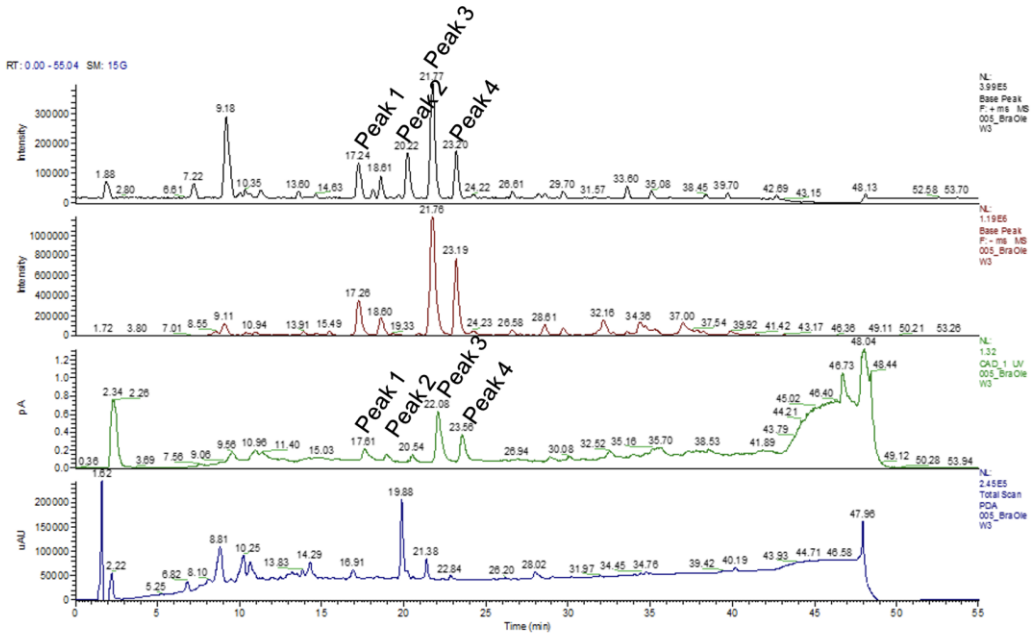

Figure 9: Representative chromatograms obtained from BraOleWFC3 by HPLC coupled with mass spectrometry (MS), positive ion mode and negative ion mode, charged aerosol detection (CAD), and photodiode array detection (PDA) (see Figure 6, p16). 4 peaks were selected for further analysis. Positive mass (black), negative mass (brown), CAD signal (green) and PDA signal (blue).

Table 12: Tentatively assigned substances that could occur in BraOleWFC3 (see Figure 6, p16). The experimental molecular weight was estimated based on the detected m/z values (positive and negative ion mode), while the theoretical molecular weights were obtained from literature sources.

Peak No.	Tentatively assigned substances	Experimental molecular weight	Theoretical molecular weight
Peak 1	Oleanolic acid or Ursolic acid	456 g/mol	456.70 g/mol
Peak 2	2-Acetoxycinnamic acid, 3 Acetoxycinnamic acid, or 4 Acetoxycinnamic acid	206 g/mol	206.20 g/mol
Peak 3	Cabbage identification factor 2	328 g/mol	328.35 g/mol
Peak 4	Vanillic acid 4-O-β-D-glucopyranoside, or Vanillic acid 1-O-β-D-glucopyranoside	330 g/mol	330.29 g/mol

In case of peak 1, the detected molecular weight is 456 g/mol (see appendix p69). Suggested triterpenes with a similar molecular weight are oleanolic or ursolic acid (see Figure 10 and Figure 11, p19) (30, 31).

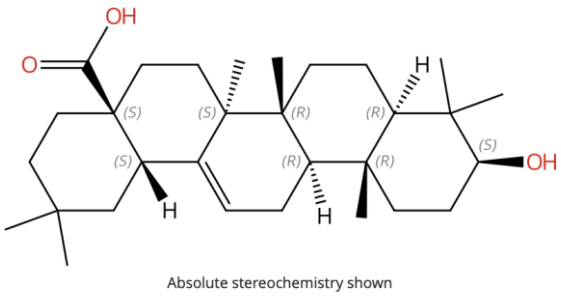

Figure 10: Structure of oleanolic acid with a molecular weight of 456.70 g/mol (30) (see Table 12, p18), a compound potentially present in the fraction BraOleWFC3 (see Figure 6, p16) and tentatively assigned to peak 1 in the CAD-detected chromatogram (green, see Figure 9, p18).

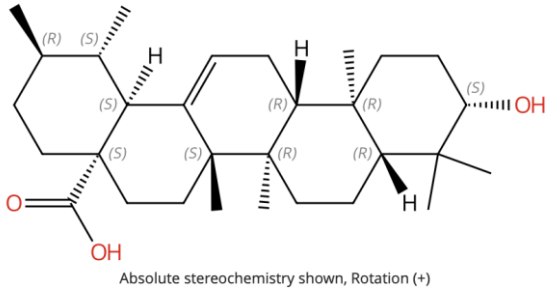

Figure 11: Structure of ursolic acid with a molecular weight of 456.70 g/mol (31) (see Table 12, p18), a compound potentially present in the fraction BraOleWFC3 (see Figure 6, p16) and tentatively assigned to peak 1 in the CAD-detected chromatogram (green, see Figure 9, p18).

When examining the UV spectrum of peak 2 (see appendix p70), it can be assumed that the substance is a hydroxycinnamic acid. Considering a molecular weight of 206 g/mol, three hydroxycinnamic acids with a similar molecular weight were identified as possible candidates: 2-acetoxycinnamic acid, 3-acetoxycinnamic acid, and 4-acetoxycinnamic acid (see Figure 12 - Figure 14, p19-20) (32-34).

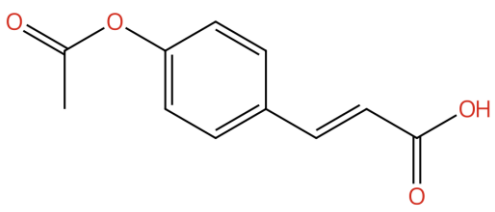

Figure 12: Structure of 4-acetoxycinnamic acid with a molecular weight of 206.20 g/mol (32) (see Table 12, p18), a compound potentially present in the fraction BraOleWFC3 (see Figure 6, p16) and tentatively assigned to peak 2 in the CAD-detected chromatogram (green, see Figure 9, p18).

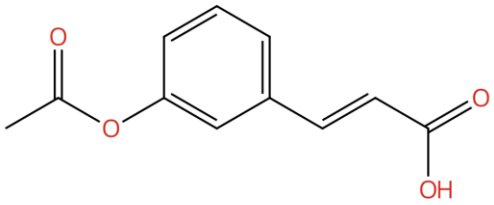

Figure 13: Structure of 3-acetoxycinnamic acid with a molecular weight of 206.20 g/mol (33) (see Table 12, p18), a compound potentially present in the fraction BraOleWFC3 (see Figure 6, p16) and tentatively assigned to peak 2 in the CAD-detected chromatogram (green, see Figure 9, p18).

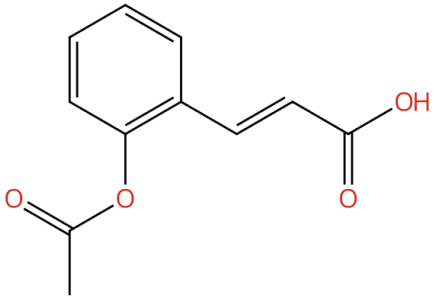

Figure 14: Structure of 2-acetoxycinnamic acid with a molecular weight of 206.20 g/mol (34) (see Table 12, p18), a compound potentially present in the fraction BraOleWFC3 (see Figure 6, p16) and tentatively assigned to peak 2 in the CAD-detected chromatogram (green, see Figure 9, p18).

Peak 3 revealed a molecular weight of 328 g/mol (see appendix p71), which corresponds to a compound described in literature as cabbage identification factor 2 (CIF2) (see Table 12, p18). CIF2 can be found on the surface of cabbage leaves and plays a role in helping certain insects recognize and select *Brassica* plants as a suitable location for egg-laying (structure see Figure 15, p20) (35-37).

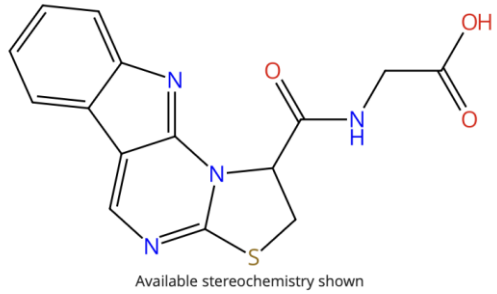

Figure 15: Structure of CIF2 with a molecular weight of 328.35 g/mol (35) (see Table 12, p18), a compound potentially present in the fraction BraOleWFC3 (see Figure 6, p16) and tentatively assigned to peak 3 in the CAD-detected chromatogram (green, see Figure 9, p18).

For peak 4 MS-DIAL® suggested the presence of methoxylated flavonoids. Yet, this was in contrast to the UV-spectra which did not point to this compound class. However, for verification quercetin-3-4-dimethylether and quercetin-3-7-dimethylether were analyzed by TLC (TLC 7, see Appendix Figure A 29), showing that none of these substances occurred in BraOleWFC3 (see Figure 6, p16).

Nevertheless, glycosides of vanillic acids with a molecular weight of 330.29 g/mol would match the m/z of peak 4 (see appendix p72), therefore, vanillic acid-4-O-β-D-glucopyranoside and vanillic acid-1-O-β-D-glucopyranoside (see Table 12, p18) were identified as possible candidates (38, 39). Due to the unavailability, no TLC comparison with pure substances was carried out.

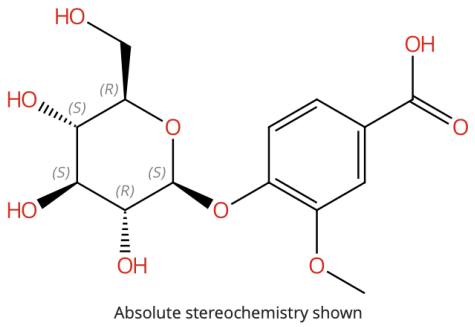

Figure 16: Structure of vanillic acid 4-O-β-D-glucopyranoside with a molecular weight of 330.29 g/mol (38) (see Table 12, p18), a compound potentially present in the fraction BraOleWFC3 (see Figure 6, p16) and tentatively assigned to peak 4 in the CAD-detected chromatogram (green, see Figure 9, p18).

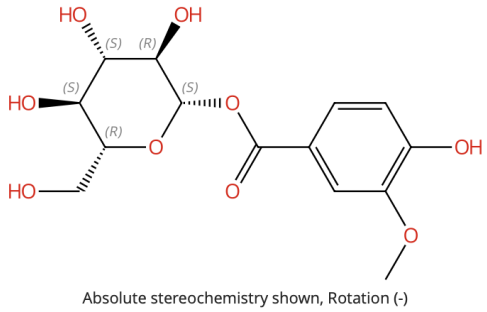

Figure 17: Structure of vanillic acid 1-O-β-D-glucopyranoside with a molecular weight of 330.29 g/mol (39) (see Table 12, p18), a compound potentially present in the fraction BraOleWFC3 (see Figure 6, p16) and tentatively assigned to peak 4 in the CAD-detected chromatogram (green, see Figure 9, p18).

4.2 Phytochemical analysis of the most active dichloromethane fractions

This chapter presents the analysis of the dichloromethane fractions BraOleD15, 40, and 70 (see 3.1.2, p5) by TLC, HPLC, and MS.

4.2.1 Extract BraOleD

The DCM extract (BraOleD, see chapter 3.1.2, p5) was prepared and fractionated via SPE in previous master theses (21). The obtained SPE fractions were then examined in bioactivity tests to assess their ability to activate Nrf2 and inhibit NF-κB, which both play an important role in wound healing (40-43). These tests

suggested that the most bioactive fractions are the 15% and 40% methanolic fraction in case of inhibiting NF-κB (BraOleD15 and BraOleD40, see chapter 3.1.2, p5) and the 70% methanolic fraction in case of activating Nrf2 (BraOleD70, see chapter 3.1.2, p5) (22). To analyze the composition of the substances in the extract, a TLC analysis was carried out with pure substances commonly found in cabbage (TLC6, see Table 3, p8). The original DCM extract (BraOleD, see chapter 3.1.2, p5) was applied and compared with the pure substances cyanidin, quercetin, kaempferol, caffeic acid, p-coumaric acid, ferulic acid, and sinapic acid. The results, which are shown below in Figure 18, suggested the presence of the following substances due to similar Rf-values and comparable colors observed under UV light between the extract and the pure substances: ferulic acid, sinapic acid, quercetin, and cyanidin

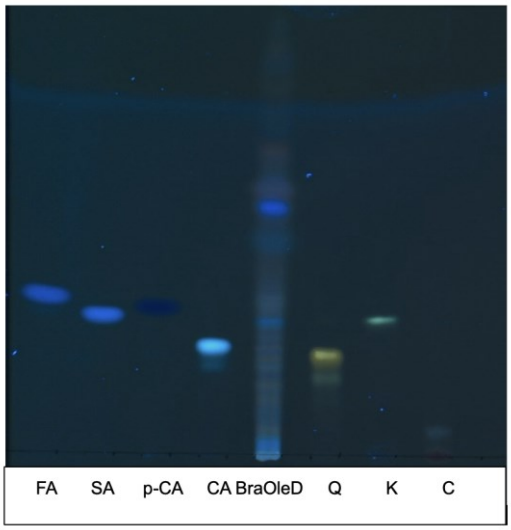

Figure 18: TLC6 analysis of ferulic acid (FA), sinapic acid (SA), p-coumaric acid (p-CA), caffeic acid (CA), extract BraOleD (see chapter 3.1.2, p5), quercetin (Q), kaempferol (K), and cyanidin (C) using TLC system 3 (see chapter 7, Table 3, p8). Detection: natural product reagent, 366 nm UV light.

To confirm the TLC-results, an HPLC analyses were carried out with BraOleD15, BraOleD40, and BraOleD70 (see chapter 3.1.2, p5) which were then compared with pure substances in HPLC run 1 and 2 (see Table 5 and Figure 4). Like in BraOleWFC3 (see Figure 6, p16), the pure substances cyanidin, quercetin, kaempferol, caffeic acid, p-coumaric acid, ferulic acid, and sinapic acid were chosen since these substances are well-known constituents occurring in cabbage (5, 19, 29). The retention times and the UV spectra of these substances were compared with those from the analyzed fractions. According to the results, none of the above-mentioned substances were detected in the fractions. However, as in the case of

BraOleWFC3 (see Figure 6, p16), when looking at the UV spectra of the analyzed hydroxycinnamic acids caffeic acid, ferulic acid and sinapic acid, all show a minimum at 260 nm and a maximum at about 320 nm. Comparing the spectrum of sinapic acid (see Figure 19, p23) with the spectrum of the peak in BraOleD70 (see Figure 20, p23, 19.802 min), similarities were observed. Therefore, different hydroxycinnamic acids or derivatives from the above-mentioned substances (e.g. sinapic acid or ferulic acid derivates) could occur in the fractions.

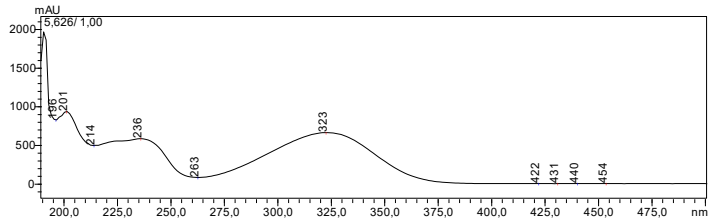

Figure 19: UV spectrum of sinapic acid.

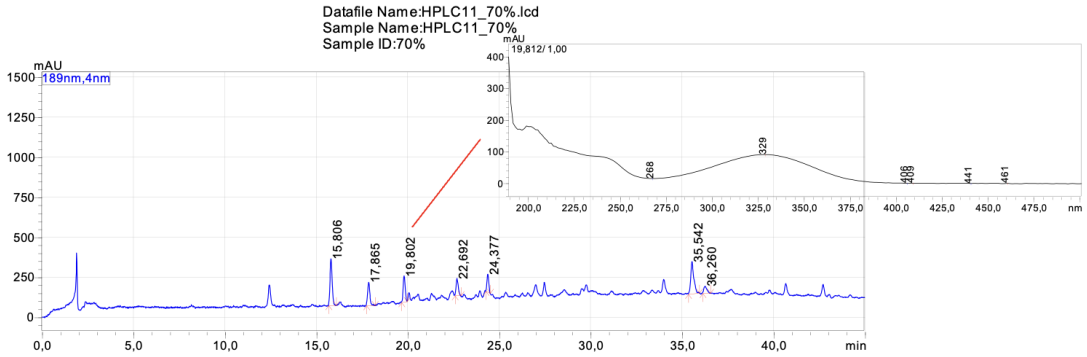

Figure 20: Analysis of fraction BraOleD70 (see chapter 3.1.2, p5) by HPLC-UV-DAD (system see Table 5, p9) and UV spectrum of the substance eluting at the retention time 19.802 min

For further identification, again an HPLC analysis hyphenated to CAD, PDA, and MS was carried out. The analysis of the different peaks in the fractions BraOleD15, BraOleD40, and BraOleD70 (see chapter 3.1.2, p5) is described in more detail in chapters 4.2.2, 4.2.3, and 4.2.4 below. Figure 21 (p24), Figure 29 (p27), and Figure 32 (p30) show the MS data, respectively. The positive ion mode is represented by the black chromatogram, while the negative ion mode is shown in brown. The CAD signal is depicted in green, and the PDA signal in blue. The peaks 1-4 in the CAD-detected chromatogram (Figure 21, Figure 29, and Figure 32, green) were assigned to the corresponding peaks in the MS-ion chromatograms. The suggested molecular weights (see Table 13, Table 14, and Table 15) from the MS data recorded in the positive and negative mode were compared with the database from CAS SciFinder®. Additionally, MS-DIAL® from CompMS® was used to analyze the MS data.

4.2.2 Fraction BraOleD15

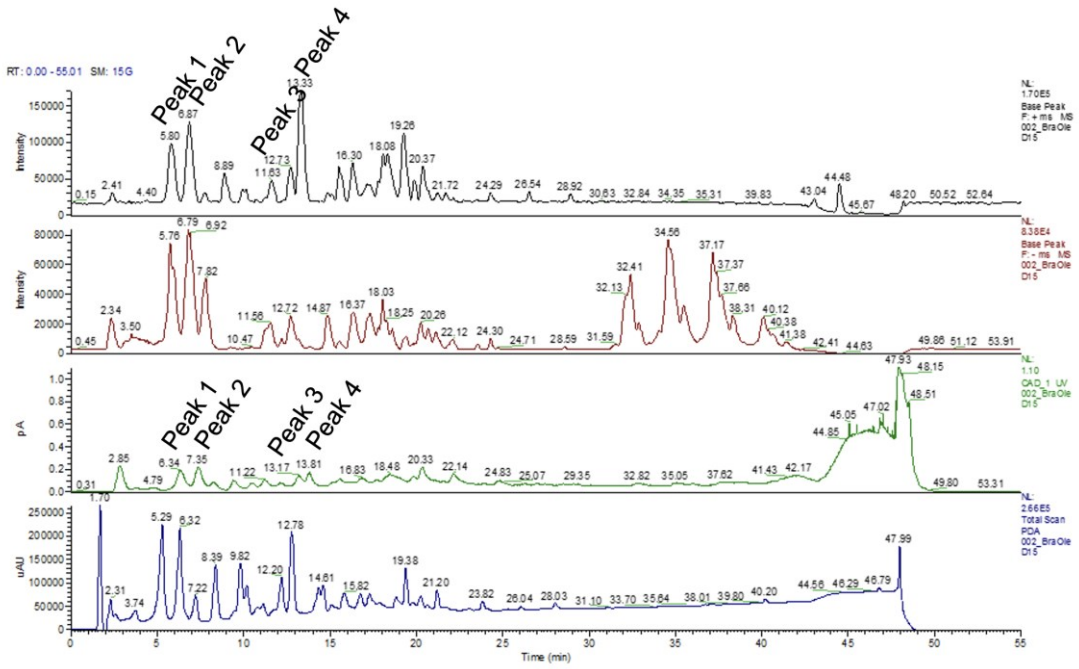

Figure 21: Representative chromatograms obtained from BraOleD15 by HPLC coupled with mass spectrometry (MS), positive ion mode and negative ion mode, charged aerosol detection (CAD), and photodiode array detection (PDA) (see chapter 3.1.2, p5). 4 peaks were selected for further analysis. Positive mass (black), negative mass (brown), CAD signal (green) and PDA signal (blue).

Table 13: Tentatively assigned substances that could occur in BraOleD15 (see chapter 3.1.2, p5). The experimental molecular weight was estimated based on the detected m/z values (positive and negative ion mode), while the theoretical molecular weights were obtained from literature sources.

Peak No.	Tentatively assigned substances	experimental molecular weight	Theoretical molecular weight
Peak 1	p-Hydroxybenzaldehyde glucoside	284 g/mol	284.26 g/mol
Peak 2	4-Carboxy-5-(2-carboxyethyl)-3-methyl-2-furanpentanoic acid	298 g/mol	298.29 g/mol
Peak 3	Ascorbigen	305 g/mol	305.28 g/mol
Peak 4	3-Butenyl isothiocyanate, 2-Thiirane-propanenitrile, 4-(Methylthio)-3-butenenitrile, or 2-Butenyl isothiocyanate	113 g/mol	113.18 g/mol

When examining the first peak, MS-DIAL® indicated that acacetin, which has a molecular weight of 284.26 g/mol (44), might be present in BraOleD15 (see chapter 3.1.2, p5). To confirm the presence of acacetin, a HPLC run was carried out with acacetin as pure substance and compared with BraOleD15 in HPLC run 6 (see Table 5 and Figure 4 in chapter 3.2.3, p8). When comparing the peak of the pure substance with the one from the fraction, no similarities could be observed as shown

in Figure A 38 on page 78. Another candidate compound was p-hydroxybenzaldehyde glucoside (see Table 13, p24) which reveals a molecular weight of 284.26 g/mol and can be seen in Figure 22 below (45). In case of this substance, the UV spectrum (typical for aromatic compounds with a maximum around 210 to 240 nm) (46) supports the assumption that p-hydroxybenzaldehyde glucoside could be present in the fraction (see appendix p77).

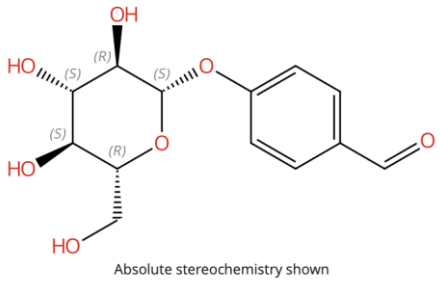

Figure 22: Structure of p-hydroxybenzaldehyde glucoside with a molecular weight of 284.26 g/mol (45) (see Table 13, p24), a compound potentially present in the fraction BraOleD15 (see chapter 3.1.2, p5) and tentatively assigned to peak 1 in the CAD-detected chromatogram (green, see Figure 21, p24)

According to the MS data, the substance from peak 2 (see appendix p79) has a molecular weight of 298 g/mol. Therefore, a furan fatty acid like 4-carboxy-5-(2-carboxyethyl)-3-methyl-2-furanpentanoic acid (see Table 13, p24), which has a comparable molecular weight of 298.29 g/mol (47), could be considered as a component of the fraction BraOleD15 (see chapter 3.1.2, p5) and is shown in Figure 23 below.

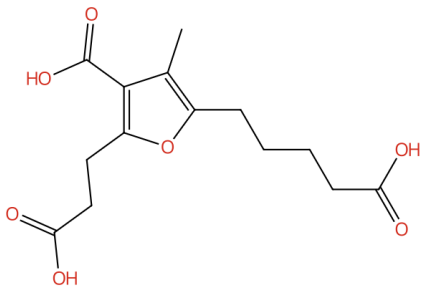

Figure 23: Structure of 4-carboxy-5-(2-carboxyethyl)-3-methyl-2-furan pentanoic acid with a molecular weight of 298.29 g/mol (47) (see Table 13, p24), a compound potentially present in the fraction BraOleD15 (see chapter 3.1.2, p5) and tentatively assigned to peak 2 in the CAD-detected chromatogram (green, see Figure 21, p24)

Regarding the third peak, various factors suggested that ascorbigen (see Table 13, p24) could be present in BraOleD15 (see chapter 3.1.2, p5). According to the MS data (see appendix p80), the substance has a molecular weight of 305 g/mol, which matches the molecular weight of ascorbigen (305.28 g/mol (48)). Furthermore, it is important to note that ascorbigen is a conjugate of ascorbic acid and indole-3-

carbinol (49). This was supported by the mass spectrum recorded in the negative mode (see appendix p80), showing a fragment with a molecular weight of 176 g/mol, corresponding to ascorbic acid. Additionally, indolic structures exhibit a UV maximum around 280 nm, which is comparable to the measured spectrum (see appendix p80) (50). The suggested structure is shown below in Figure 24.

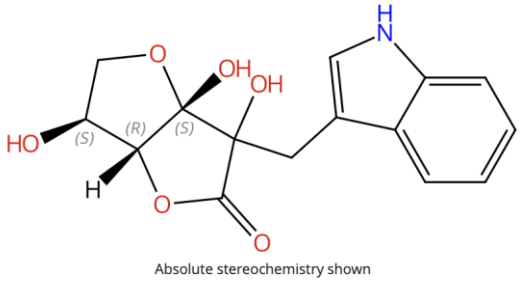

Figure 24: Structure of ascorbigen with a molecular weight of 305.28 g/mol (48) (see Table 13, p24), a compound potentially present in the fraction BraOleD15 (see chapter 3.1.2, p5) and tentatively assigned to peak 3 in the CAD-detected chromatogram (green, see Figure 21, p24)

Based on the MS data corresponding to peak 4 (see appendix p81), the positive ion signal was significantly more intense than the corresponding negative ion signal, suggesting a molecular weight of approximately 113 g/mol. Considering this value, various thiocyanates and nitriles could be proposed as potential candidates. The molecular weight of certain thiocyanates, such as 113.18 g/mol, fits well with the observed MS data (see Table 13, p24). These thiocyanates include 3-butenyl isothiocyanate, 2-thiirane-propanenitrile, 4-(methylthio)-3-butenenitrile, and 2-butenyl isothiocyanate (51-54) and are shown below in Figure 25 to Figure 28.

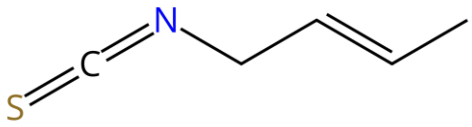

Figure 25: Structure of 2-butenyl isothiocyanate with a molecular weight of 113.18 g/mol (51) (see Table 13, p24), a compound potentially present in the fraction BraOleD15 (see chapter 3.1.2, p5) and tentatively assigned to peak 4 in the CAD-detected chromatogram (green, see Figure 21, p24)

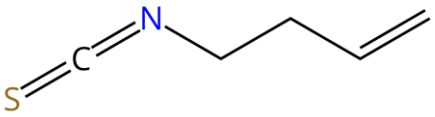

Figure 26: Structure of 3-butenyl isothiocyanate with a molecular weight of 113.18 g/mol (52) (see Table 13, p24), a compound potentially present in the fraction BraOleD15 (see chapter 3.1.2, p5) and tentatively assigned to peak 4 in the CAD-detected chromatogram (green, see Figure 21, p24)

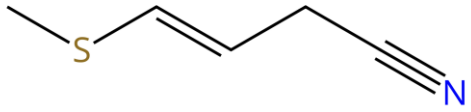

Figure 27: Structure of 4-(methylthio)-3-butenenitrile with a molecular weight of 113.18 g/mol (53) (see Table 13, p24), a compound potentially present in the fraction BraOleD15 (see chapter 3.1.2, p5) and tentatively assigned to peak 4 in the CAD-detected chromatogram (green, see Figure 21, p24)

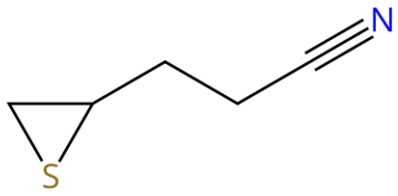

Figure 28: Structure of 2-thiirane-propanenitrile with a molecular weight of 113.18 g/mol (54) (see Table 13, p24), a compound potentially present in the fraction BraOleD15 (see chapter 3.1.2, p5) and tentatively assigned to peak 4 in the CAD-detected chromatogram (green, see Figure 21, p24)

4.2.3 Fraction BraOleD40

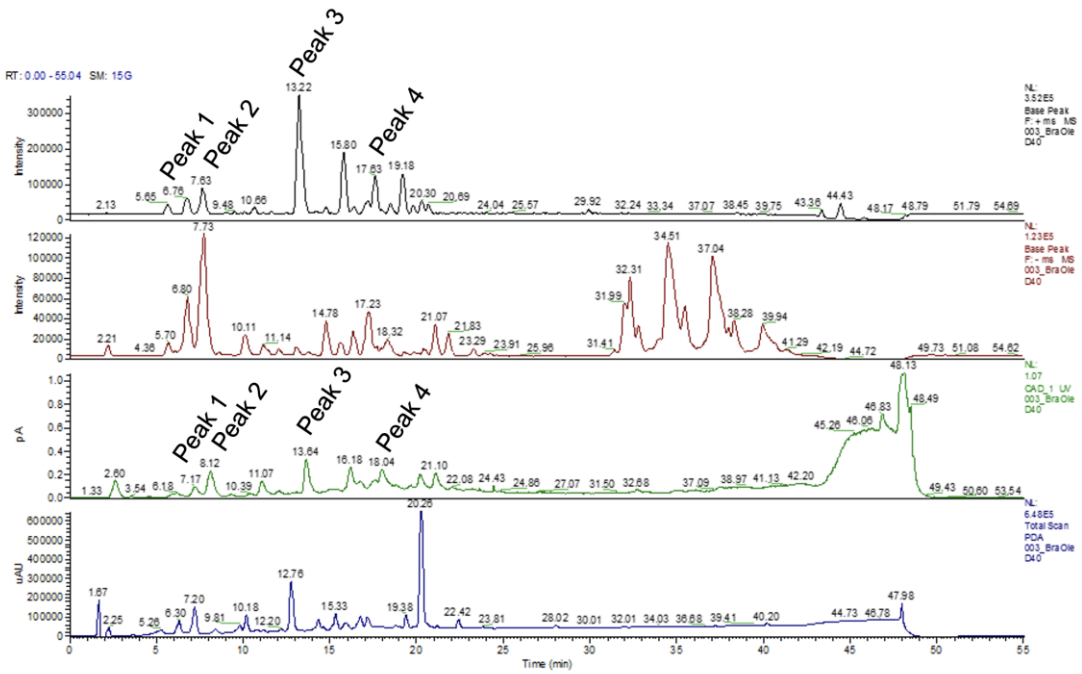

Figure 29: Representative chromatograms obtained from BraOleD40 by HPLC coupled with mass spectrometry (MS), positive ion mode and negative ion mode, charged aerosol detection (CAD), and photodiode array detection (PDA) (see chapter 3.1.2, p5). 4 peaks were selected for further analysis. Positive mass (black), negative mass (brown), CAD signal (green) and PDA signal (blue).

Table 14: Tentatively assigned substances that could occur in BraOleD40 (see chapter 3.1.2, p5). The experimental molecular weight was estimated based on the detected m/z values (positive and negative ion mode), while the theoretical molecular weights were obtained from literature sources.

Peak No.	Tentatively assigned substances	experimental molecular weight	Theoretical molecular weight
Peak 1	4-Carboxy-5-(2-carboxyethyl)-3-methyl-2-furanpentanoic acid	298 g/mol	298.29 g/mol
Peak 2	Linoleic acid 13-hydroperoxide	312 g/mol	312.44 g/mol
Peak 3	3-Butenyl isothiocyanate, 2-Thiirane-propanenitrile, 4-(Methylthio)-3-butenenitrile, or 2-Butenyl isothiocyanate	113 g/mol	113.18 g/mol
Peak 4	1,2-Disinapoylglucose	592 g/mol	592.55 g/mol

For the first peak, the molecular weight is 298 g/mol (see appendix p83). Therefore, a furan fatty acid such as 4-carboxy-5-(2-carboxyethyl)-3-methyl-2-furanpentanoic acid (see Table 14, p28) could again be considered as a component of the fraction, as observed in BraOleD15 peak 2 (see chapter 4.2.2, p24 and Figure 23, p25). The MS data of peak 2 from BraOleD40 (see chapter 3.1.2, p5) aligns with the molecular weight of caftaric acid of 312.23 g/mol (see appendix p84) (55). To confirm its presence, caftaric acid as a pure substance was analyzed by using HPLC (see HPLC run 3 in Table 5 and Figure 4). Initially, the pure substance showed the same retention time as the peak in the fraction (see appendix p85). However, caftaric acid showed a different UV spectrum than the corresponding peak in BraOleD40. Therefore, another HPLC run was carried out using a different solvent gradient (see HPLC run 4 in Table 4 and Figure 4 in chapter 3.2.3, p8). As a result, caftaric acid pure substance peak did not align with the peak from the fraction anymore as shown in Figure A 52 (see appendix p85). Consequently, no caftaric acid was found. But, assuming a molecular weight of 312 g/mol, a fatty acid with a hydroperoxide function could be considered (see Table 14, p28). A fatty acid like linoleic acid 13-hydroperoxide would have a comparable molecular weight (56, 57) and is shown below in Figure 30.

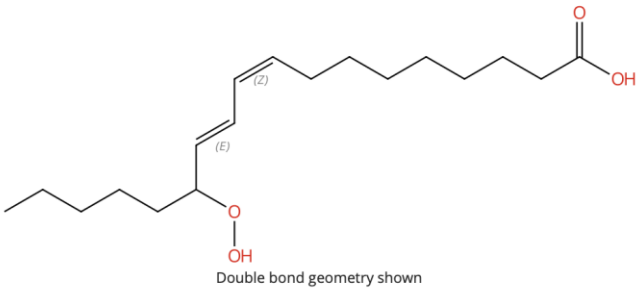

Figure 30: Structure of linoleic acid 13-hydroperoxide with a molecular weight of 312.44 g/mol (56) (see Table 14, p28), a compound potentially present in the fraction BraOleD40 (see chapter 3.1.2, p5) and tentatively assigned to peak 2 in the CAD-detected chromatogram (green, see Figure 29, p27)

For peak 3, thiocyanates or nitriles could again be considered as possible substances, similar to those identified in BraOleD15 peak 4 (see chapter 4.2.2, p24 and Figure 25 to Figure 28, p26). When examining peak 4, a hydroxycinnamic acid derivative could be considered as a possible candidate (see Table 14, p28). The peak not only displays a UV spectrum characteristic for hydroxycinnamic acids but also is in good agreement with the MS data (see appendix p87). In the negative mass spectrum, a peak at 591.41 g/mol is observed, which is close to the molecular weight of 1,2-disinapoylglucose (592.20 g/mol) (58). Additionally, the MS2 data (see appendix p88) reveals a fragment with a molecular weight similar to that of sinapic acid, with 224.21 g/mol (59) (see Figure A 57, p88). This could indicate the cleavage of sinapic acid and the glucose. The structure is shown below in Figure 31.

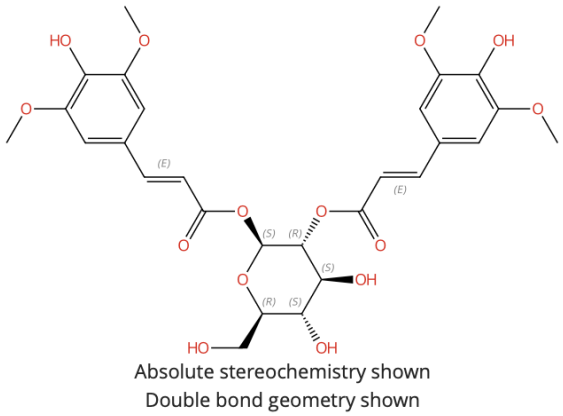

Figure 31: Structure of 1,2-disinapoylglucose with a molecular weight of 592.55 g/mol (58) (see Table 14, p28), a compound potentially present in the fraction BraOleD40 (see chapter 3.1.2, p5) and tentatively assigned to peak 4 in the CAD-detected chromatogram (green, see Figure 29, p27)

4.2.4 Fraction BraOleD70

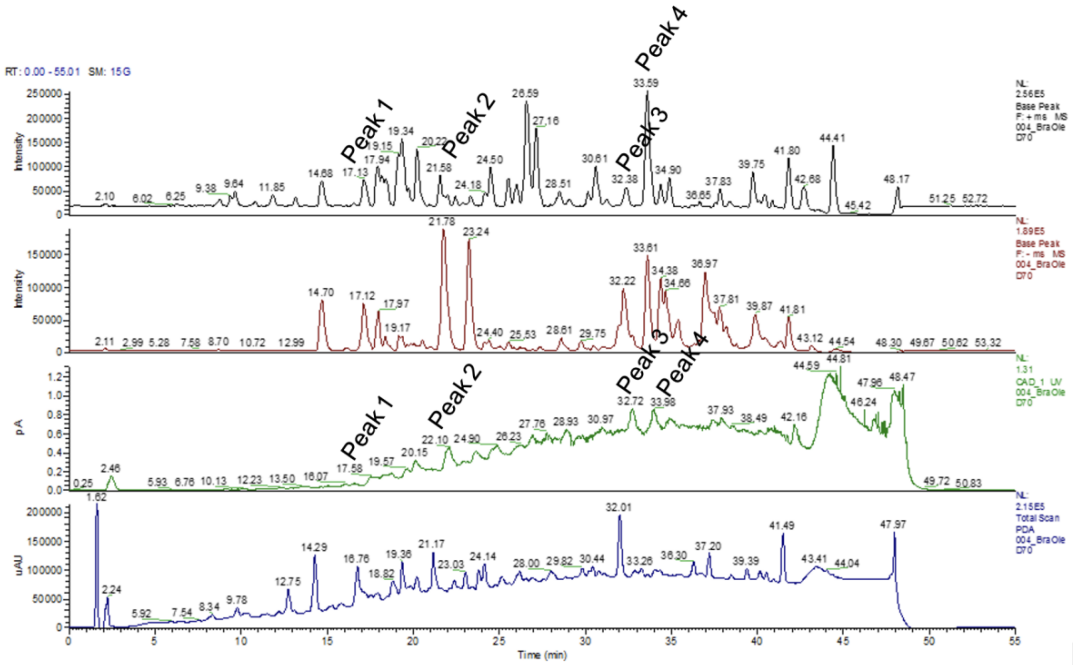

Figure 32: Representative chromatograms obtained from BraOleD70 by HPLC coupled with mass spectrometry (MS), positive ion mode and negative ion mode, charged aerosol detection (CAD), and photodiode array detection (PDA) (see chapter 3.1.2, p5). 4 peaks were selected for further analysis. Positive mass (black), negative mass (brown), CAD signal (green) and PDA signal (blue).

Table 15: Tentatively assigned substances that could occur in BraOleD70 (see chapter 3.1.2, p5). The experimental molecular weight was estimated based on the detected m/z values (positive and negative ion mode), while the theoretical molecular weights were obtained from literature sources.

Peak No.	**Tentatively assigned substances**	**experimental molecular weight**	**Theoretical molecular weight**
Peak 1	3-Feruloylquinic acid, or 1,2-Disinapoylglucose	368 (positive ion mode), or 592 (negative ion mode)	368.34, or 592.55
Peak 2	Cabbage identification factor 2	328	328.25
Peak 3	Methoxybrassinin	266	266.38
Peak 4	Methyl α-linolenate, or Methyl γ-linolenate	292	292.46

Upon examining the UV spectrum of the peak 1 (see appendix p90), it can be assumed that the substance is a hydroxycinnamic acid. A molecular weight of 368 g/mol, corresponding to the positive ion MS data (see appendix p90), would match 3-feruloylquinic acid (60). Since no pure substance was available for direct comparison, an acid hydrolysis was carried out to separate ferulic acid from quinic acid. For this purpose, sulfuric acid was diluted to 0.5 M and added to the fraction at a 1:2 ratio. The mixture was then heated in an oven at 110°C for 10 minutes. After

hydrolysis, BraOleD70 (see chapter 3.1.2, p5) was compared with pure ferulic acid using HPLC (run 5, see Table 5, p9) showing similar retention times and UV spectra (see appendix p91). Co-chromatography (HPLC run 6, see Table 5, p9) further confirmed the presence of ferulic acid, as the peak area increased when the pure substance was mixed with the hydrolyzed fraction (see Figure 34 and Figure 35). Additionally, quinic acid was analyzed by HPLC (run 5, see Table 5, p9). The ELSD signals revealed similar retention times between quinic acid and the corresponding peak in the hydrolyzed fraction (see appendix p91). Importantly, neither ferulic acid nor quinic acid was detected in the fraction before hydrolysis (see HPLC run 1, Table 5 and Figure 4 in chapter 3.2.3, p8), indicating that both compounds were artefacts resulting from the acid hydrolysis. The combined results from the MS data and UV spectra, before and after hydrolysis results strongly supports the occurrence of 3-feruloylquinic acid in BraOleD70 (see chapter 3.1.2, p5).

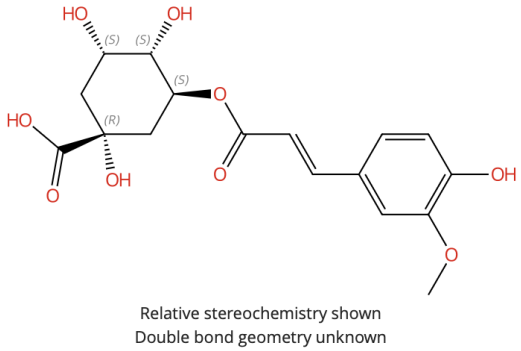

Figure 33: Structure of 3-feruloylquinic acid with a molecular weight of 368.34 g/mol (60) (see Table 15, p30), a compound potentially present in the fraction BraOleD70 (see chapter 3.1.2, p5) and tentatively assigned to peak 1 in the CAD-detected chromatogram (green, see Figure 32, p30)

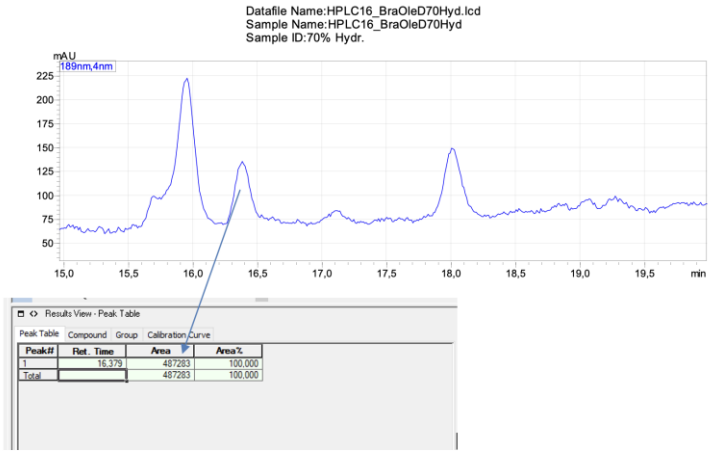

Figure 34: Analysis of fraction BraOleD70 (see chapter 3.1.2, p5) after hydrolysis by HPLC-UV-DAD (system see Table 5, p9). Ferulic acid eluting at the retention time 16.379 min. Peak area: 487293

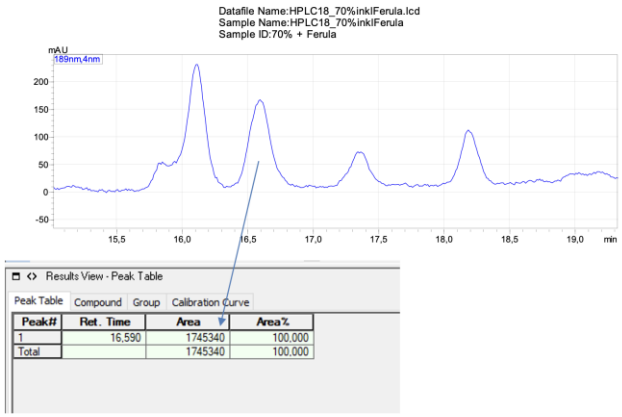

Figure 35: Analysis of fraction BraOleD70 (see chapter 3.1.2, p5) after hydrolysis mixed with ferulic acid pure substance by HPLC-UV-DAD (system see Table 5, p9). Ferulic acid eluting at the retention time 16.590 min. Peak area: 1745340.

When examining the mass spectrum in the positive mode of the first peak (see appendix p90), the data suggests the presence of 3-feruloylquinic acid, as previously described. However, when considering the corresponding mass spectrum in the negative mode, a peak at m/z 591.20 was observed, which corresponds to 1,2-disinapoylglucose (molecular weight 592.55 g/mol) (58). Therefore, similar to the observation made for BraOleD40 peak 4 (see chapter 4.2.3, p27), 1,2-disinapoylglucose could also be considered a possible candidate for BraOleD70 peak 1 (see chapter 3.1.2, p5). When examining the MS data from BraOleD70 peak 2 (see chapter 3.1.2, p5), a molecular weight of 328 g/mol was observed (see appendix p92). Given this molecular weight, cabbage identification factor 2 (CIF2), which shows a similar molecular weight, could be considered (35). Furthermore, the UV spectrum displays maxima at approximately 210 and 290 nm, which is similar to the UV spectra from indolic structures (50). CIF2 has already been described for peak 3 of BraOleWFC3 (see chapter 4.1.2, p16). The MS data of peak 3 from BraOleD70 (see chapter 3.1.2, p5), corresponds to the molecular weight of methoxybrassinin (266.38 g/mol) (61). Additionally, the UV spectrum displays a maximum around 280 nm, which is typical for indolic structures (see appendix p93) (50).

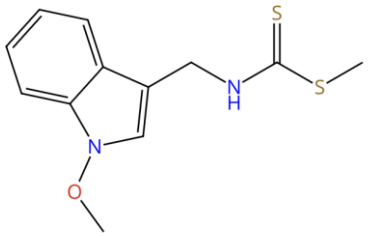

Figure 36: Structure of methoxybrassinin with a molecular weight of 266.38 g/mol (61) (see Table 15, p30), a compound potentially present in the fraction BraOleD70 (see chapter 3.1.2, p5) and tentatively assigned to peak 3 in the CAD-detected chromatogram (green, see Figure 32, p30)

Upon examining the fourth peak a molecular weight of approximately 292 g/mol was observed (see appendix p94). In this case, a fatty acid derivative could be considered as a potential substance, such as a methyl ester of linolenic acid (e.g., methyl α-linolenate or methyl γ-linolenate) (62, 63). Additionally, the UV spectrum showed similarities to that of α-linolenic acid (see appendix p94) (64).

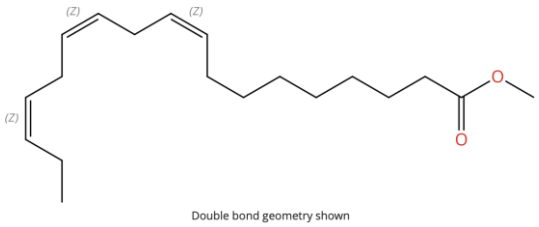

Figure 37: Structure of methyl α-linolenate with a molecular weight of 292.46 g/mol (62) (see Table 15, p30), a compound potentially present in the fraction BraOleD70 (see chapter 3.1.2, p5) and tentatively assigned to peak 4 in the CAD-detected chromatogram (green, see Figure 32, p30)

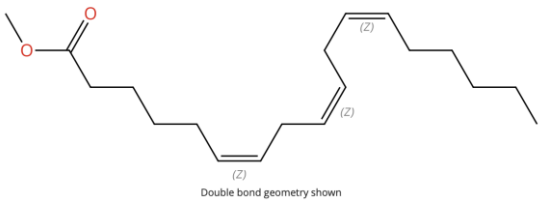

Figure 38: Structure of methyl γ-linolenate with a molecular weight of 292.36 g/mol (63) (see Table 15, p30), a compound potentially present in the fraction BraOleD70 (see chapter 3.1.2, p5) and tentatively assigned to peak 4 in the CAD-detected chromatogram (green, see Figure 32, p30)

4.3 GC-MS analysis of volatile components in the dichloromethane extract

This chapter presents the analysis of the freshly prepared DCM extract (see 3.1.2, p5) with GC-MS to investigate its volatile components.

4.3.1 Comparison of German and Austrian cabbage

Initially, the already existing DCM extract (see chapter 3.1.2, p5) which had been isolated approximately six months ago, was checked for any volatile components. However, after GC examination, it was observed that most of the substances had already evaporated. To ensure that the volatile components do not evaporate, fresh DCM extracts were prepared shortly before the GC-MS analysis described in chapter 3.1.2, p5. The dry extracts were then dissolved in 100 µL DCM, centrifuged, diluted to 1:100 and analyzed by GC-MS (see chapter 3.2.4 and Table 7) The cabbages used for this GC-MS analysis were a cabbage originating from Germany and a cabbage originating from Austria. The aim was to check for any qualitative differences between these two extracts. The results, which can be seen in Figure 39, suggest very similar components with a few quantitative deviations between the two extracts.

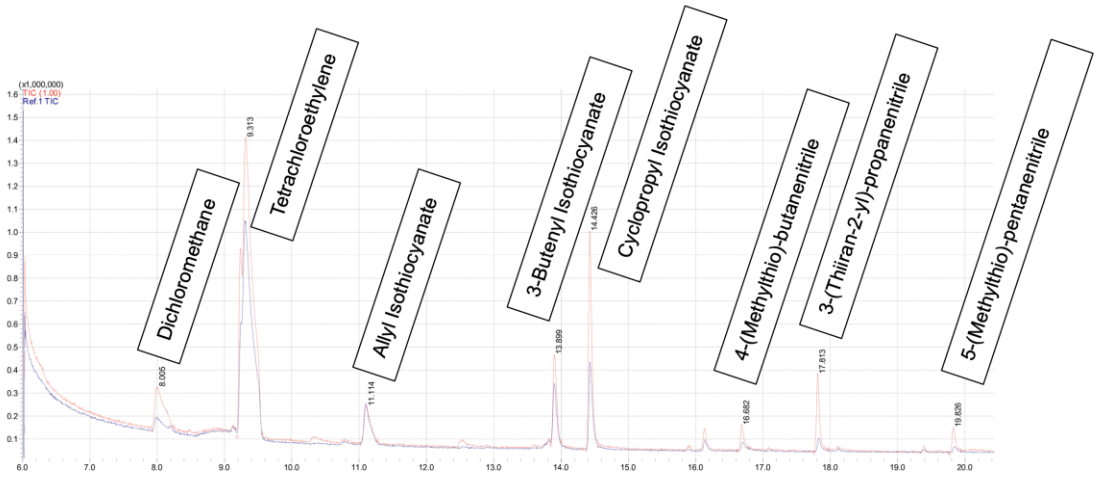

Figure 39: Comparison of the peaks from Austrian cabbage (GCMS run 1, red) with German cabbage (GCMS run 2, blue) along with possible substance identifications based on NIST® and WILEY® databases (see chapter 3.2.4 and Table 7)

4.3.2 Identification of substances in the DCM extract from the Austrian cabbage

To identify certain substances in the DCM extracts (see chapter 3.1.2, p5), the similarity search function of GCMSsolution 4.11 software was used. The obtained MS spectra were compared with library databases such as NIST® or WILEY®. Based on these comparisons, allyl isothiocyanate, 3-butenyl isothiocyanate, cyclopropyl isothiocyanate, 4-(methylthio)-butanenitrile, 3-(thiiran-2-yl)-propanenitrile, and 5-

(methylthio)-pentanenitrile were tentatively identified as possible substances, as shown in Table 16 below and in the appendix section on page 95.

Table 16: Tentatively identified volatile substances detected in the DCM extracts (see chapter 3.1.2, p5)

Substance	**Similarity score (%) according to databases**	**Compared with pure substances**
3-butenyl isothiocyanate	94	yes
4-(methylthio)-butanenitrile	92	no
allyl isothiocyanate	91	yes
5-(methylthio)-pentanenitrile	82	no
3-(thiiran-2-yl)-propanenitrile	80	no
cyclopropyl isothiocyanate	79	no

The substances mentioned above have already been described in cabbage before (5, 65). Further substances found by the databases were the used DCM solvent as well as tetrachloroethylene which acts as stabilizer in the DCM (see Figure 39, p34). To confirm these tentative assignments, available pure compounds were analyzed to identify the substances (see Table 16, p35). Allyl isothiocyanate (AITC) and 3-butenyl isothiocyanate (3-BITC) were diluted 1:25.000 and analyzed using the GC-MS (see chapter 3.2.4 and Table 7, p10). The comparison of the MS spectra and the retention times of the pure substances with those of the DCM extract supports the assumption that AITC and 3-BITC occur in the freshly prepared DCM extract (see chapter 3.1.2, p5). The chemical structures of AITC and 3-BITC are shown in Figure 41 and Figure 42 on p36. However, to confirm this statement, a co-chromatography was carried out (GC-MS runs 5-8, see Table 7, p10). For this purpose, the pure substances were combined with the DCM extract and again analyzed using GC-MS. The respective peak areas were then compared with the ones from the pure cabbage extract. The peak areas indicated that the AITC and 3-BITC peaks were approximately twice as intense as in the DCM extract (see chapter 3.1.2, p5) was mixed with the pure substances. This can be seen in Figure 40 and Table 17 below and further confirms the presence of AITC and 3-BITC. All the abovementioned data of the GC-MS analysis can be found in the appendix section (Figure A 70 to Figure A 90 on pages 95-100).

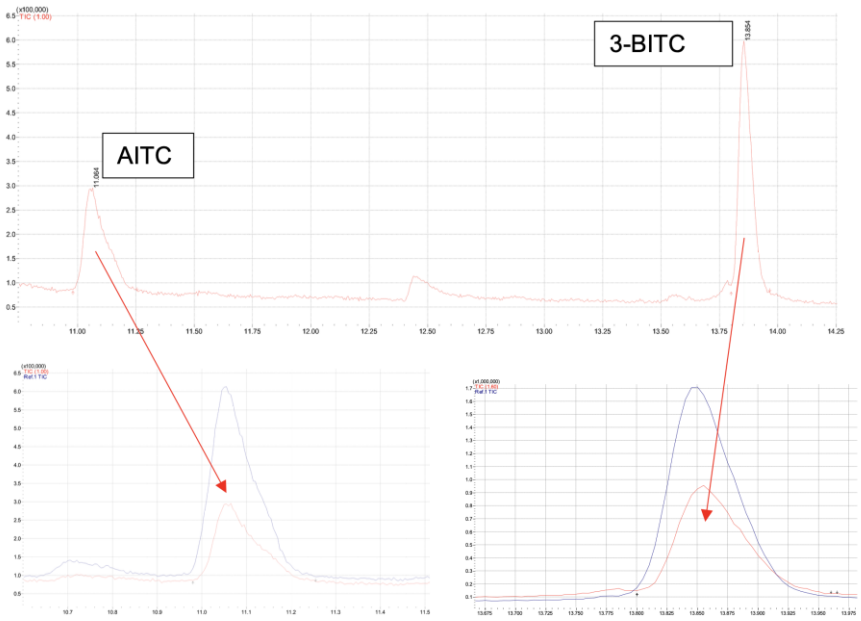

Figure 40: Top panel: GC-MS run 5 (see Table 7, p10), analyzed DCM extract (see chapter 3.1.2, p5). Bottom panel: GC-MS run 6-8 (see Table 7, p10), Comparison of peak areas indicated that the AITC and 3-BITC peaks were approximately twice as intense when the DCM extract (see chapter 3.1.2, p5) was mixed with the pure substances. Bottom left panel: AITC peak from DCM extract (red) and AITC peak from DCM extract mixed with pure substance (blue). Bottom right panel: 3-BITC peak from DCM extract (red) and 3-BITC peak from DCM extract mixed with pure substance (blue).

Table 17: Peak areas of AITC and 3-BITC in the analyzed DCM extract (see chapter 3.1.2, p5) and in the corresponding pure substances

Used extract / substances	**AITC peak area**	**3-BITC peak area**
DCM extract	1.370.883	1.951.877
pure substance	1.868.083	1.325.153
DCM extract combined with AITC and 3-BITC pure substances (measured)	3.319.854	3.474.983
Calculated peak area	3.238.966	3.277.030

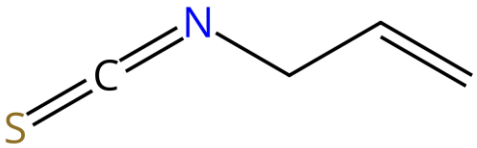

Figure 41: Structure of allyl isothiocyanate with a molecular weight of 99.16 g/mol (66) (see Table 16, p35), a compound potentially present in the fresh DCM extract (see chapter 3.1.2, p5) and tentatively assigned to peak eluting at 11.114 min in the GC-MS chromatogram (see Figure 39, p34)

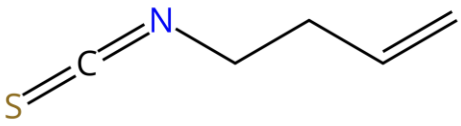

Figure 42: Structure of 3-butenyl isothiocyanate with a molecular weight of 113.18 (52) (see Table 16, p35), a compound potentially present in the fresh DCM extract (see chapter 3.1.2, p5) and tentatively assigned to peak eluting at 13.899 min in the GC-MS chromatogram (see Figure 39, p34)

5 Discussion and conclusion

In this master thesis, various cabbage extracts were analyzed with regard to their phytochemical composition. Identification of volatile isothiocyanates reported earlier in literature for cabbage (5, 65) was achieved for the fresh DCM extract (see chapter 3.1.2, p5) employing GC-MS (see chapter 4.3, p33). Allyl isothiocyanate and 3-butenyl isothiocyanate were identified by comparison with pure substances. Further compounds such as cyclopropyl isothiocyanate, 4-(methylthio)-butanenitrile, 3-(thiiran-2-yl)-propane-nitrile, and 5-(methylthio)-pentanenitrile were tentatively identified based on the comparison with libraries (5, 65) (see Table 16). Although these compounds were not confirmed by reference substances due to their unavailability, they are well-documented constituents occurring in cabbage (5, 65). The presence of 4-(methylthio)-butanenitrile appears particularly likely, as the received similarity score of 92% closely matches the score of the two identified substances (see Table 16, p35). Isothiocyanates and nitriles show antioxidative and anti-inflammatory effects and may therefore contribute positively to wound healing (67). Therefore, they can serve as marker substances for quality control.

In the case of BraOleD15 (see chapter 3.1.2, p5), which was selected for further analysis due to its inhibitory effects on NF-κB (22), p-hydroxybenzaldehyde glucoside, furan fatty acids, ascorbigen, various thiocyanates, and nitriles were tentatively identified (see chapter 4.2.2, p24). Based on MS data and UV spectra, the most promising compound in the fraction appears to be ascorbigen (see Figure 24, p26). This compound is formed from glucobrassicin, has been described as a constituent of cabbage and is known for its anti-inflammatory properties (49, 68). Furthermore, MS data point to the presence of a glycosylated form of p-hydroxybenzaldehyde (see Figure 22, p25). The glucoside of p-hydroxybenzaldehyde has not yet been reported as a cabbage constituent up to now, but its presence is plausible, since “the aglycone” p-hydroxybenzaldehyde has already been identified in cabbage (69, 70). Other present compounds are thiocyanates and nitriles (see Figure 25 - Figure 28, p26). As previously mentioned, these substances are well-established constituents of cabbage and are also associated with antioxidative and anti-inflammatory effects (5, 18, 65, 67). Typically, they are formed through enzymatic hydrolysis of glucosinolates by myrosinase. However, it has also been reported that these breakdown products could possibly

be generated through the degradation of glucosinolates during mass spectrometry fragmentation. Specific fragments related to isothiocyanates can be formed during MS/MS experiments, even though complete isothiocyanates are primarily generated enzymatically or chemically before MS analysis. Therefore, the observed peaks at 113 g/mol (see Table 13) might result from a fragmentation of glucosinolates rather than from intact isothiocyanates (71). Furan fatty acids may also be present in the fraction (see Figure 23, p25). These fatty acids show anti-inflammatory and antioxidative effects and are known constituents of white cabbage (72-74). Moreover, the UV spectrum shows a maximum in the range of 210–240 nm, which is typical for aromatic compounds (46). In summary, all the above-mentioned substances could occur in the fraction BraOleD15 (see chapter 3.1.2, p5). All these substances also possess anti-inflammatory or antioxidant properties and, therefore, could have a positive effect on wound healing (49, 67, 70, 73). In terms of NF-κB inhibition, BraOleD40 (see chapter 3.1.2, p5) exhibited effects comparable to those of BraOleD15 (see chapter 3.1.2, p5) (22). This observation is supported by MS data, which suggest that BraOleD40 may also contain similar compounds, including furan fatty acids, thiocyanates, and nitriles. In addition, fatty acids with hydroperoxide functionalities or 1,2-disinapoylglucose may be present in the fraction (see chapter 4.2.3, p27). The presence of 1,2-disinapoylglucose (see Figure 31, p29) appears plausible, as both the UV spectrum and MS data support this assumption. Moreover, when looking at the MS data, a peak corresponding to the mass of sinapinic acid was observed, which could indicate the fragmentation of 2-disinapoylglucose by MS. So, it may be possible that a glycosylated variant of sinapic acid could occur in BraOleD40 (see chapter 3.1.2, p5), particularly since sinapic acid has been identified as a constituent of cabbage (19). Additionally, cabbage is known to contain fatty acids such as linoleic acid (75). Although linoleic acid itself was not detected in this extract, it cannot be excluded that the fatty acids present include hydroperoxide derivatives. Such hydroperoxide fatty acids are typically formed via lipoxygenase activity as part of the plant's defense response (75-77). When considering the possible constituents of BraOleD40 (see chapter 3.1.2, p5), three of the four above mentioned substances exhibit antioxidant and anti-inflammatory properties, and could benefit wound healing (19, 67, 73). BraOleD70 (see chapter 3.1.2, p5), which exhibited effects related to Nrf2 activation (22), may again contain 1,2-disinapoylglucose, as strongly supported by MS and UV

spectral data (see chapter 4.2.4, p30). Additional possible constituents include 3-feruloylquinic acid, CIF2, methoxybrassinin, and a fatty acid methyl ester (see chapter 4.2.4, p30). The presence of 3-feruloylquinic acid appears particularly likely, as evidenced by comparison with pure substances after hydrolysis (see Figure 33, p31). CIF2 (see Figure 15, p20) is a compound involved in the interaction between the cabbage and insects. This substance helps the cabbage the root fly selecting *Brassica* plants as suitable spots for egg-laying (36, 37). Since there is no information about this substance's wound-healing properties, it will not be discussed further. In contrast to CIF2, methoxybrassinin (see Figure 36, p33) possesses antimicrobial properties and may positively contribute to wound healing (78, 79). This compound has already been described as a constituent of white cabbage (80). Furthermore, a fatty acid methyl ester (see Figure 37 and Figure 38, p33) could be considered as a possible substance inside BraOLeD70 (see chapter 3.1.2, p5). This is strengthened by the fact that cabbage contains fatty acids such as α-linolenic acid (75). Although α-linolenic acid itself was not detected, it is possible that methyl ester derivatives of such fatty acids are present in the fraction. In summary, among the four discussed constituents in BraOleD70 (see chapter 3.1.2, p5), three exhibit antioxidative, anti-inflammatory, or antimicrobial activities, and could therefore contribute positively to wound healing (19, 78, 79). Fraction 3 from the aqueous extract (see chapter 3.1.1, p5) was selected for further analysis, as TLC results indicated that this fraction contains the highest number of yet unidentified compounds (see Figure 5, p15). In the case of BraOleWFC3, again CIF2 could be present (see Figure 15, p20). However, since no information is available regarding the potential role of this compound in wound healing, it will not be discussed further. In contrast, triterpenes, cinnamic acids, and derivatives of vanillic acid (see Table 12, p18), that may be present in this fraction are known to exhibit antioxidative or anti-inflammatory properties, and could therefore positively contribute to wound healing (19, 81, 82). Oleanonic acid (see Figure 10, p19) is one such triterpene that might be present in BraOleWFC3 (see chapter 3.1.1, p5). Additionally, triterpenes such as α-amyrin, β-amyrin, and lupeol have been identified in the epicuticular wax of cabbage. According to the literature, the presence of other triterpenes such as oleanonic or ursolic aldehydes also cannot be ruled out (83). Particularly promising substances may include vanillic acid derivatives (see Figure 16 and Figure 17, p21), especially since such compounds have already been reported in cabbage (81).

Furthermore, hydroxycinnamic acids are also well-established constituents of cabbage (19).

Considering all four fractions, several of the compounds potentially present exhibit antioxidative, anti-inflammatory, or antimicrobial activities. These bioactivities are all highly relevant to wound healing and support the assumption that cabbage extracts may contribute positively to this process (5, 8, 17). The most promising substances could be allyl isothiocyanate, 3-butenyl isothiocyanate (see chapter 4.3, p33), and 3-feruloylquinic acid (see chapter 4.2.4, p30) based on the comparison with pure substances. Other notable candidates are p-hydroxybenzaldehyde glucoside, ascorbigen, 1,2-disinapoylglucose, methoxybrassinin, various cinnamic acids (e.g., 2-acetoxycinnamic acid, 3-acetoxycinnamic acid, and 4-acetoxycinnamic acid), as well as vanillic acid derivatives (e.g., vanillic acid 4-O-β-D-glucopyranoside and vanillic acid 1-O-β-D-glucopyranoside) (see chapters 4.1.2, 4.2.2, 4.2.3, and 4.2.4). However, these compounds still require isolation and structural elucidation, or confirmation via comparison with standards in order to provide clear evidence of their occurrence, which could be addressed in future studies.

Table 18: Overview of the most promising substances identified in the analyzed extract fractions, including the corresponding fraction and whether comparison with pure substances was performed (see chapters 4.1.2, 4.2.2, 4.2.3, 4.2.4, and 4.3).

Substance	**Fraction**	**Compared with pure substances**
Allyl isothiocyanate	Fresh DCM extract	yes
3-Butenyl isothiocyanate	Fresh DMC extract	yes
4-(Methylthio)-butanenitrile	Fresh DMC extract	no
Vanillic acid derivates	BraOleWFC3	no
Cinnamic acids	BraOleWFC3	no
p-Hydroxybenzaldehyde glucoside	BraOleD15	no
Ascorbigen	BraOleD15	no
1,2-Disinapoylglucose	BraOleD40, BraOleD70	no
3-Feruloylquinic acid	BraOleD70	yes (after hydrolysis)
Methoxybrassinin	BraOleD70	no

Noteworthy, sinapic acid and ferulic acid are frequently reported in cabbage. However, in this master thesis, the sinapic acid and ferulic acid identified were bound to glucose (1,2-disinapoylglucose) or quinic acid (3-feruloylquinic acid), which is rarely mentioned in literature (19). This suggests that different extraction

agents, possibly involving acids, may have been used in some of the cited studies. Such extraction methods could facilitate the separation of glucose during the extraction process. Therefore, it is recommended that future studies explore the use of alternative extraction agents, for example, those supplemented with acids. Furthermore, given the high chemical diversity associated with cabbage constituents, the use of high-resolution mass spectrometry techniques such as Q-TOF is suggested. This could help reduce the large number of hits in database comparisons and improve the precision of compound identification. Although several substances with antioxidative and anti-inflammatory properties were identified via comparison with pure reference compounds, further work is required to isolate and characterize the active constituents responsible for the wound-healing effects of cabbage.

6 Abstract

White cabbage has been cultivated worldwide for centuries. Because of its global occurrence, it is not surprising that cabbage plays an important role in traditional medicine, for example, in wound treatment. Although cabbage has been cultivated for a long time, more information is needed about all its constituents and their effects on wound healing.

This work aimed to fractionate and analyze the aqueous cabbage extract using flash chromatography. The second aim was to analyze the already fractionated dichloromethane extract based on the results of the bioactivity tests. The third aim was to prepare fresh dichloromethane extract for the analysis of volatile components via GC-MS.

After optimizing the settings for flash chromatography and carrying out several runs, four fractions were obtained from the aqueous extract. One of them was selected for further analysis. Following the bioactivity test results, three dichloromethane extract fractions were chosen for further phytochemical examination. When comparing these fractions with pure substances by using HPLC and TLC, no matches were found. Additionally, MS analysis was carried out, which allowed further suggestions regarding the constituents present in the fractions. Hits suggested by the databases NIST®, CAS SciFinder®, and MS-DIAL® included p-hydroxybenzaldehyde glucoside, ascorbigen, 1,2-disinapoylglucose, 4-(methylthio)-butanenitrile, cinnamic acid-, and vanillic acid-derivatives. Unfortunately, none of these constituents were confirmed by comparison with reference substances due to their unavailability. However, 3-feruloylquinic acid, allyl isothiocyanate, and 3-butenyl isothiocyanate were identified by co-chromatography with reference compounds.

7 Zusammenfassung

Weißkohl wird seit Jahrhunderten weltweit kultiviert. Aufgrund seiner weiten Verbreitung ist es nicht überraschend, dass er eine bedeutende Rolle in der traditionellen Medizin einnimmt. So wird Weißkohl beispielsweise zur Unterstützung der Wundheilung eingesetzt. Trotz des langjährigen medizinischen Gebrauchs sind weiterführende Untersuchungen zu den Inhaltsstoffen und deren Wirkung auf den Heilungsprozess erforderlich.

Ziel dieser Masterarbeit war es, den wässrigen Kohl-Extrakt mittels Flash-Chromatographie aufzutrennen und die erhaltenen Fraktionen zu analysieren. Zusätzlich sollten die bereits vorhandenen Dichlormethan-Fraktionen, nach Erhalt der Bioaktivitätsergebnisse, einer vertieften Analyse unterzogen werden. Ein weiteres Ziel bestand in der Herstellung von frischen Dichlormethan-Extrakten zur Analyse flüchtiger Komponenten.

Mehrere Flash-Chromatographie Durchgänge und die Optimierung der Trennparameter lieferten vier Fraktionen des wässrigen Extraktes, von denen die dritte Fraktion für eine weiterführende Analyse ausgewählt wurde. Basierend auf den Ergebnissen der Bioaktivitätstests wurden zudem drei Dichlormethan-Fraktionen für eine detaillierte phytochemische Analyse herangezogen.

Der Vergleich dieser Fraktionen mit Referenzsubstanzen mittels HPLC und DC ergab keine Übereinstimmungen. Die zur weiteren Charakterisierung durchgeführte massenspektrometrische Analyse lieferte jedoch Hinweise auf mögliche Inhaltsstoffe. Mithilfe der Datenbanken NIST®, CAS SciFinder® und MS-DIAL® konnten p-Hydroxybenzaldehyd Glucosid, Ascorbigen, 1,2-Disinapoylglucose, 4-(Methylthio)-butyronitril, Zimtsäure- und Vanillinsäure-Derivate vorläufig identifiziert werden. Aufgrund des Fehlens authentischer Referenzsubstanzen konnte das Vorliegen dieser Substanzen jedoch nicht bestätigt werden. Im Gegensatz dazu erfolgte die Identifizierung von 3-Feruloylchinasäure, Allylisothiocyanat und 3-Butenyl Isothiocyanat durch den Abgleich mit Referenzsubstanzen.

8 References

1. Wickett RR, Visscher MO. Structure and function of the epidermal barrier. American Journal of Infection Control. 2006;34(10):98-110.
2. Velnar T, Bailey T, Smrkolj V. The wound healing process: an overview of the cellular and molecular mechanisms. Journal of International Medical Research. 2009;37(5):1528-42.
3. Sorg H, Tilkorn DJ, Hager S, Hauser J, Mirastschijski U. Skin wound healing: an update on the current knowledge and concepts. European Surgical Research. 2017;58(1-2):81-94.
4. Shedoeva A, Leavesley D, Upton Z, Fan C. Wound healing and the use of medicinal plants. Evidence-Based Complementary and Alternative Medicine. 2019.
5. Šamec D, Pavlović I, Salopek-Sondi B. White cabbage (Brassica oleracea var. capitata f. alba): botanical, phytochemical and pharmacological overview. Phytochemistry Reviews. 2017;16:117-35.
6. Ştefan IMA, Ona AD. Cabbage (Brassica oleracea L.). overview of the health benefits and therapeutical uses. Hop and Medicinal Plants. 2020;28:150-69.
7. Ray LR, Alam MS, Junaid M, Ferdousy S, Akter R, Hosen S, et al. Brassica oleracea var. capitata f. alba: A Review on its Botany, Traditional uses, Phytochemistry and Pharmacological Activities. Mini Reviews in Medicinal Chemistry. 2021;21(16):2399-417.
8. Eichenauer E, Saukel J, Glasl S. VOLKSMED Database: A Source for Forgotten Wound Healing Plants in Austrian Folk Medicine. Planta Medica. 2023(89):1-14.
9. Droz C, Rilliot-Droz F, Rilliot-Droz F. Von den wunderbaren Heilwirkungen des Kohlblattes. 12 ed. Les Geneveys-sur-Coffrane Sudden Inspiration Verlag; 1971.
10. Gonçalves RV, Sarandy MM, da Matta SLP, Novaes RD, de Mello Pinto MV. Comparative study of the effects of laser photobiomodulation and extract of Brassica oleracea on skin wounds in wistar rats: a histomorphometric study. Pathology - Research and Practice. 2013;209(10):648-53.
11. Sarandy MM, Novaes RD, da Matta SLP, Mezencio JMdS, da Silva MB, Zanuncio JC, et al. Ointment of Brassica oleracea var. capitata matures the extracellular matrix in skin wounds of wistar rats. Evidence-Based Complementary and Alternative Medicine. 2015.
12. Miranda LL, Sarandy MM, Altoé LS, Bastos DSS, Melo FCSA, Novaes RD, et al. Antioxidant and Anti-Inflammatory Potential of Brassica oleracea Accelerates Third-Degree Burn Healing in Rats. Cosmetics. 2024;11(1):27.
13. Rebolla A, Arisawa EALS, Barja PR, Posso MBS, Carvalho CdS. Effect of Brassica oleracea in rats skin wound healing. Acta Cirúrgica Brasileira. 2013;28(9):664-9.
14. Tanaka T, Horiuchi G, Matsuoka M, Hirano K, Tokumura A, Koike T, et al. Formation of lysophosphatidic acid, a wound-healing lipid, during digestion of cabbage leaves. Bioscience, Biotechnology, and Biochemistry. 2009;73(6):1293-300.
15. Samuelsen AB, Westereng B, Yousif O, Holtekjølen AK, Michaelsen TE, Knutsen SH. Structural features and complement-fixing activity of pectin from three Brassica oleracea varieties: white cabbage, kale, and red kale. Biomacromolecules. 2007;8(2):644-9.

16. Westereng B, Yousif O, Michaelsen TE, Knutsen SH, Samuelsen AB. Pectin isolated from white cabbage--structure and complement-fixing activity. Molecular Nutrition & Food Research. 2006;50(8):746-55.
17. Comino-Sanz IM, López-Franco MD, Castro B, Pancorbo-Hidalgo PL. The role of antioxidants on wound healing: A review of the current evidence. Journal of Clinical Medicine. 2021;10(16).
18. Zayed A, Sheashea M, Kassem IA, Farag MA. Red and white cabbages: An updated comparative review of bioactives, extraction methods, processing practices, and health benefits. Critical Reviews in Food Science and Nutrition. 2023;63(24):7025-42.
19. Park S, Arasu MV, Jiang N, Choi S-H, Lim YP, Park J-T, et al. Metabolite profiling of phenolics, anthocyanins and flavonols in cabbage (Brassica oleracea var. capitata). Industrial Crops and Products. 2014;60:8-14.
20. Zimmerl M. Herstellung von Dichlormethan-Extrakten aus Weisskohlblättern [Bachelorarbeit]: Universität Wien; 2023.
21. Haury M. Phytochemische Analyse von Weißkohlextrakten [Masterarbeit]: Universität Wien; 2024.
22. Eichenauer E. Traditional Austrian Herbal Medicines for Wound Healing - Analytics and Bioactivity [Doctoral Thesis]: University of Vienna; 2024.
23. Gey MH. Instrumentelle Analytik und Bioanalytik: Biosubstanzen, Trennmethoden, Strukturanalytik, Applikationen. 4 ed. Berlin, Heidelberg: Springer; 2021.
24. Swathi G, Srividya A, Ajitha A, Uma Maheswar Rao V. Review on: flash chromatography. World Journal of Pharmacy and Pharmaceutical Sciences. 2015;4(8):281-96.
25. GenTech. A Brief Overview Of PDA Detectors in HPLC 2023. accessed on 16.03.2024 [Available from: https://gentechscientific.com/brief-overview-of-pda-detectors-in-hplc/#:~:text=A%20common%20type%20of%20detector,they%20exit%20the%20HPLC%20column.
26. Bmcbride. What are Evaporative Light-Scattering Detectors? 2017. accessed on 16.03.2024 [Available from: https://www.peakscientific.com/discover/news/what-are-evaporative-light-scattering-detectors/#:~:text=ELSDs%20are%20aerosol%2Dbased%20HPLC,only%20the%20mobile%20phase%20evaporates.
27. Cebolla VL, Membrado L, Vela J, Ferrando AC. Evaporative light-scattering detection in the quantitative analysis of semivolatile polycyclic aromatic compounds by high-performance liquid chromatography. Journal of Chromatographic Science. 1997;35(4):141-50.
28. Vervoort N, Daemen D, Török G. Performance evaluation of evaporative light scattering detection and charged aerosol detection in reversed phase liquid chromatography. Journal of Chromatography A. 2008;1189:92-100.
29. Mageney V, Neugart S, Albach DC. A guide to the variability of flavonoids in Brassica oleracea. Molecules. 2017;22(2):252.
30. Society AC. AS Registry Number: 508-02-1 2024. accessed on 12.08.2024 [Available from: https://scifinder-n-cas-org.uaccess.univie.ac.at/searchDetail/substance/66bb1fb8a217821612b267f0/substanceDetails.
31. Society AC. CAS Registry Number: 77-52-1 2024. accessed on 12.08.2024 [Available from: https://scifinder-n-cas-

org.uaccess.univie.ac.at/searchDetail/substance/66bb1fbca217821612b2687d/substanceDetails.
32. Society AC. CAS Registry Number: 15486-19-8 2024. accessed on 10.08.2024 [Available from: https://scifinder-n-cas-org.uaccess.univie.ac.at/searchDetail/substance/66b8a030fc2c2c06827fe7ca/substanceDetails.
33. Society AC. CAS Registry Number: 20375-42-2 2024. accessed on 10.08.2024 [Available from: https://scifinder-n-cas-org.uaccess.univie.ac.at/searchDetail/substance/66b36a14584bd85018130a98/substanceDetails.
34. Society AC. CAS Registry Number: 55620-18-3 2024. accessed on 10.08.2024 [Available from: https://scifinder-n-cas-org.uaccess.univie.ac.at/searchDetail/substance/66b8a02efc2c2c06827fe7bd/substanceDetails.
35. Society AC. CAS Registry Number: 238757-91-0 2024. accessed on 11.08.2024 [Available from: https://scifinder-n-cas-org.uaccess.univie.ac.at/searchDetail/substance/66b9cb2efdc9142729e9eac9/substanceDetails.
36. Hurter J, Ramp T, Patrian B, Städler E, Roessingh P, Baur R, et al. Oviposition stimulants for the cabbage root fly: isolation from cabbage leaves. Phytochemistry. 1999;51(3):377-82.
37. de Jong R, Maher N, Patrian B, Städler E, Winkler T. Rutabaga roots, a rich source of oviposition stimulants for the cabbage root fly. Chemoecology. 2000;10:205-9.
38. Society AC. CAS Registry Number: 32142-31-7 2024. accessed on 10.08.2024 [Available from: https://scifinder-n-cas-org.uaccess.univie.ac.at/searchDetail/substance/66b8a52dfc2c2c06828009a4/substanceDetails.
39. Society AC. CAS Registry Number: 68985-14-8 2024. accessed on 10.08.2024 [Available from: https://scifinder-n-cas-org.uaccess.univie.ac.at/searchDetail/substance/66b8a540fc2c2c06828009f4/substanceDetails.
40. Süntar I, Çetinkaya S, Panieri E, Saha S, Buttari B, Profumo E, et al. Regulatory role of Nrf2 signaling pathway in wound healing process. Molecules. 2021;26(9).
41. Victor P, Sarada D, Ramkumar KM. Pharmacological activation of Nrf2 promotes wound healing. European Journal of Pharmacology. 2020;886.
42. Park YR, Sultan MT, Park HJ, Lee JM, Ju HW, Lee OJ, et al. NF-κB signaling is key in the wound healing processes of silk fibroin. Acta Biomaterialia. 2018;67:183-95.
43. Ambrozova N, Ulrichova J, Galandakova A. Models for the study of skin wound healing. The role of Nrf2 and NF-κB. Biomedical Papers of the Medical Faculty of Palacky University in Olomouc. 2017;161(1).
44. Society AC. CAS Registry Number: 480-44-4 2024. accessed on 21.06.2024 [Available from: https://scifinder-n-cas-org.uaccess.univie.ac.at/searchDetail/substance/66757ffda0417771baf092f0/substanceDetails.
45. Society AC. CAS Registry Number: 26993-16-8 2024. accessed on 09.08.2024 [Available from: https://scifinder-n-cas-

org.uaccess.univie.ac.at/searchDetail/substance/66b1c91d8c19d02a0db8fddf/substanceDetails.
46. McMurry J. Spectroscopy of Aromatic Compounds accessed on 10.08.2024 [Available from: https://chem.libretexts.org/Bookshelves/Organic_Chemistry/Organic_Chemistry_(OpenStax)/15%3A_Benzene_and_Aromaticity/15.08%3A_Spectroscopy_of_Aromatic_Compounds.
47. Society AC. CAS Registry Number: 121434-55-7 2024. accessed on 10.08.2024 [Available from: https://scifinder-n-cas-org.uaccess.univie.ac.at/searchDetail/substance/66b7207487c519727a6043a5/substanceDetails.
48. Society AC. CAS Registry Number: 8075-98-7 2024. accessed on 10.08.2024 [Available from: https://scifinder-n-cas-org.uaccess.univie.ac.at/searchDetail/substance/66d7024e80979a348dd978a1/substanceDetails.
49. Wagner AE, Rimbach G. Ascorbigen: chemistry, occurrence, and biologic properties. Clinics in Dermatology. 2009;27(2):217-24.
50. Li Z, Wei X, Li L, Liu Y, Fang Z, Yang L, et al. Development of a simple method for determination of anti-cancer component of indole-3-carbinol in cabbage and broccoli. Journal of Food and Nutrition Research. 2017;5:642-8.
51. Society AC. CAS Registry Number: 2253-93-2 2024. accessed on 21.06.2024 [Available from: https://scifinder-n-cas-org.uaccess.univie.ac.at/searchDetail/substance/66b736c0d43b7c54f21b9d90/substanceDetails.
52. Society AC. CAS Registry Number: 3386-97-8 2024. accessed on 21.06.2024 [Available from: https://scifinder-n-cas-org.uaccess.univie.ac.at/searchDetail/substance/66b1ee1c8c19d02a0dbca34a/substanceDetails.
53. Society AC. CAS Registry Number: 36756-71-5 2024. accessed on 21.06.2024 [Available from: https://scifinder-n-cas-org.uaccess.univie.ac.at/searchDetail/substance/66b736bed43b7c54f21b9d70/substanceDetails.
54. Society AC. CAS Registry Number: 54096-45-6 2024. accessed on 21.06.2024 [Available from: https://scifinder-n-cas-org.uaccess.univie.ac.at/searchDetail/substance/66b73686d43b7c54f21b9b18/substanceDetails.
55. Society AC. CAS Registry Number: 67879-58-7 2024. accessed on 21.06.2024 [Available from: https://scifinder-n-cas-org.uaccess.univie.ac.at/searchDetail/substance/667580f6a0417771baf0a544/substanceDetails.
56. Society AC. CAS Registry Number: 23017-93-8 2024. accessed on 12.08.2024 [Available from: https://scifinder-n-cas-org.uaccess.univie.ac.at/searchDetail/substance/66bb10d2a217821612b0d553/substanceDetails.
57. Society AC. CAS Registry Number: 33964-75-9 2024. accessed on 12.08.2024 [Available from: https://scifinder-n-cas-org.uaccess.univie.ac.at/searchDetail/substance/66bb10dba217821612b0d619/substanceDetails.
58. Society AC. CAS Registry Number: 91095-79-3 2024. accessed on 11.08.2024 [Available from: https://scifinder-n-cas-

org.uaccess.univie.ac.at/searchDetail/substance/66b86eaedeca172a6d09cb6e/substanceDetails.
59. Society AC. CAS Registry Number: 530-59-6 2024. accessed on 10.08.2024 [Available from: https://scifinder-n-cas-org.uaccess.univie.ac.at/searchDetail/substance/66b872a9deca172a6d09e775/substanceDetails.
60. Society AC. CAS Registry Number: 1899-29-2 2024. accessed on 21.06.2024 [Available from: https://scifinder-n-cas-org.uaccess.univie.ac.at/searchDetail/substance/6672a253fd4ce818093a617a/substanceDetails.
61. Society AC. CAS Registry Number: 105748-60-5 2024. accessed on 10.08.2024 [Available from: https://scifinder-n-cas-org.uaccess.univie.ac.at/searchDetail/substance/66b87d9adeca172a6d0a2d3f/substanceDetails.
62. Society AC. CAS Registry Number: 301-00-8 2024. accessed on 11.08.2024 [Available from: https://scifinder-n-cas-org.uaccess.univie.ac.at/searchDetail/substance/66ba0b72fdc9142729ef39ab/substanceDetails.
63. Society AC. CAS Registry Number: 16326-32-2 2024. accessed on 11.08.2024 [Available from: https://scifinder-n-cas-org.uaccess.univie.ac.at/searchDetail/substance/66ba0b7ffdc9142729ef3b09/substanceDetails.
64. Yang Q, Cao W, Zhou X, Cao W, Xie Y, Wang S. Anti-thrombotic effects of α-linolenic acid isolated from Zanthoxylum bungeanum Maxim seeds. BMC Complementary and Alternative Medicine. 2014;14.
65. Wei S, Xiao X, Wei L, Li L, Li G, Liu F, et al. Development and comprehensive HS-SPME/GC–MS analysis optimization, comparison, and evaluation of different cabbage cultivars (Brassica oleracea L. var. capitata L.) volatile components. Food Chemistry. 2021;340.
66. Society AC. CAS Registry Number: 57-06-7 2025. accessed on 21.04.2025 [Available from: https://scifinder-n-cas-org.uaccess.univie.ac.at/searchDetail/substance/68060c5184d8ec263d326889/substanceDetails.
67. Chandler JD, Day BJ. Thiocyanate: a potentially useful therapeutic agent with host defense and antioxidant properties. Biochemical Pharmacology. 2012;84(11):1381-7.
68. Medtigo. ascorbigen 2025. accessed on 26.04.2025 [Available from: https://medtigo.com/drug/ascorbigen/#:~:text=Ascorbigen%20found%20in%20broccoli%20and%20related%20vegetables%2C,properties%20and%20is%20used%20in%20cancer%20treatment.
69. Wang Y, Liu W, Dong B, Wang D, Nian Y, Zhou H. Isolation and Identification of Herbicidal Active Compounds from Brassica oleracea L. and Exploration of the Binding Sites of Brassicanate A Sulfoxide. Plants. 2023;12(13).
70. Brito TBN, Lima LRS, Santos MCB, Moreira RFA, Cameron LC, Fai AEC, et al. Antimicrobial, antioxidant, volatile and phenolic profiles of cabbage-stalk and pineapple-crown flour revealed by GC-MS and UPLC-MSE. Food Chemistry. 2021;339:1-11.
71. Bianco G, Pascale R, Lelario F, Bufo SA, Cataldi TR. Investigation of glucosinolates by mass spectrometry. Glucosinolates. Cham Springer; 2017. p. 431-61.

72. Hannemann K, Puchta V, Simon E, Ziegler H, Ziegler G, Spiteller G. The common occurrence of furan fatty acids in plants. Lipids. 1989;24(4):296-8.
73. Coudray C, Durand E, Balas L, Sultan A, Casas F, Feillet-Coudray C. Potential favourable health effects of some dietary uncommon fatty acids. Oilseeds and fats, Crops and Lipids. 2021;28, 41.
74. Xu L, Sinclair AJ, Faiza M, Li D, Han X, Yin H, et al. Furan fatty acids–Beneficial or harmful to health? Progress in Lipid Research. 2017;68:119-37.
75. Žnidarčič D, Vidrih R. Content of essential fatty acids in cabbage (Brassica oleracea L.). Acta Agriculturae Slovenica. 2009;93(2):225-30
76. Zheng S-J, van Dijk JP, Bruinsma M, Dicke M. Sensitivity and speed of induced defense of cabbage (Brassica oleracea L.): dynamics of BoLOX expression patterns during insect and pathogen attack. Molecular Plant-Microbe Interactions. 2007;20(11).
77. Savchenko T, Zastrijnaja O, Klimov V. Oxylipins and plant abiotic stress resistance. Biochemistry (Moscow). 2014;79(4):362-75.
78. Budovská M, Krochtová K, Michalková R, Mojžiš J. Aminoanalogues of isobrassinin, erucalexin and isocyclobrassinin: Synthesis and evaluation of the antiproliferative and cytotoxic properties. Tetrahedron. 2022;120.
79. Pedras MSC, Minic Z, Sarma-Mamillapalle VK. Synthetic inhibitors of the fungal detoxifying enzyme brassinin oxidase based on the phytoalexin camalexin scaffold. Journal of Agricultural and Food Chemistry. 2009;57(6):2429-35.
80. Monde K, Sasaki K, Shirata A, Takasugi M. 4-Methoxybrassinin, a sulphur-containing phytoalexin from Brassica oleracea. Phytochemistry. 1990;29(5):1499-500.
81. Schmidtlein H, Herrmann K. On phenolic acids of vegetables: I. Hydroxycinnamic acids and hydroxybenzoic acids of Brassica-Species and leaves of other cruciferae. Zeitschrift für Lebensmittel-Untersuchung und Forschung. 1975;159:139-48.
82. Jasemi SV, Khazaei H, Morovati MR, Joshi T, Aneva IY, Farzaei MH, et al. Phytochemicals as treatment for allergic asthma: Therapeutic effects and mechanisms of action. Phytomedicine. 2024;122.
83. Martelanc M, Vovk I, Simonovska B. Determination of three major triterpenoids in epicuticular wax of cabbage (Brassica oleracea L.) by high-performance liquid chromatography with UV and mass spectrometric detection. Journal of Chromatography A. 2007;1164:145-52.

9 List of abbreviations

AITC	allyl isothiocyanate
3-BITC	3-butenyl isothiocyanate
C	cyanidin
CA	caffeic acid
DC	Dünnschichtchromatographie
DCM	dichloromethane
ELSD	evaporative light scattering detector
FA	ferulic acid
FC	flash chromatography
GC	gas chromatography
g/mol	grams per mol
K	kaempferol
LC-MS	liquid chromatography mass spectrometry
LPA	lysophosphatidic acid
mbar	millibars
mg	milligrams
mm	millimeters
MS	mass spectrometry
MeOH	methanol
m/z	mass to charge ratio
nm	nanometers
PA	phosphatidic acid
p-CA	p-coumaric acid
PDA	photodiode array detector
Q	quercetin
Q-TOF	quadrupole time of flight
RP	reverse phase
SA	sinapic acid
SPE	solid phase extraction
TOF	time of flight

10 Appendix

Solvent A : H2O	Solvent C :
Solvent B : MeOH	Solvent D :
Channel 1 : UV600:SIG1 ==> 254 nm	Channel 2 : UV600:SCAN ==> 200-600
Channel 3 : ELSD ==> 49°	
Equil+Inject Mode : Equil. (Simple) + Valve Inj. + Wait	Stop Mode : Pause
RUN Time : 3/13/2024 3:27:41 PM	

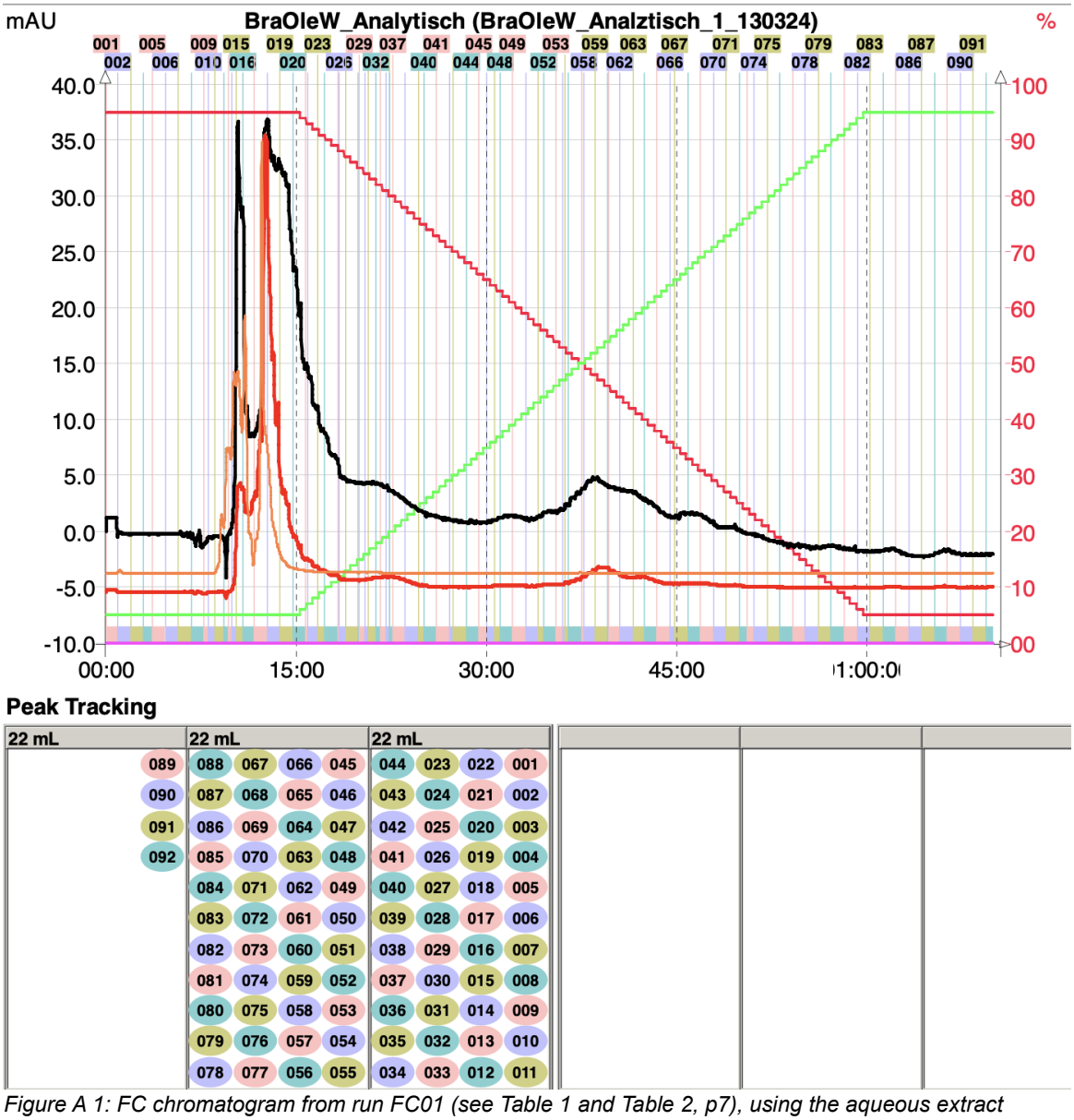

Figure A 1: FC chromatogram from run FC01 (see Table 1 and Table 2, p7), using the aqueous extract BraOleW1 (see chapter 3.1.1, p5)

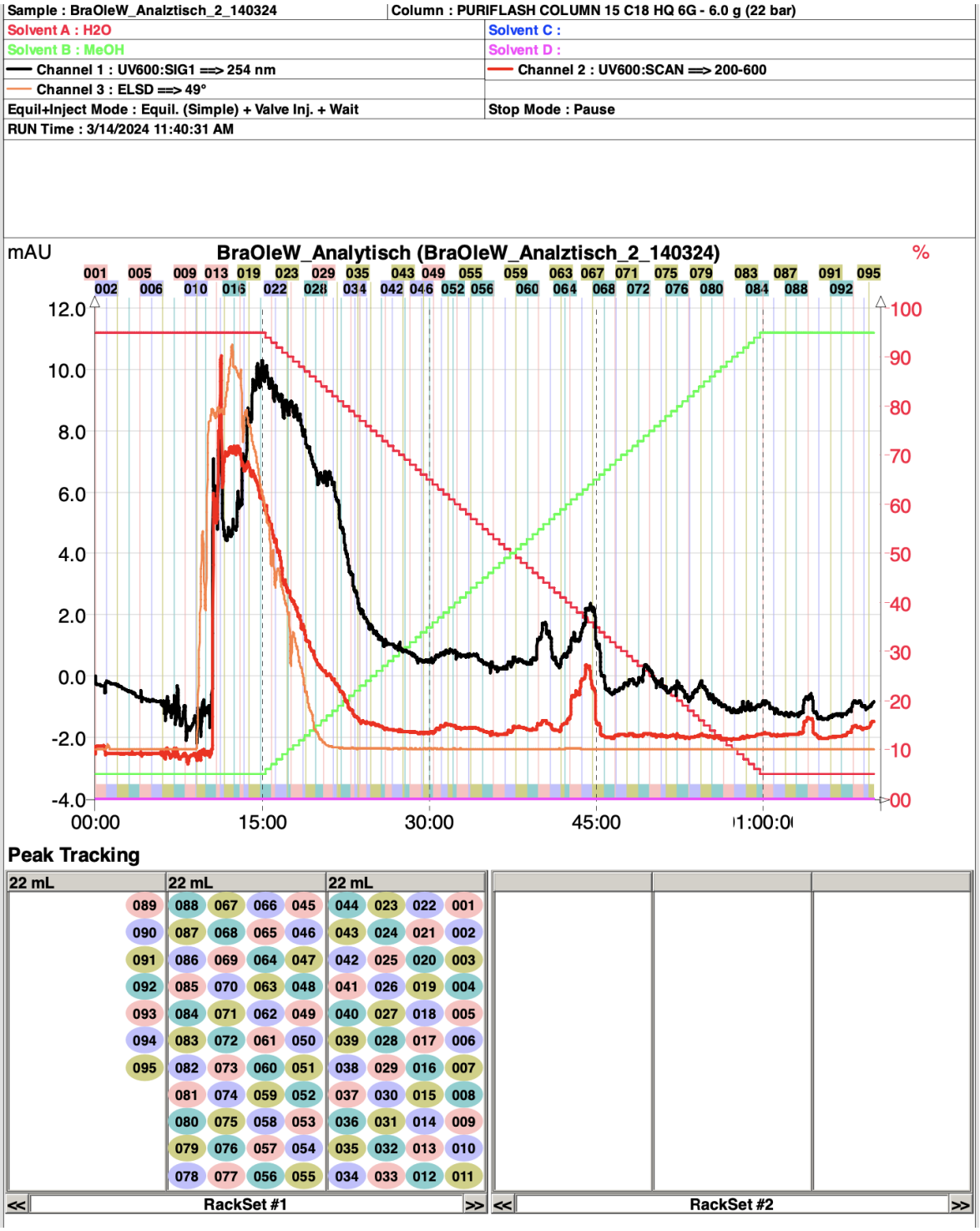

Figure A 2: FC chromatogram from run FC02 (see Table 1 and Table 2, p7), using the aqueous extract BraOleW1 (see chapter 3.1.1, p5)

The 95 various fractions were united into 6 fractions: fraction 1 = 001-020, fraction 2 = 021-042, fraction 3 = 043-059, fraction 4 = 060-064, fraction 5 = 065-070, fraction 6 = 071-095

Solvent A : H2O	Solvent C :
Solvent B : MeOH	Solvent D :
Channel 1 : UV600:SIG1 ==> 254 nm	Channel 2 : UV600:SCAN ==> 200-600
Channel 3 : ELSD ==> 49°	
Equil+Inject Mode : Equil. (Simple) + Valve Inj. + Wait	Stop Mode : Pause
RUN Time : 3/18/2024 11:07:04 AM	

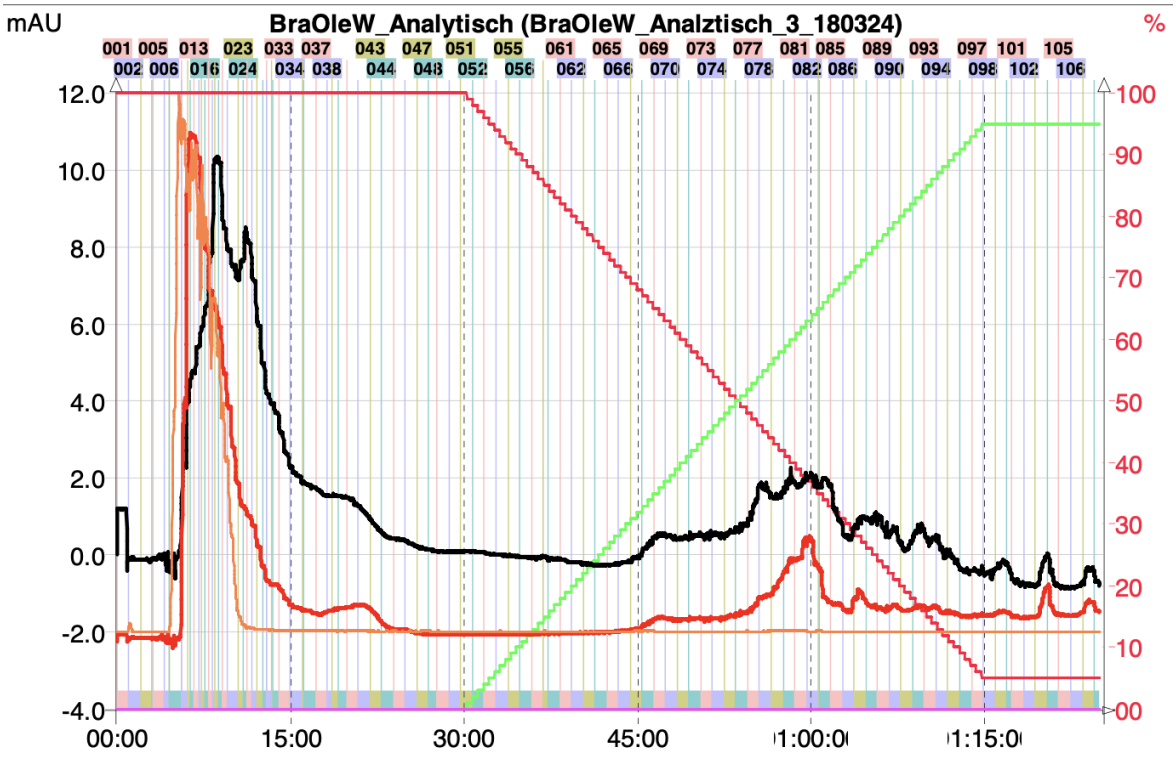

Peak Tracking

22 mL	22 mL	22 mL	
089	088 067 066 045	044 023 022 001	
090	087 068 065 046	043 024 021 002	
108 091	086 069 064 047	042 025 020 003	
107 092	085 070 063 048	041 026 019 004	
106 093	084 071 062 049	040 027 018 005	
105 094	083 072 061 050	039 028 017 006	
104 095	082 073 060 051	038 029 016 007	
103 096	081 074 059 052	037 030 015 008	
102 097	080 075 058 053	036 031 014 009	
101 098	079 076 057 054	035 032 013 010	
100 099	078 077 056 055	034 033 012 011	

Figure A 3: FC chromatogram from run FC03 (see Table 1 and Table 2, p7), using the aqueous extract BraOleW1 (see chapter 3.1.1, p5)

The 108 various fractions were united into 6 fractions: fraction 1 = 001-033, fraction 2 = 034-044, fraction 3 = 045-066, fraction 4 = 067-076, fraction 5 = 077-086, fraction 6 = 087-108

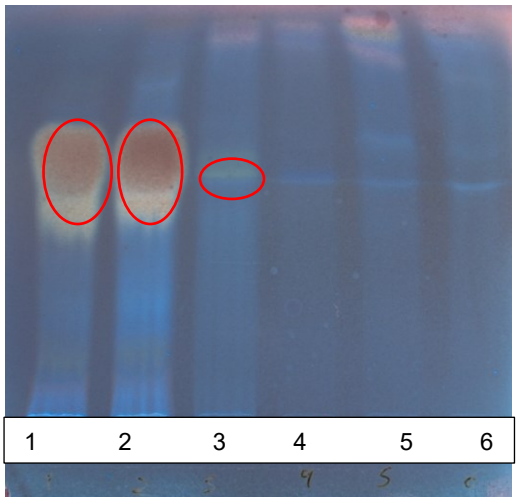

Figure A 4: TLC 1 (see Table 3, p8), analysis of the 6 fractions from run FC02 (see chapter 4.1.1, p14). Many sugars can still be found in fraction 1 and fraction 2, with a few sugars also present in fraction 3 (marked red). 366 nm, after derivatization.

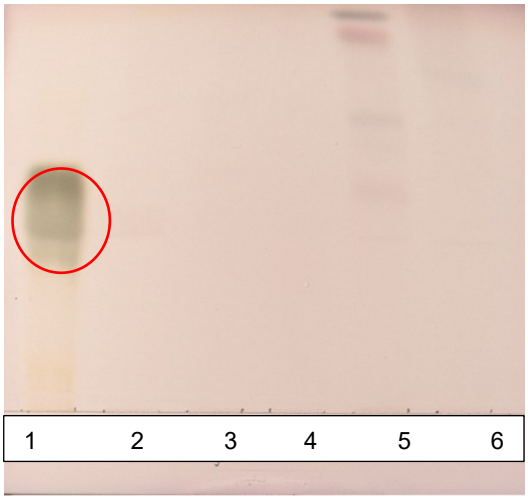

Figure A 5: TLC 2 (see Table 3, p8), analysis of the 6 fractions from run FC03 (see chapter 4.1.1, p14). Sugars can only be found in fraction 1 and are marked red. Natural light, after derivatization.

Figure A 6: TLC 3 (see Table 3, p8), analysis of the 6 fractions from run FC03 (see chapter 4.1.1, p14). Sugars can only be found in fraction 1 and are marked red. Natural light, after derivatization.

Solvent A : H2O	Solvent C :
Solvent B : MeOH	Solvent D :
Channel 1 : UV600:SIG1 ==> 254 nm	Channel 2 : UV600:SCAN ==> 200-600
Channel 3 : ELSD ==> 49°	
Equil+Inject Mode : Equil. (Simple) + Valve Inj. + Wait	Stop Mode : Pause
RUN Time : 3/22/2024 9:34:25 AM	

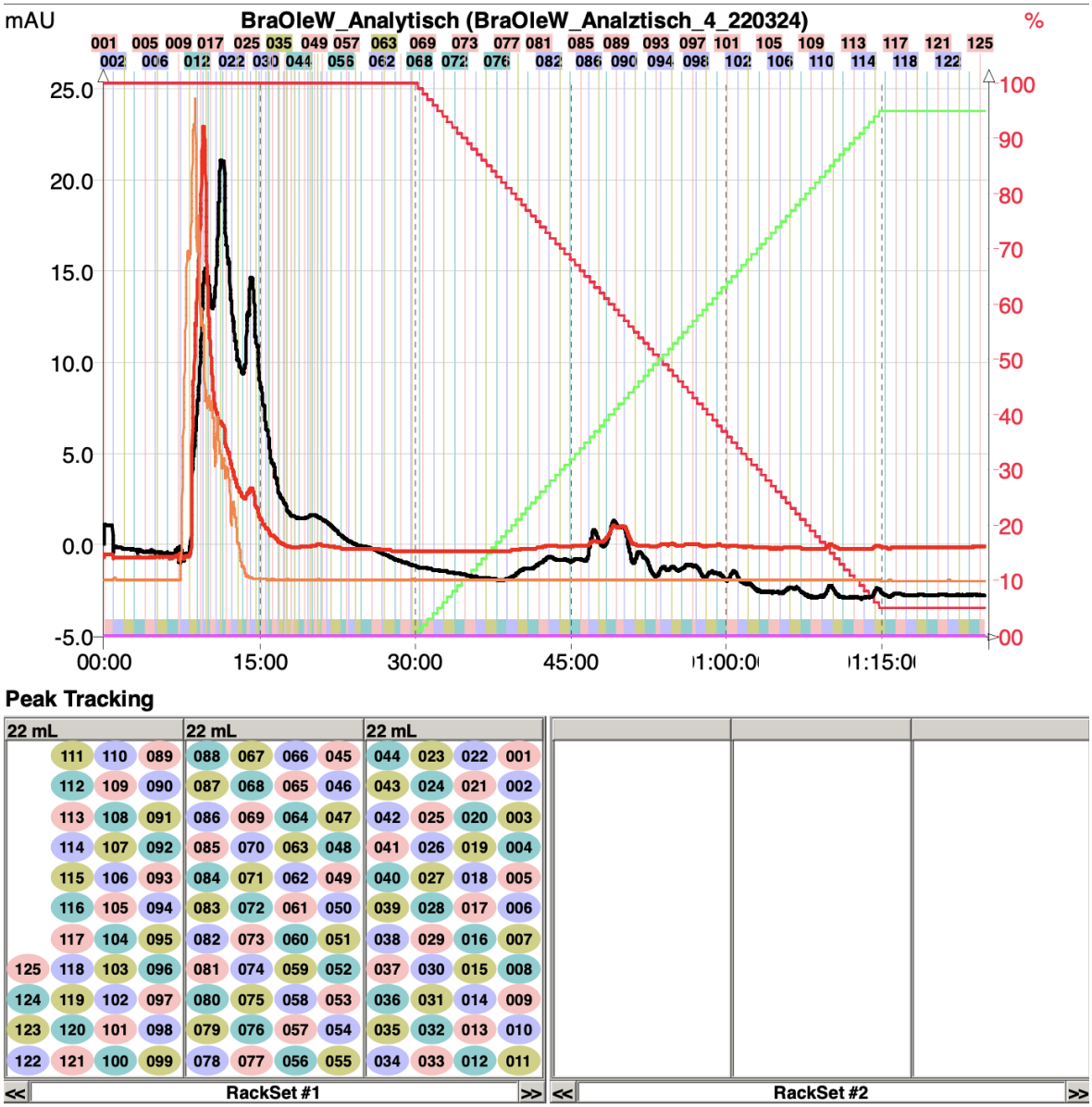

Figure A 7: FC chromatogram from run FC04 (see Table 1 and Table 2, p7), using the aqueous extract BraOleW1 (see chapter 3.1.1, p5)

The 125 various fractions were united into 4 fractions: fraction 1 = 001-039, fraction 2 = 040-084, fraction 3 = 085-108, fraction 4 = 109-125.

Solvent A : H2O	Solvent C :
Solvent B : MeOH	Solvent D :
Channel 1 : UV600:SIG1 ==> 254 nm	Channel 2 : UV600:SCAN ==> 200-600
Channel 3 : ELSD ==> 49°	
Equil+Inject Mode : Equil. (Simple) + Valve Inj. + Wait	Stop Mode : Pause
RUN Time : 3/22/2024 11:52:56 AM	

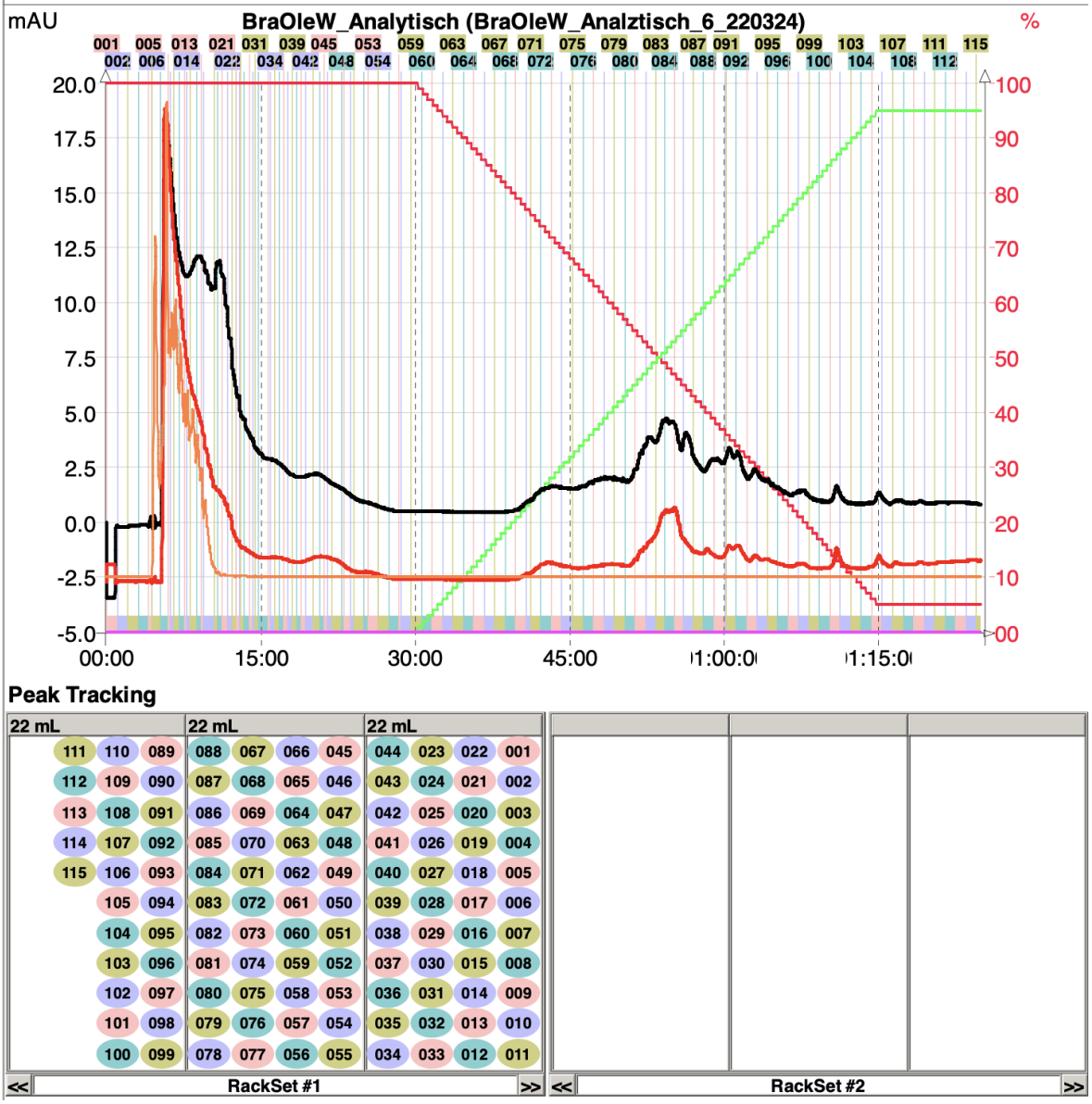

Figure A 8: FC chromatogram from run FC05 (see Table 1 and Table 2, p7), using the aqueous extract BraOleW1 (see chapter 3.1.1, p5)

The 115 various fractions were united into 4 fractions: fraction 1 = 001-039, fraction 2 = 040-079, fraction 3 = 080-099, fraction 4 = 100-115.

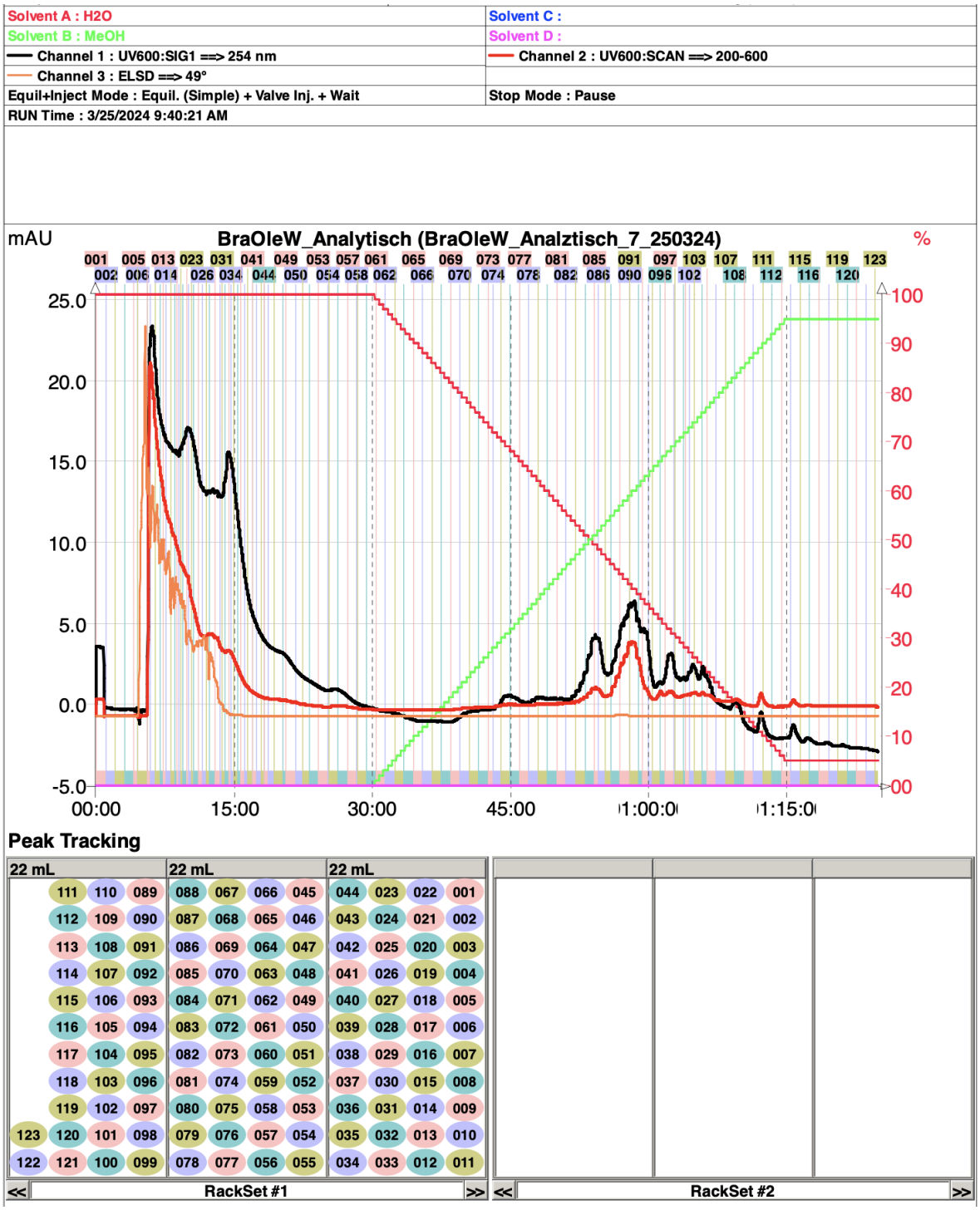

Figure A 9: FC chromatogram from run FC06 (see Table 1 and Table 2, p7), using the aqueous extract BraOleW1 (see chapter 3.1.1, p5)

The 123 various fractions were united into 4 fractions: fraction 1 = 001-047, fraction 2 = 048-080, fraction 3 = 081-109, fraction 4 = 110-123.

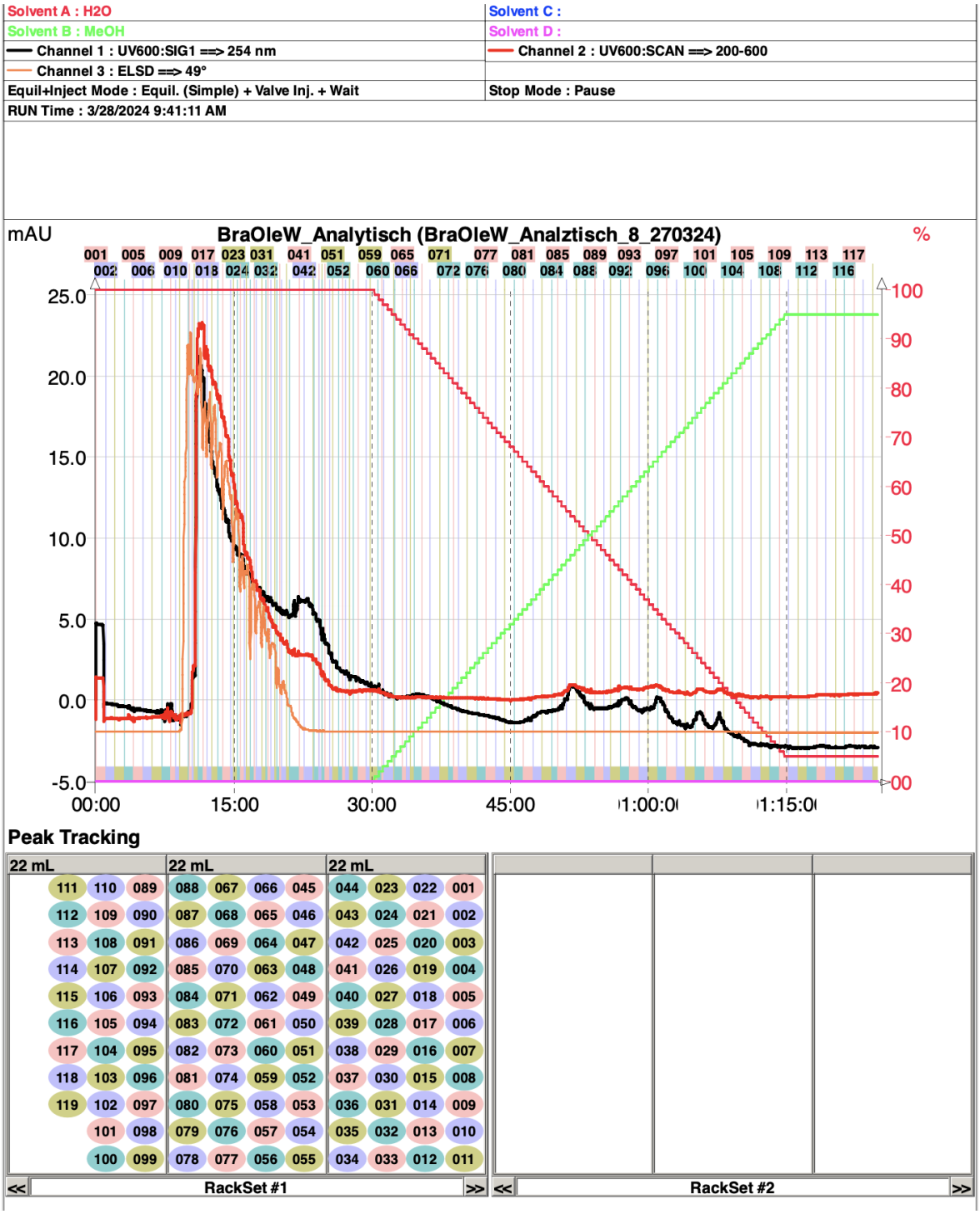

Figure A 10: FC chromatogram from run FC07 (see Table 1 and Table 2, p7), using the aqueous extract BraOleW2 (see chapter 3.1.1, p5)

The 119 various fractions were united into 4 fractions: fraction 1 = 001-047, fraction 2 = 048-080, fraction 3 = 081-109, fraction 4 = 110-119.

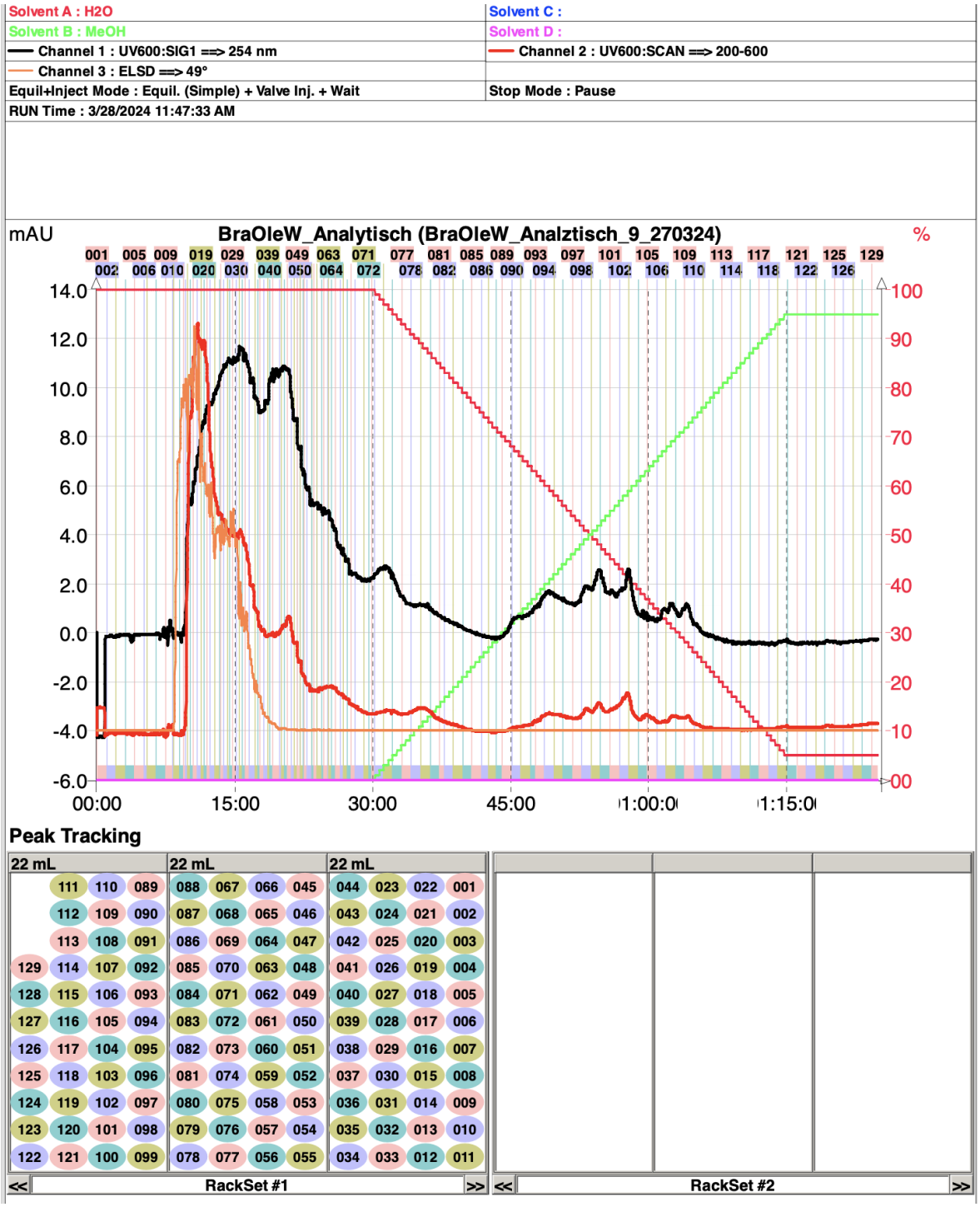

Figure A 11: FC chromatogram from run FC08 (see Table 1 and Table 2, p7), using the aqueous extract BraOleW2 (see chapter 3.1.1, p5)

The 129 various fractions were united into 4 fractions: fraction 1 = 001-047, fraction 2 = 048-090, fraction 3 = 091-112, fraction 4 = 113-129.

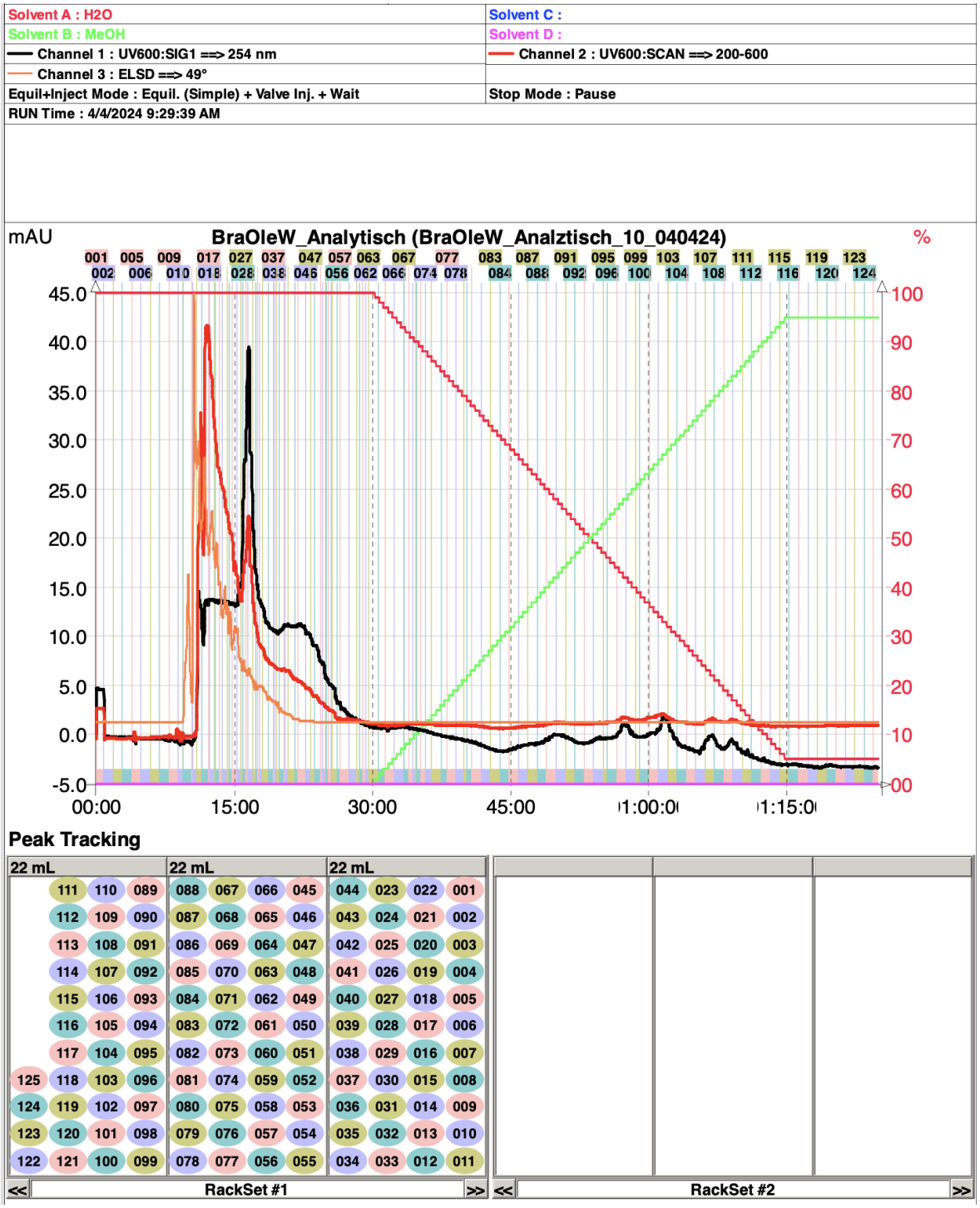

Figure A 12: FC chromatogram from run FC09 (see Table 1 and Table 2, p7), using the aqueous extract BraOleW2 (see chapter 3.1.1, p5)

The 125 various fractions were united into 4 fractions: fraction 1 = 001-039, fraction 2 = 040-092, fraction 3 = 093-111, fraction 4 = 112-125.

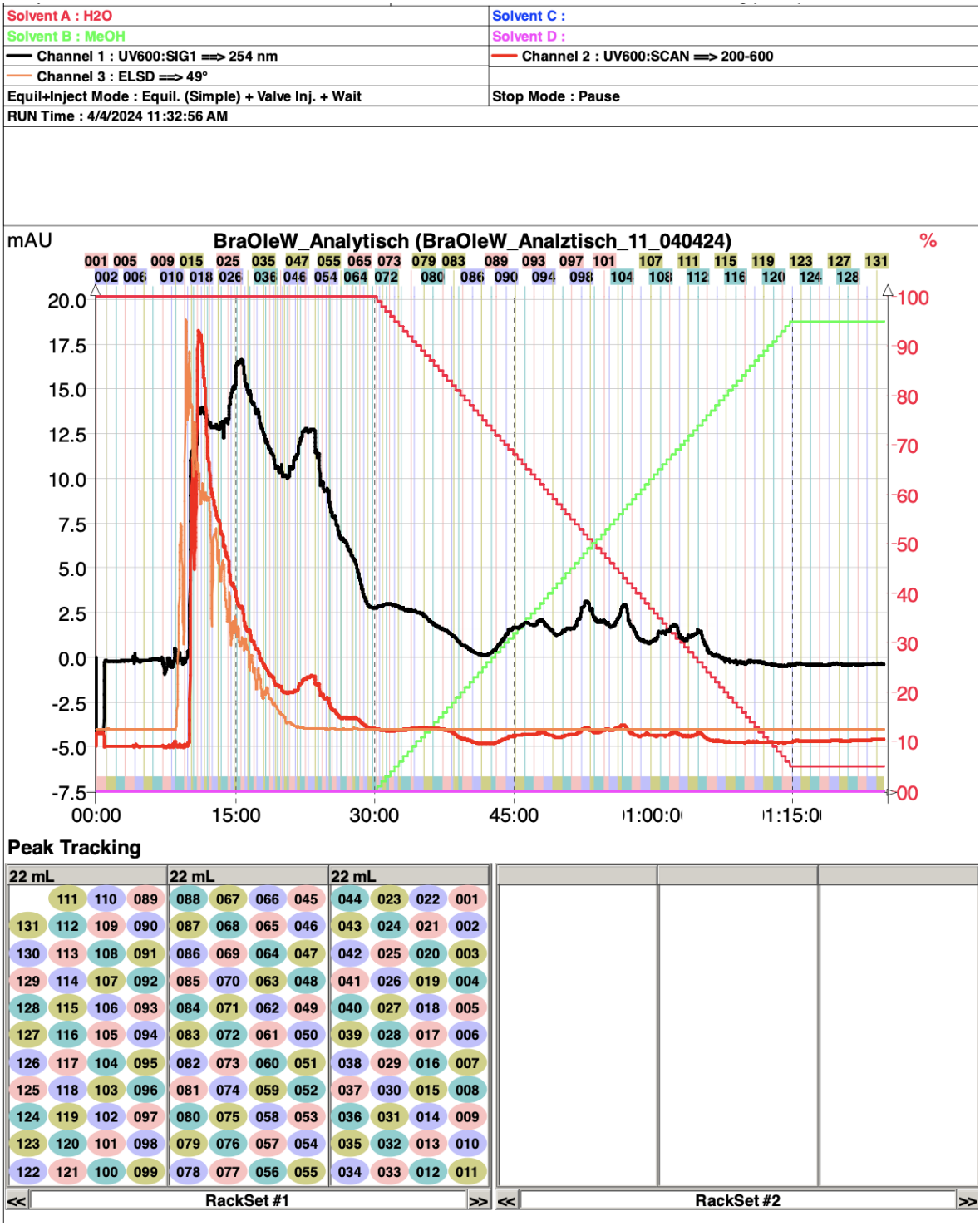

Figure A 13: FC chromatogram from run FC10 (see Table 1 and Table 2, p7), using the aqueous extract BraOleW2 (see chapter 3.1.1, p5)

The 131 various fractions were united into 4 fractions: fraction 1 = 001-068, fraction 2 = 069-095, fraction 3 = 096-115, fraction 4 = 116-131.

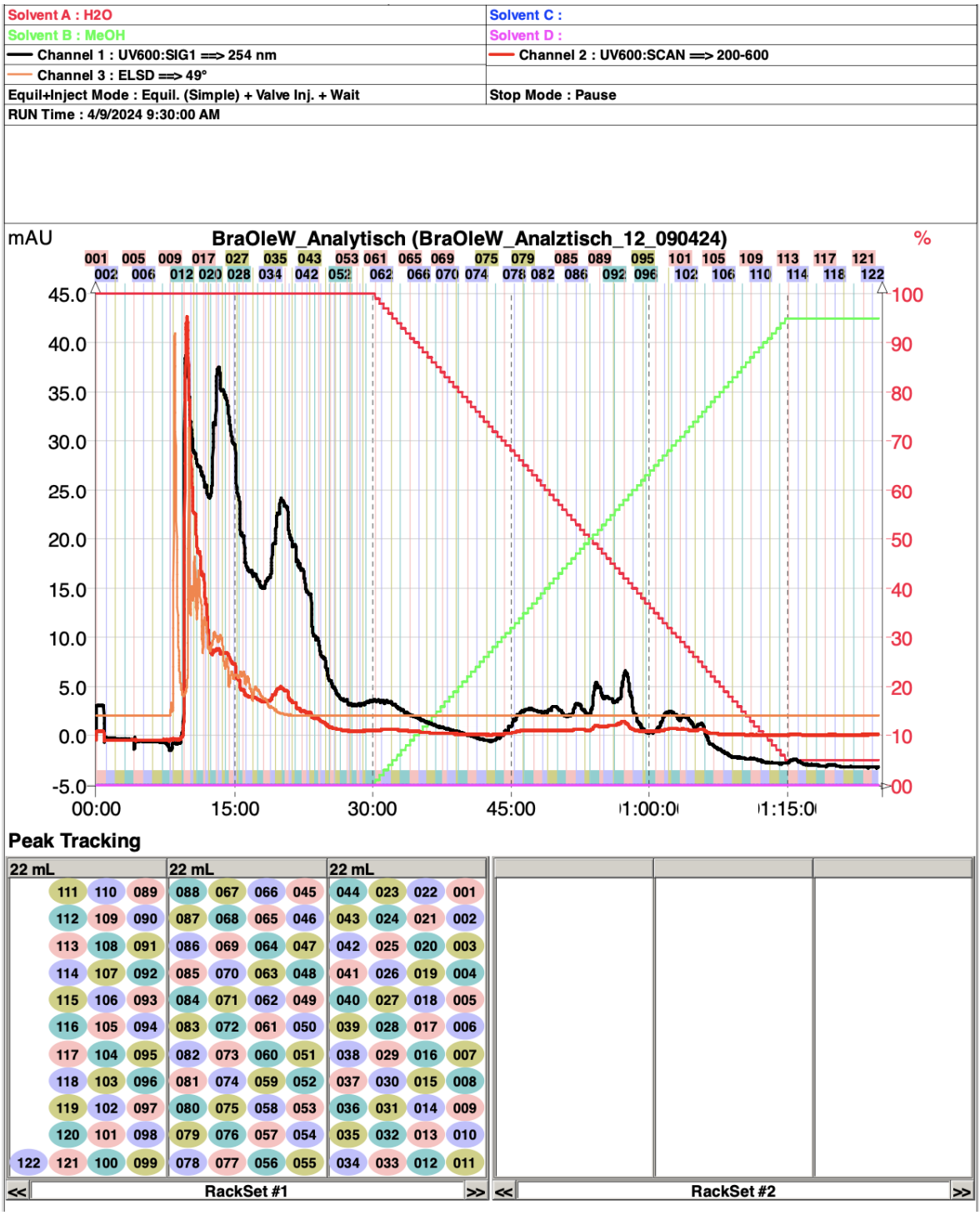

Figure A 14: FC chromatogram from run FC11 (see Table 1 and Table 2, p7), using the aqueous extract BraOleW2 (see chapter 3.1.1, p5)

The 122 various fractions were united into 4 fractions: fraction 1 = 001-056, fraction 2 = 057-086, fraction 3 = 087-105, fraction 4 = 106-122.

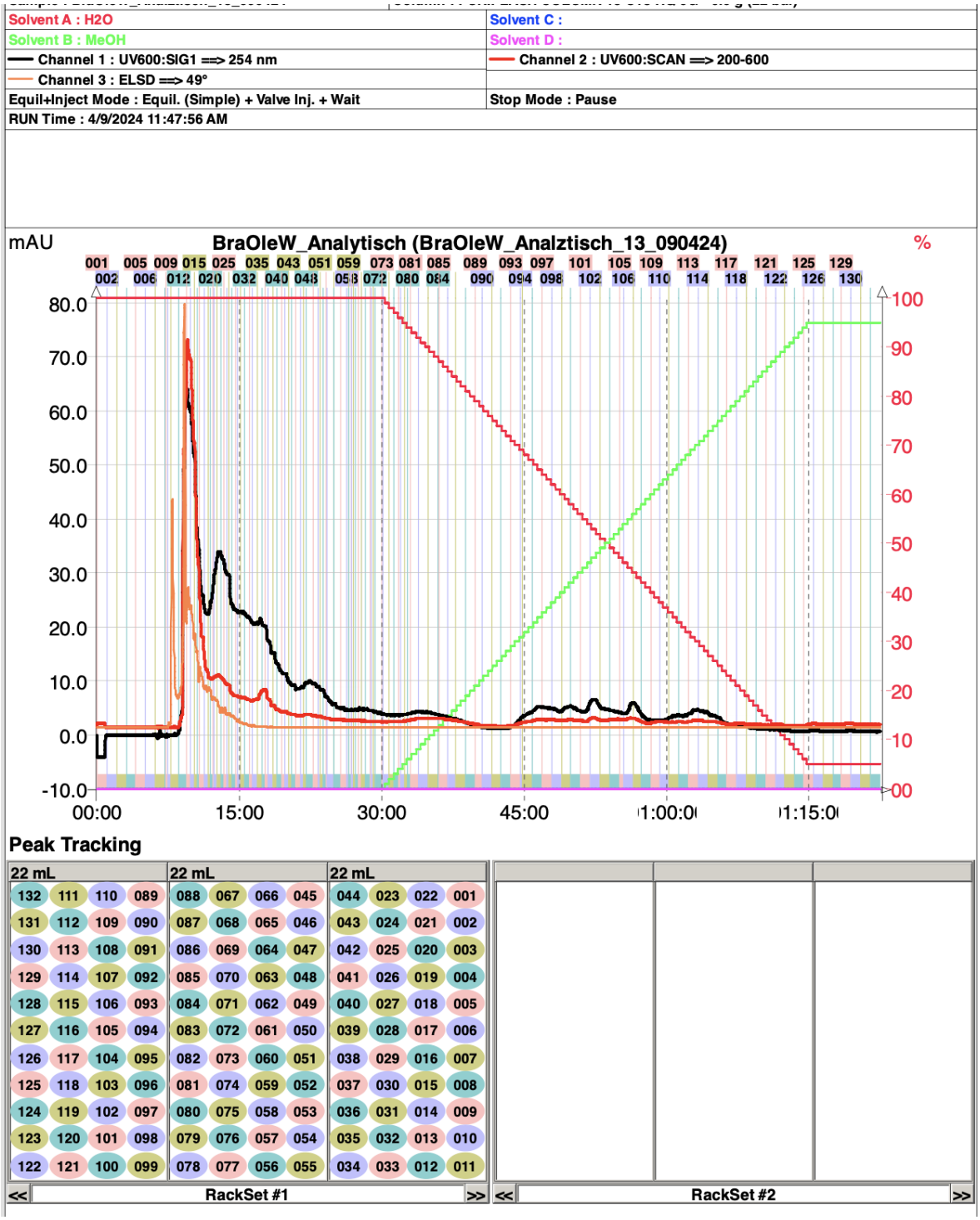

Figure A 15: FC chromatogram from run FC12 (see Table 1 and Table 2, p7), using the aqueous extract BraOleW2 (see chapter 3.1.1, p5)

The 132 various fractions were united into 4 fractions: fraction 1 = 001-073, fraction 2 = 074-100, fraction 3 = 101-117, fraction 4 = 118-132.

Solvent A : H2O	Solvent C :
Solvent B : MeOH	Solvent D :
Channel 1 : UV600:SIG1 ==> 254 nm	Channel 2 : UV600:SCAN ==> 200-600
Channel 3 : ELSD ==> 49°	
Equil+Inject Mode : Equil. (Simple) + Valve Inj. + Wait	Stop Mode : Pause
RUN Time : 4/12/2024 9:13:19 AM	

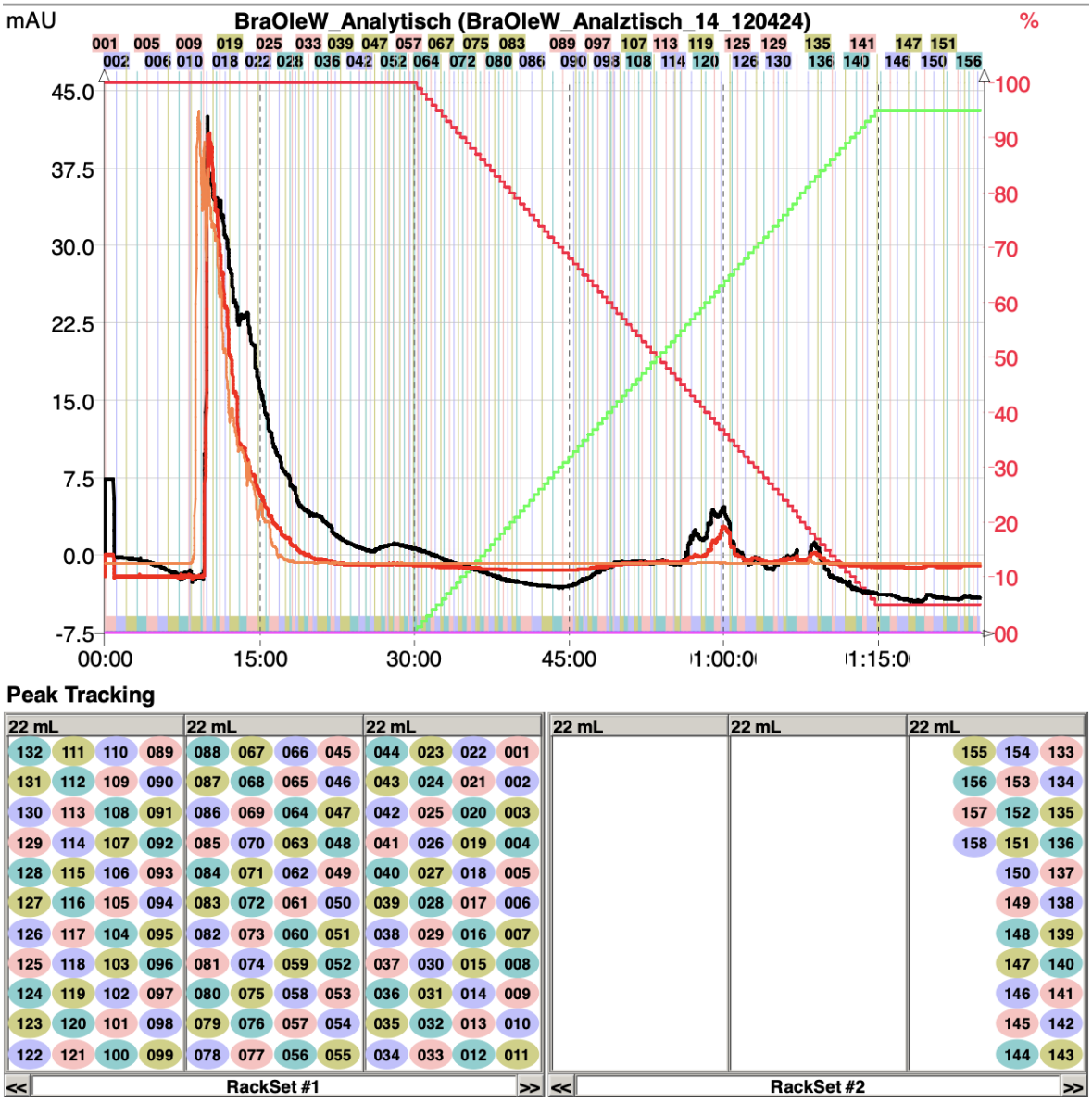

Figure A 16: FC chromatogram from run FC13 (see Table 1 and Table 2, p7), using the aqueous extract BraOleW3 (see chapter 3.1.1, p5).

The 158 various fractions were united into 4 fractions: fraction 1 = 001-051, fraction 2 = 052-116, fraction 3 = 117-143, fraction 4 = 144-158.

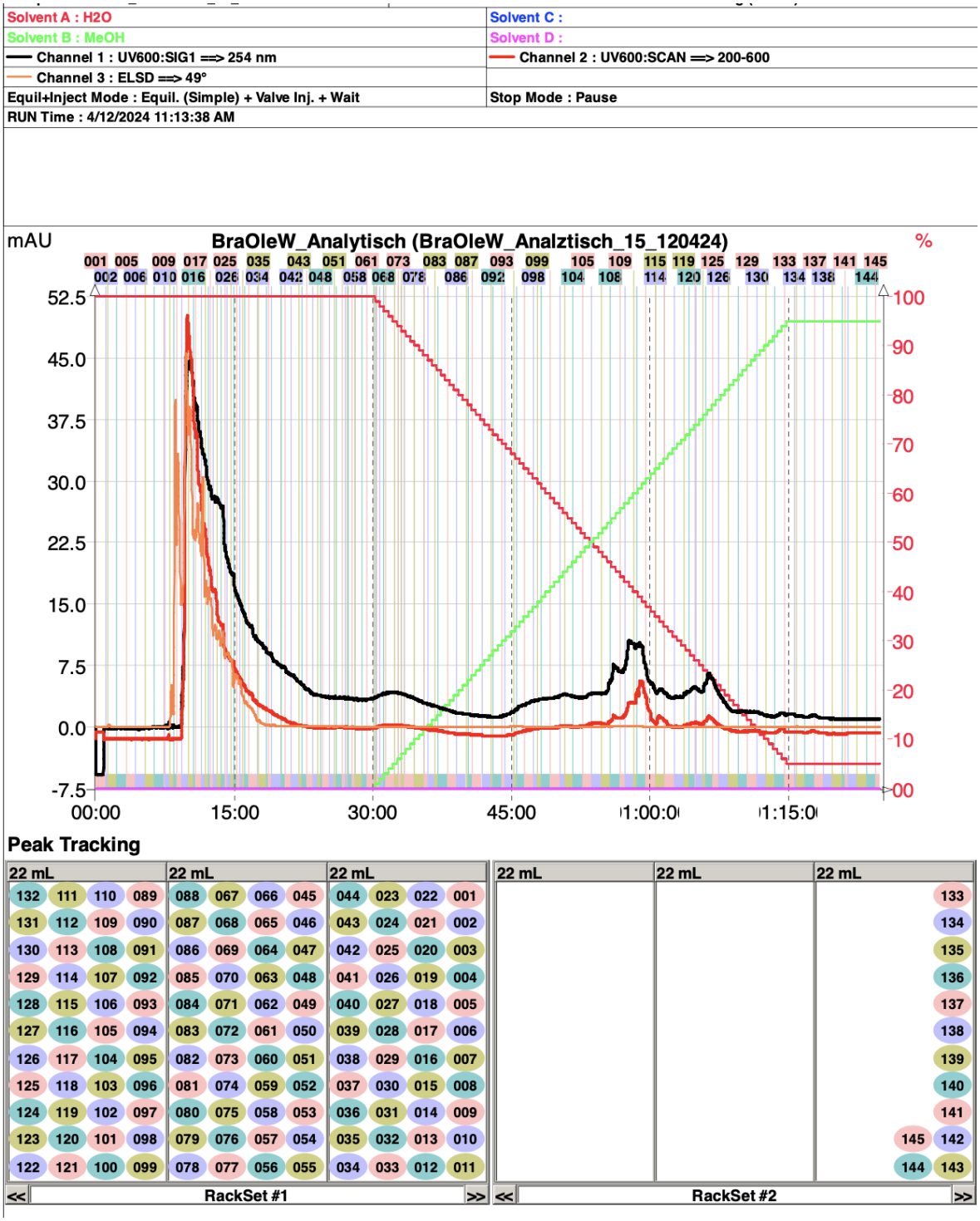

Figure A 17: FC chromatogram from run FC14 (see Table 1 and Table 2, p7), using the aqueous extract BraOleW3 (see chapter 3.1.1, p5).

The 145 various fractions were united into 4 fractions: fraction 1 = 001-061, fraction 2 = 062-104, fraction 3 = 105-128, fraction 4 = 129-145.

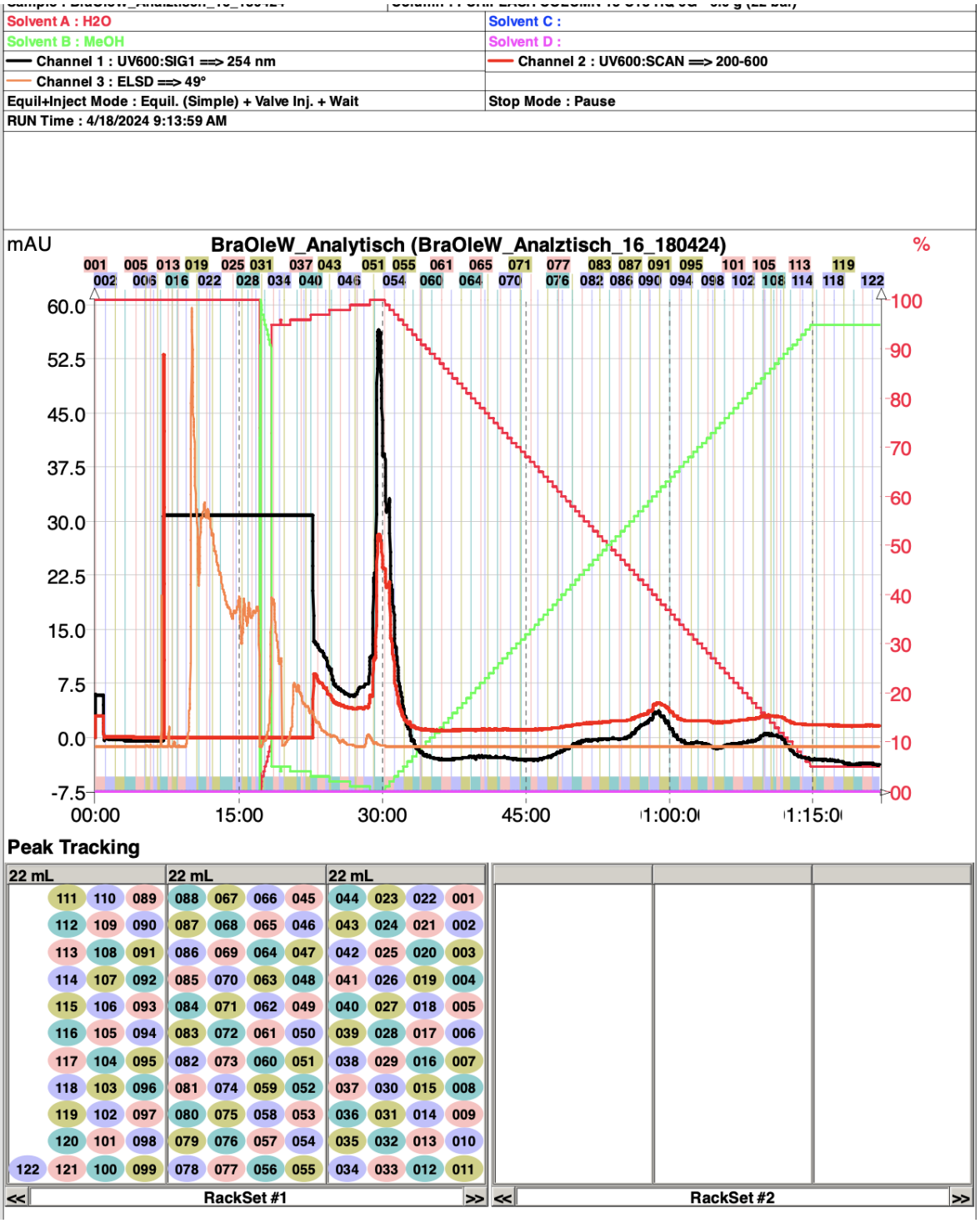

Figure A 18: FC chromatogram from run FC15 (see Table 1 and Table 2, p7), using the aqueous extract BraOleW3 (see chapter 3.1.1, p5).

The 122 various fractions were united into 4 fractions: fraction 1 = 001-060, fraction 2 = 061-87, fraction 3 = 088-113, fraction 4 = 114-122.

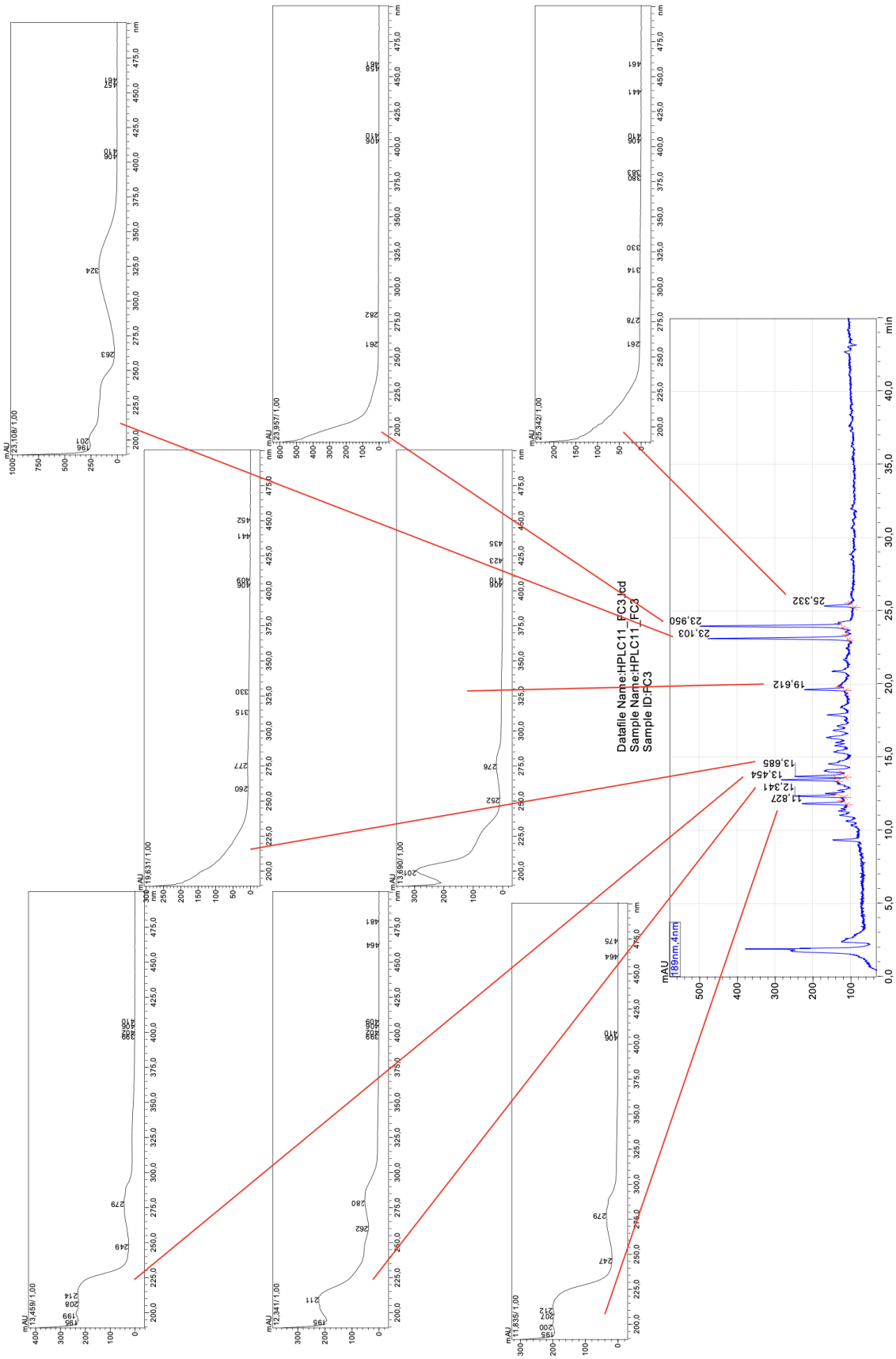

Figure A 19: HPLC chromatogram and associated UV-spectra from BraOleWFC3 (see Figure 6, p16). HPLC run 1 (see Table 5, p9)

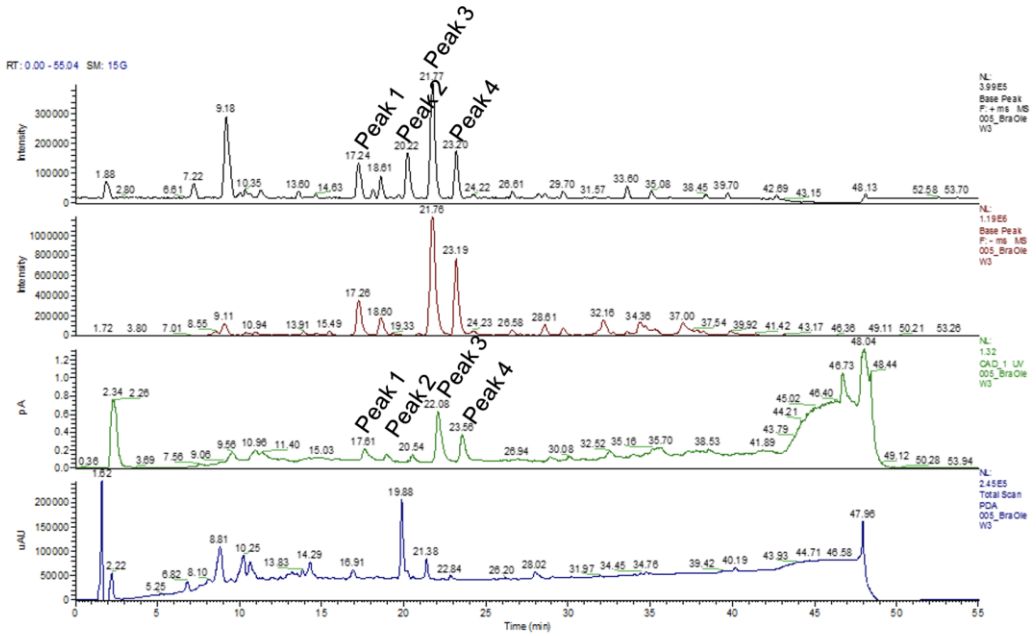

Figure A 20: Representative chromatograms obtained from BraOleWFC3 by HPLC coupled with mass spectrometry (MS), positive ion mode and negative ion mode, charged aerosol detection (CAD), and photodiode array detection (PDA) (see Figure 6, p16). 4 peaks were selected for further analysis. Positive mass (black), negative mass (brown), CAD signal (green) and PDA signal (blue).

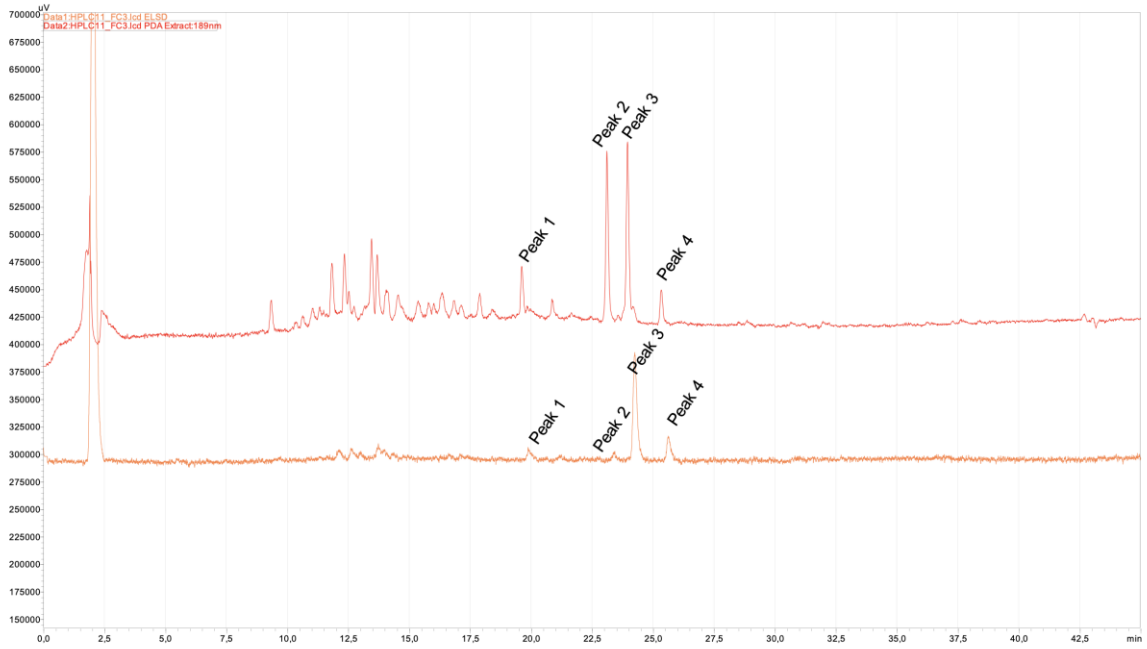

Figure A 21: HPLC data from BraOleWFC3 (see Figure 6, p16). 4 peaks were selected for further analysis. HPLC run 1 (see Table 5, p9). ELSD signal (orange) and PDA signal (red)

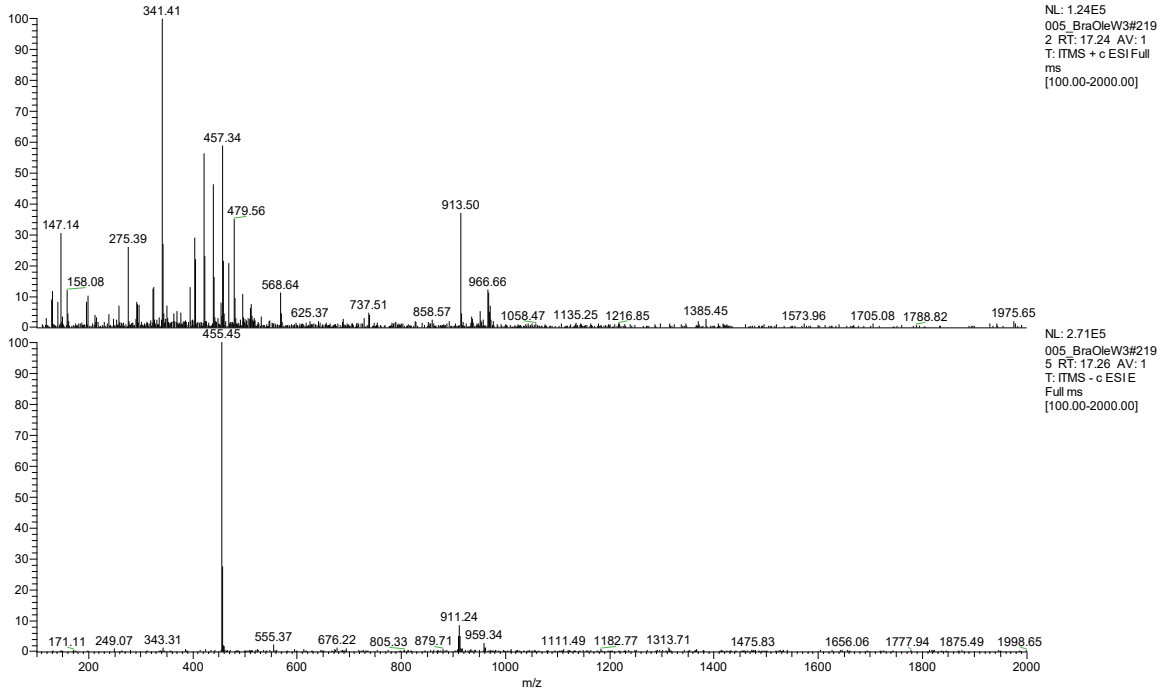

Figure A 22: MS spectra from BraOleWFC3 (see Figure 6, p16) corresponding to peak 1 (Figure 9, p18). Top: positive ion mode (RT 17.24 min); bottom: negative ion mode (RT 17.26 min).

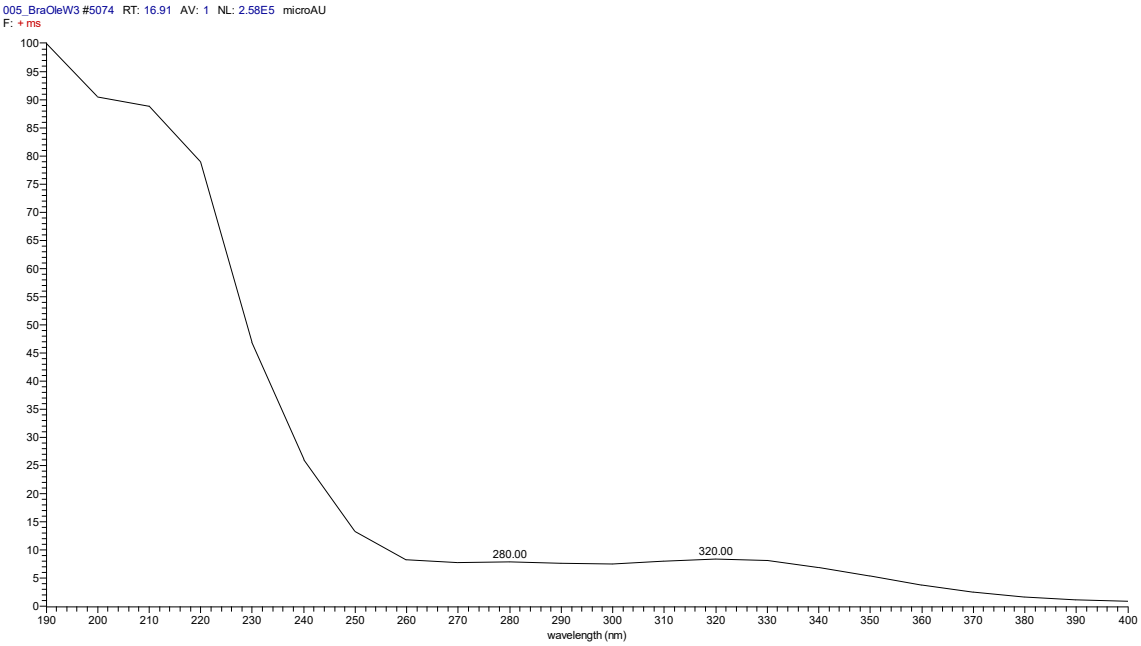

Figure A 23: UV spectrum from BraOleWFC3 (see Figure 6, p16) corresponding to peak 1 (Figure 9, p18).

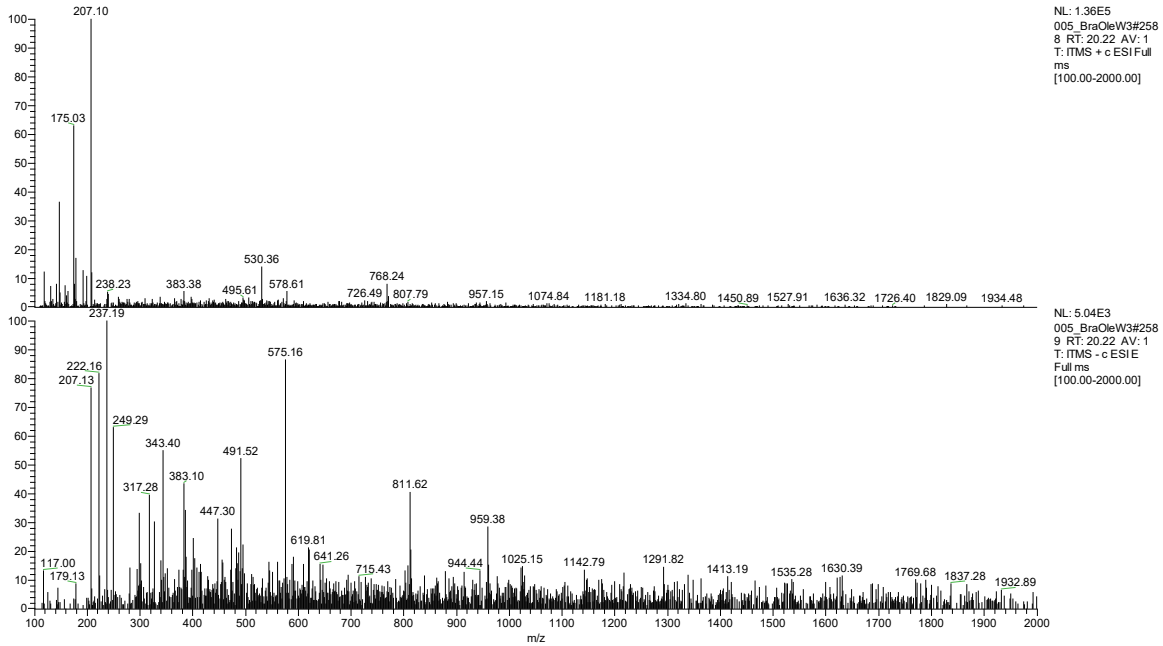

Figure A 24: MS spectra from BraOleWFC3 (see Figure 6, p16) corresponding to peak 2 (Figure 9, p18). Top: positive ion mode (RT 20.22 min); bottom: negative ion mode (RT 20.22 min).

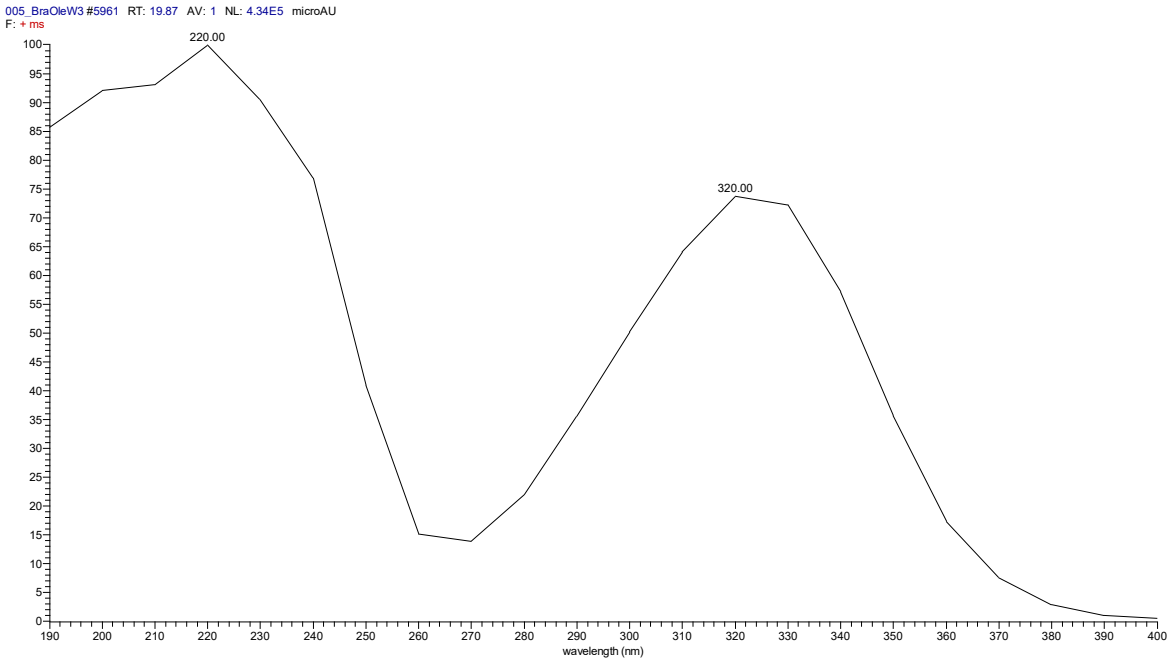

Figure A 25: UV spectrum from BraOleWFC3 (see Figure 6, p16) corresponding to peak 2 (Figure 9, p18).

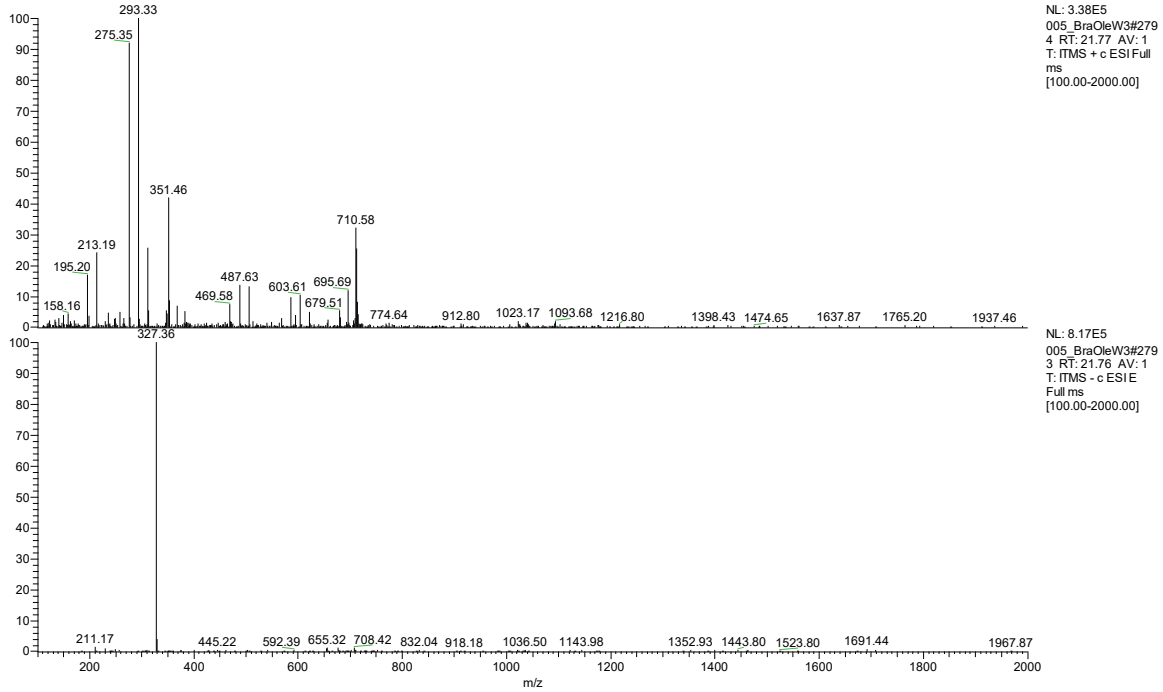

Figure A 26: MS spectra from BraOleWFC3 (see Figure 6, p16) corresponding to peak 3 (Figure 9, p18). Top: positive ion mode (RT 21.77 min); bottom: negative ion mode (RT 21.76 min).

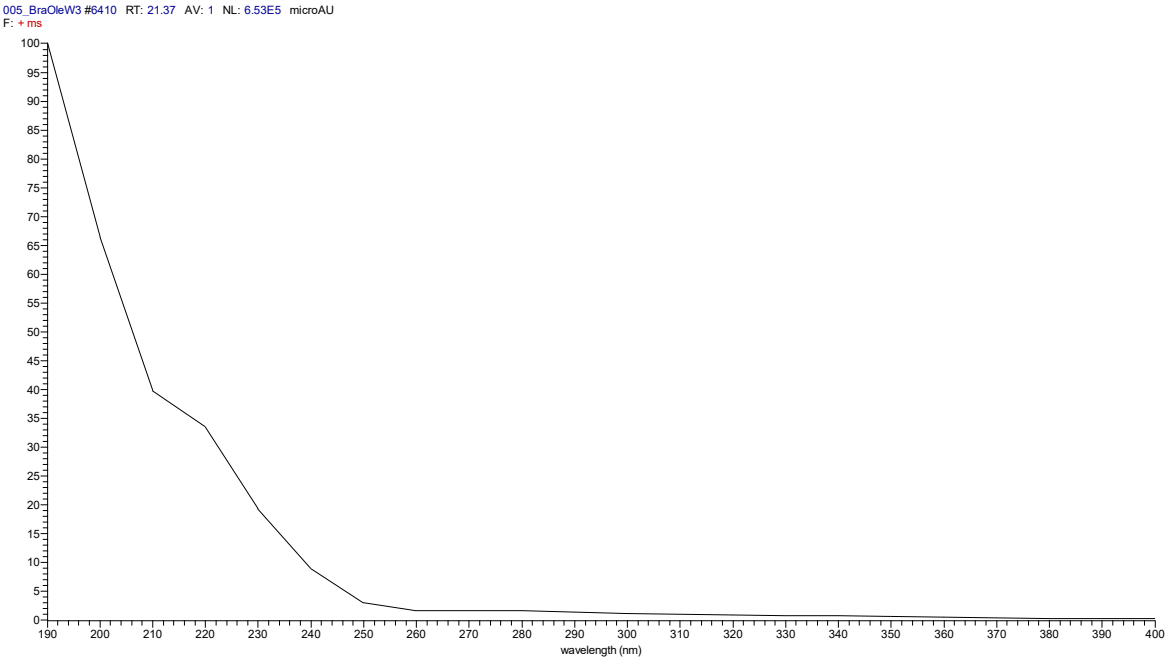

Figure A 27: UV spectrum from BraOleWFC3 (see Figure 6, p16) corresponding to peak 3 (Figure 9, p18).

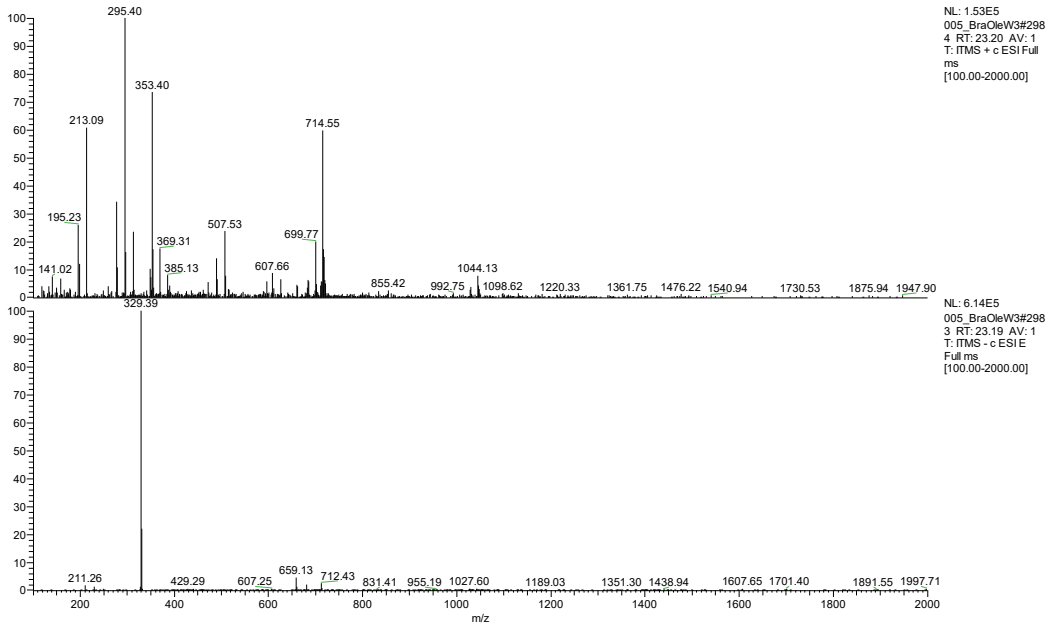

Figure A 28: MS spectra from BraOleWFC3 (see Figure 6, p16) corresponding to peak 4 (Figure 9, p18). Top: positive ion mode (RT 23.20 min); bottom: negative ion mode (RT 23.19 min).

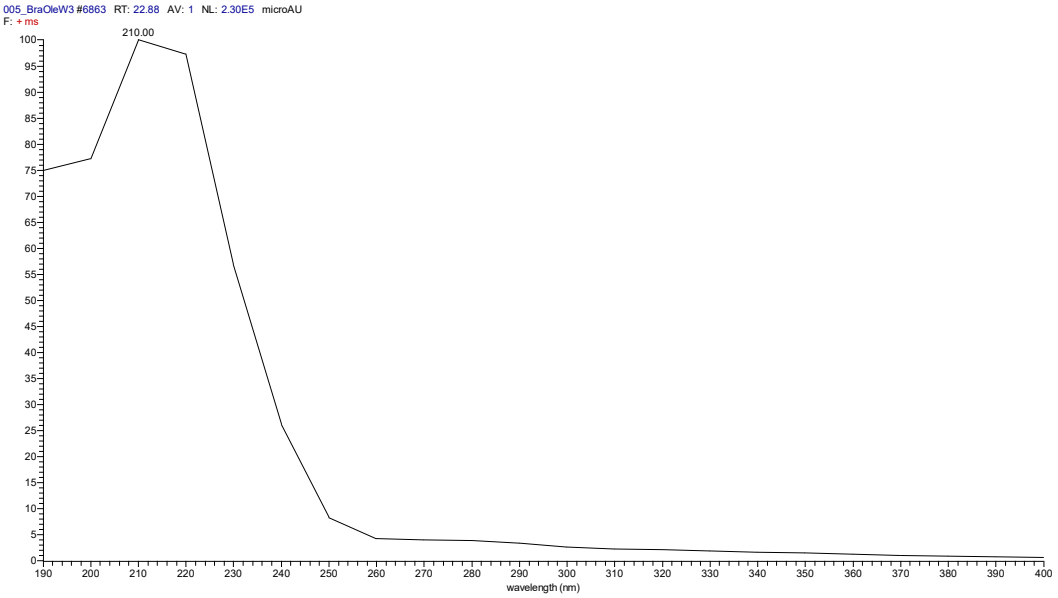

Figure A 29: UV spectrum from BraOleWFC3 (see Figure 6, p16) corresponding to peak 4 (Figure 9, p18).

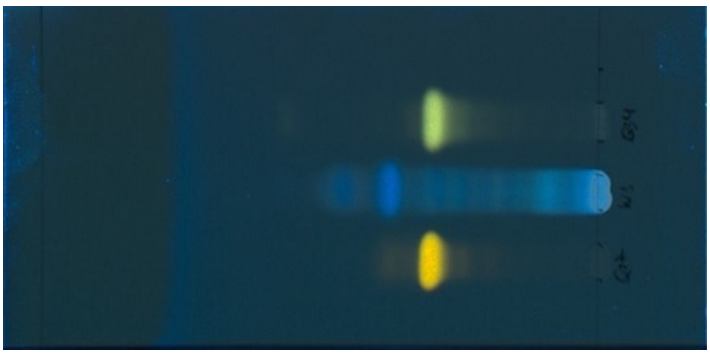

Figure A 30: TLC 7 (see Table 3, p8), comparison of BraOleWFC3 in the middle (see Figure 6, p16) with quercetin-3,4-dimethylether (left) and quercetin-3,7-dimethylether (right). Based on the TLC pattern, neither reference compound could be identified in BraOleWFC3 (see chapter 4.1.2, p16).

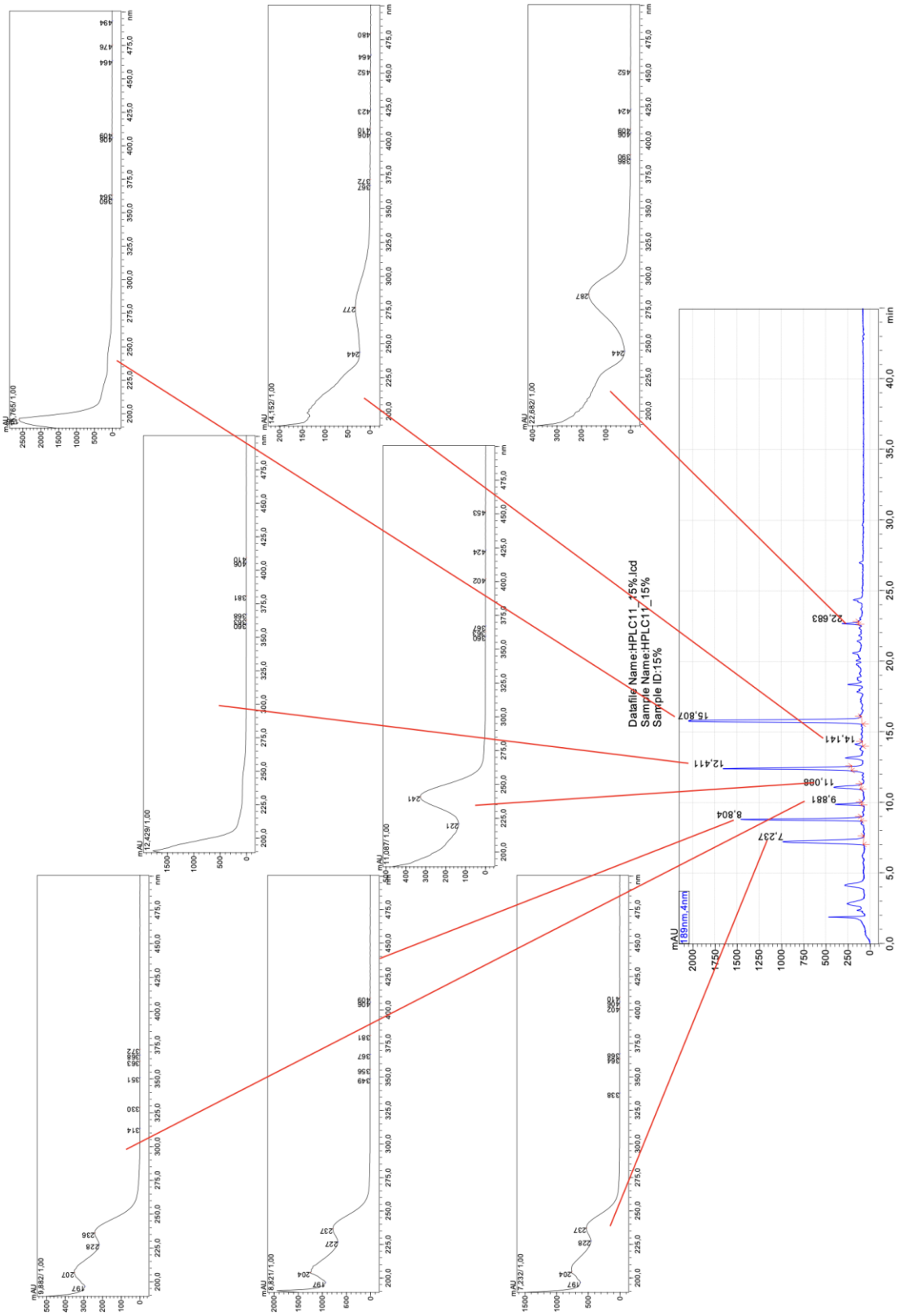

Figure A 31: HPLC chromatogram and associated UV-spectra from BraOleD15 (see chapter 3.1.2, p5). HPLC run 1 (see Table 5, p9)

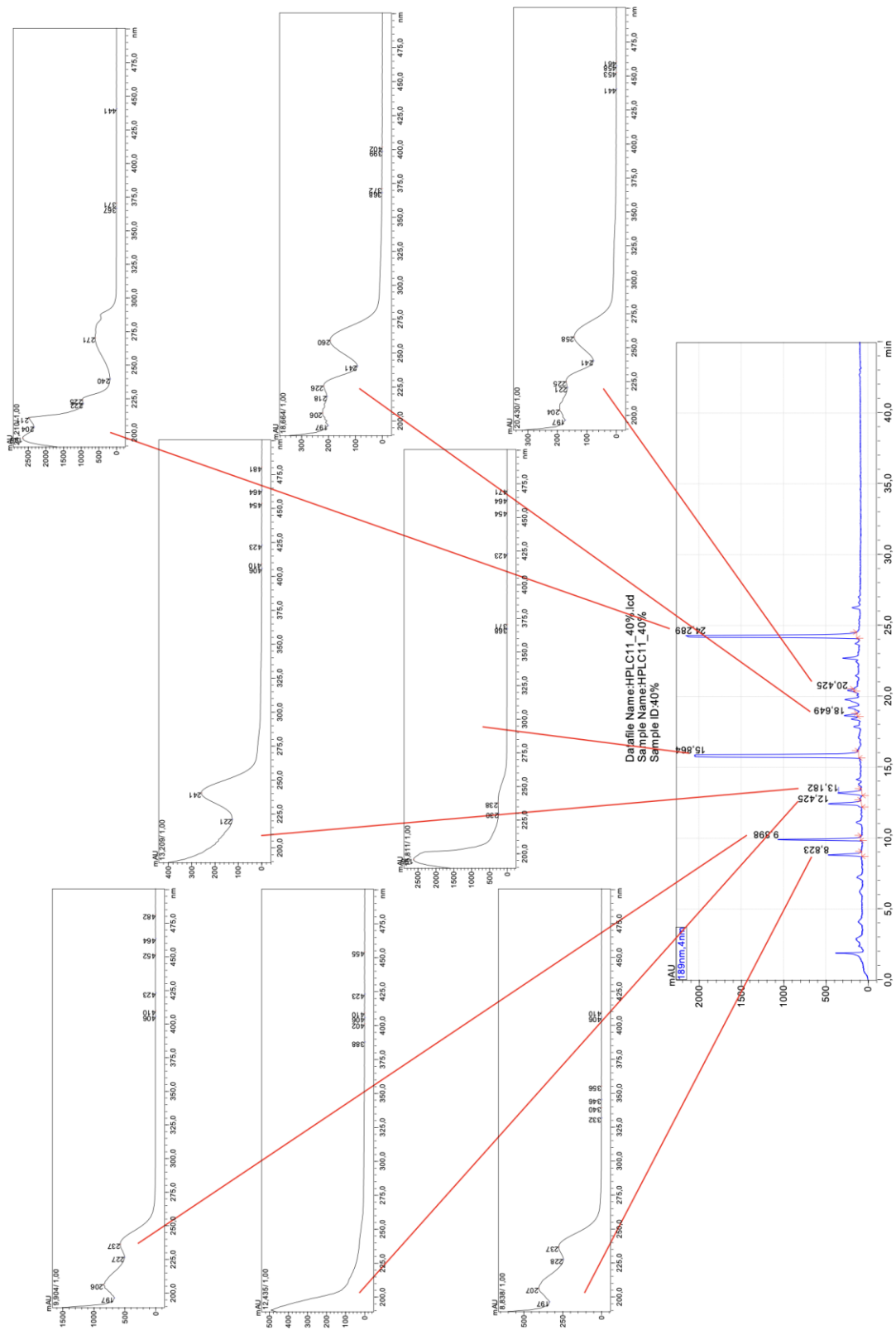

Figure A 32: HPLC chromatogram and associated UV-spectra from BraOleD40 (see chapter 3.1.2, p5). HPLC run 1 (see Table 5, p9)

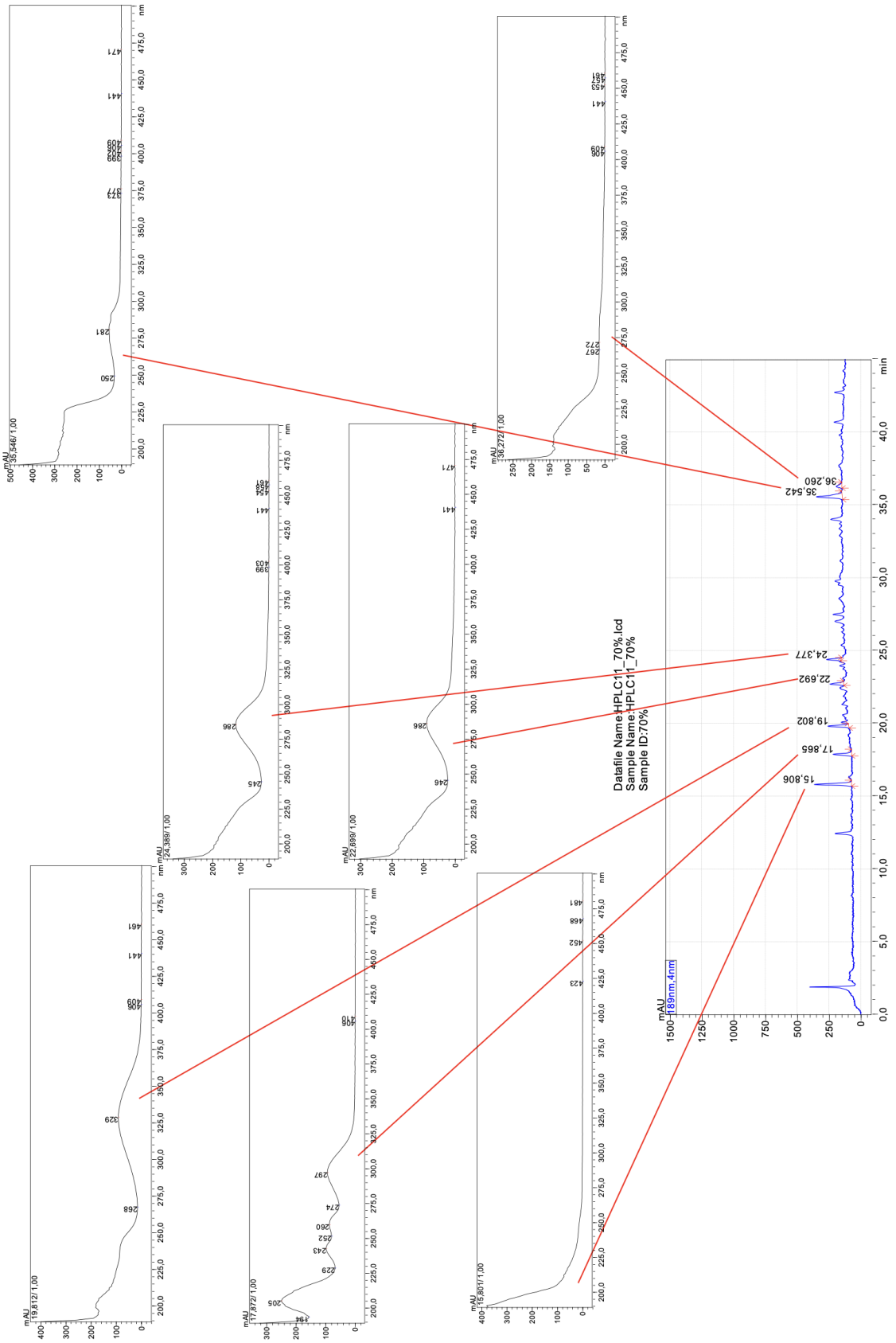

Figure A 33: HPLC chromatogram and associated UV-spectra from BraOleD70 (see chapter 3.1.2, p5). HPLC run 1 (see Table 5, p9)

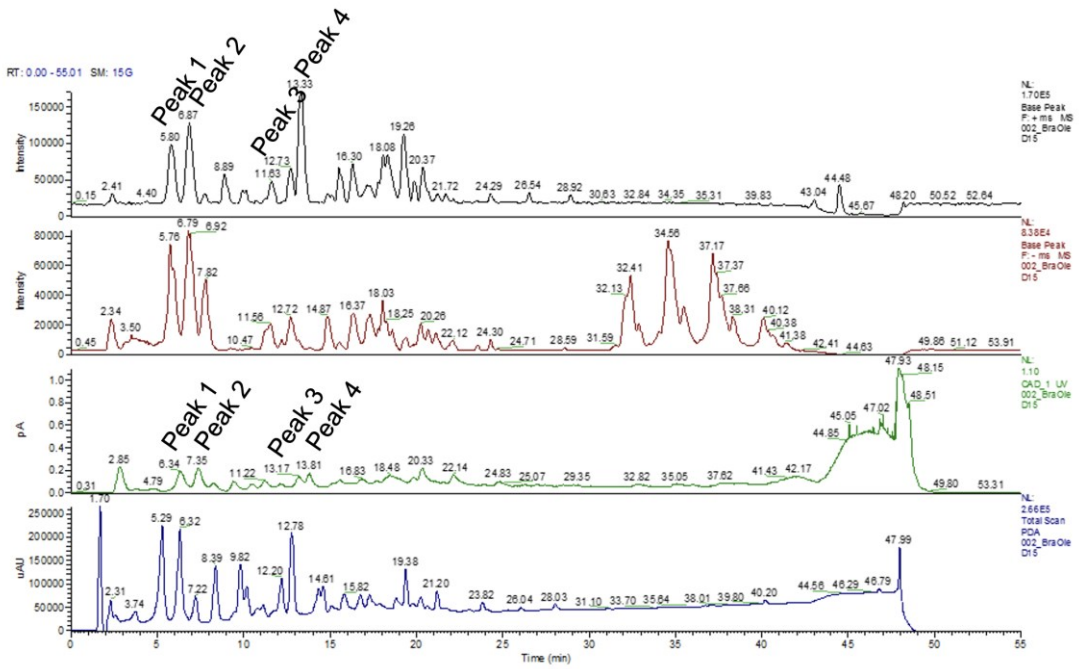

Figure A 34: Representative chromatograms obtained from BraOleD15 by HPLC coupled with mass spectrometry (MS), positive ion mode and negative ion mode, charged aerosol detection (CAD), and photodiode array detection (PDA) (see chapter 3.1.2, p5). 4 peaks were selected for further analysis. Positive mass (black), negative mass (brown), CAD signal (green) and PDA signal (blue).

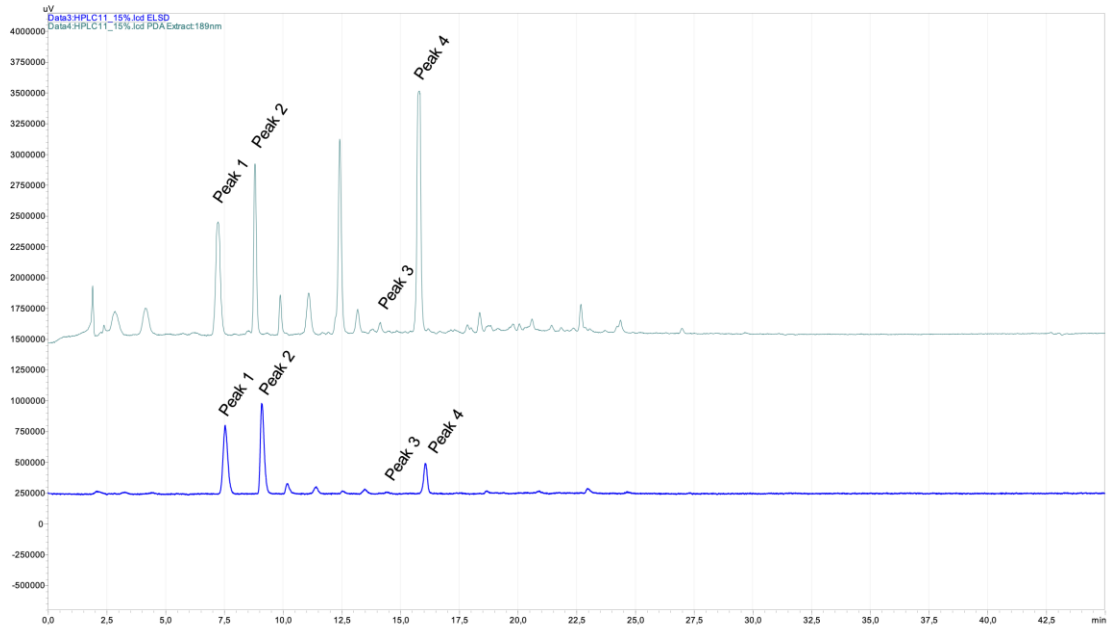

Figure A 35: HPLC data from BraOleD15 (see chapter 3.1.2, p5). 4 peaks were selected for further analysis. HPLC run 1 (see Table 5, p9). ELSD signal (blue) and PDA signal (grey)

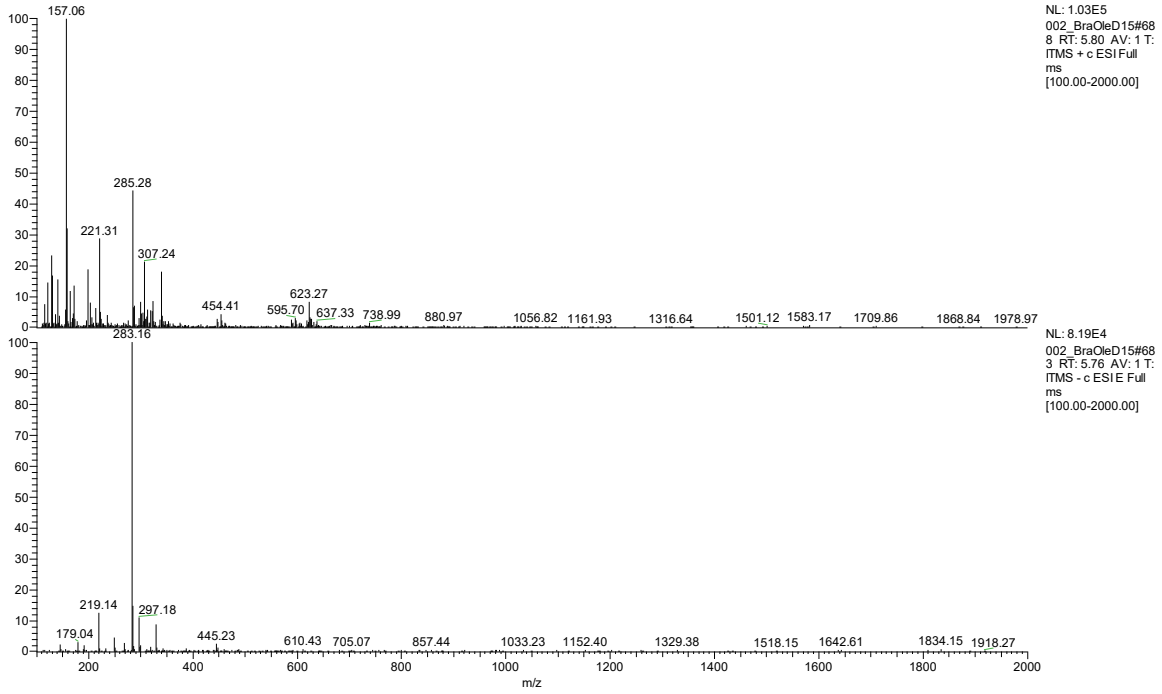

Figure A 36: MS spectra from BraOleD15 (see chapter 3.1.2, p5) corresponding to peak 1 (see Figure 21, p24). Top: positive ion mode (RT 5.80 min); bottom: negative ion mode (RT 5.76 min).

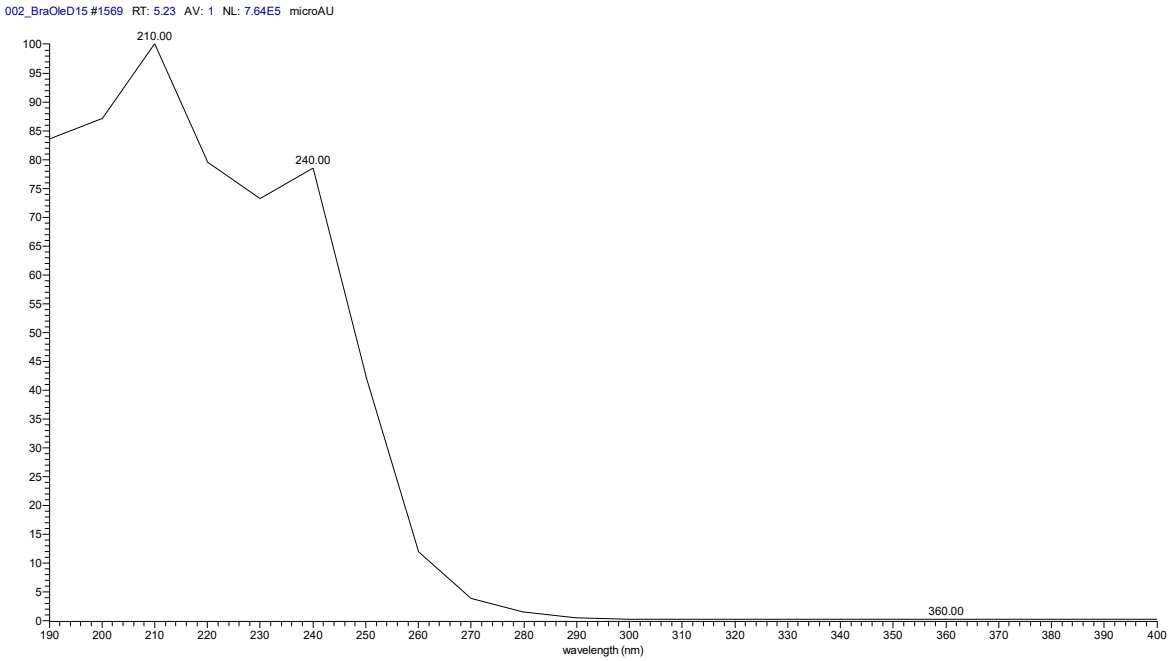

Figure A 37: UV spectrum from BraOleD15 (see chapter 3.1.2, p5) corresponding to peak 1 (see Figure 21, p24).

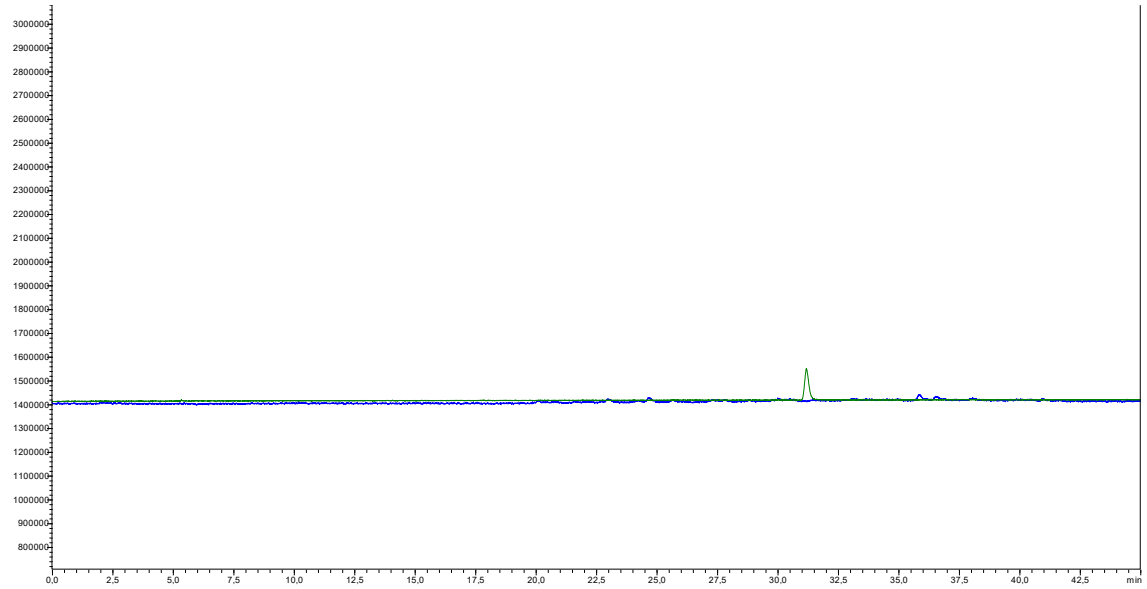

Figure A 38: Comparison of the acacetin pure substance ELSD peak (green) with the ELSD peak (blue) from BraOLeD15 (see chapter 3.1.2, p5). HPLC run 6 (see Table 5, p9). Based on the HPLC chromatogram, acacetin reference compound was not identified in BraOleD15 (see chapter 4.2.2, p24).

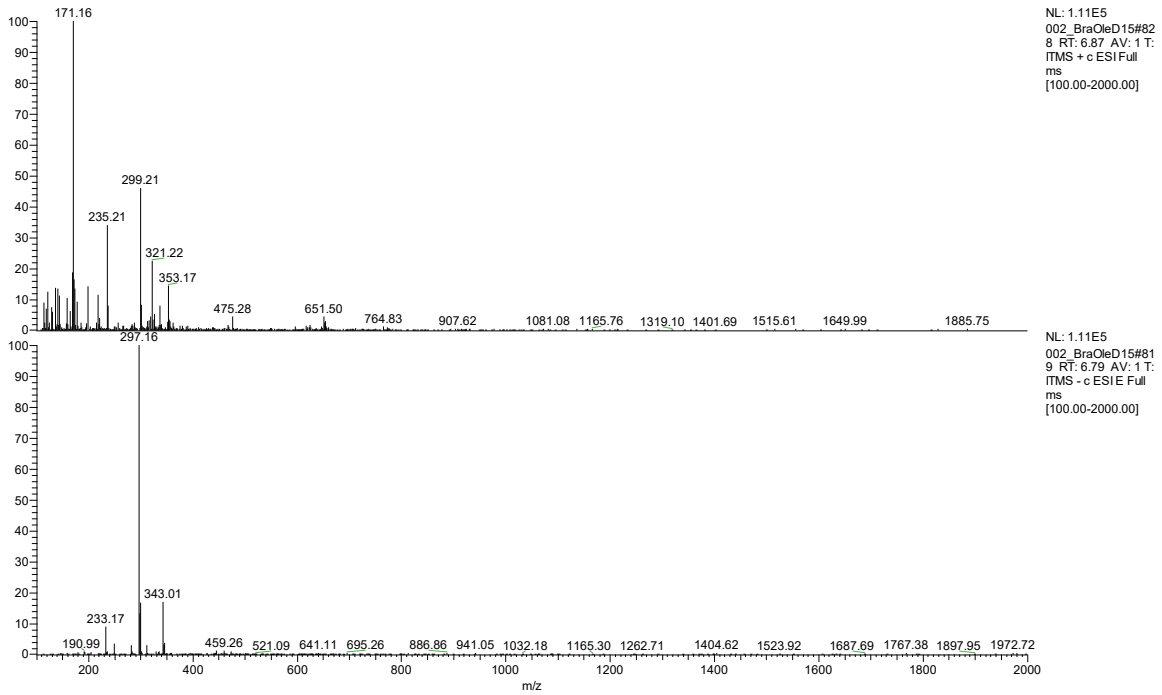

Figure A 39: MS spectra from BraOleD15 (see chapter 3.1.2, p5) corresponding to peak 2 (see Figure 21, p24). Top: positive ion mode (RT 6.87 min); bottom: negative ion mode (RT 6.79 min).

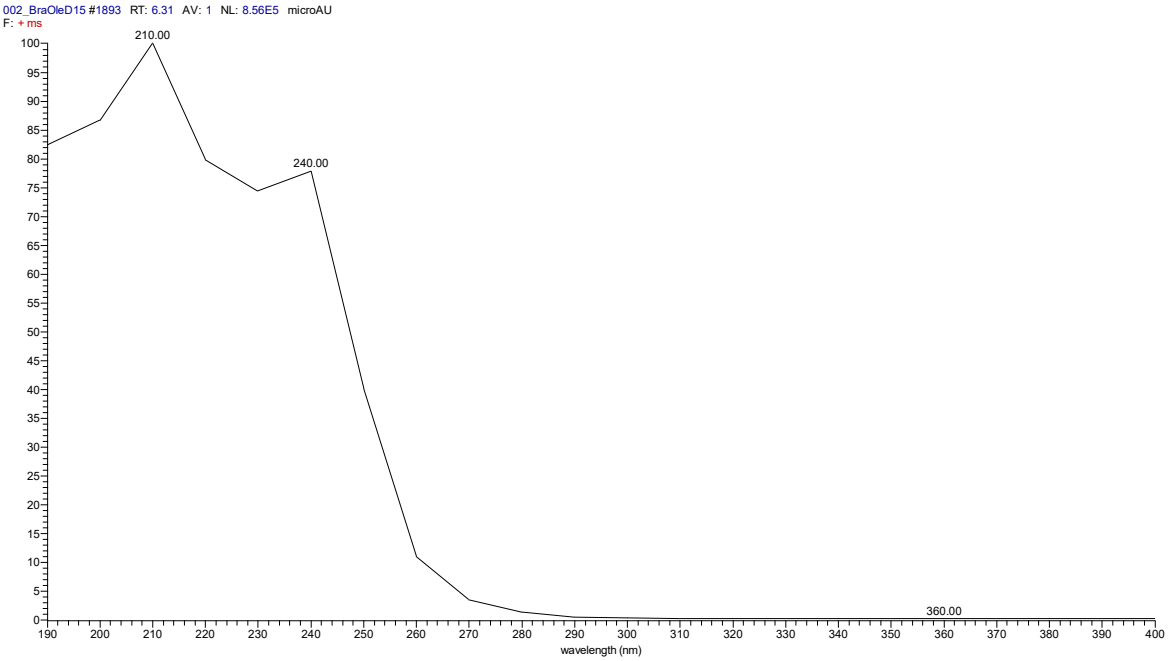

Figure A 40: UV spectrum from BraOleD15 (see chapter 3.1.2, p5) corresponding to peak 2 (see Figure 21, p24).

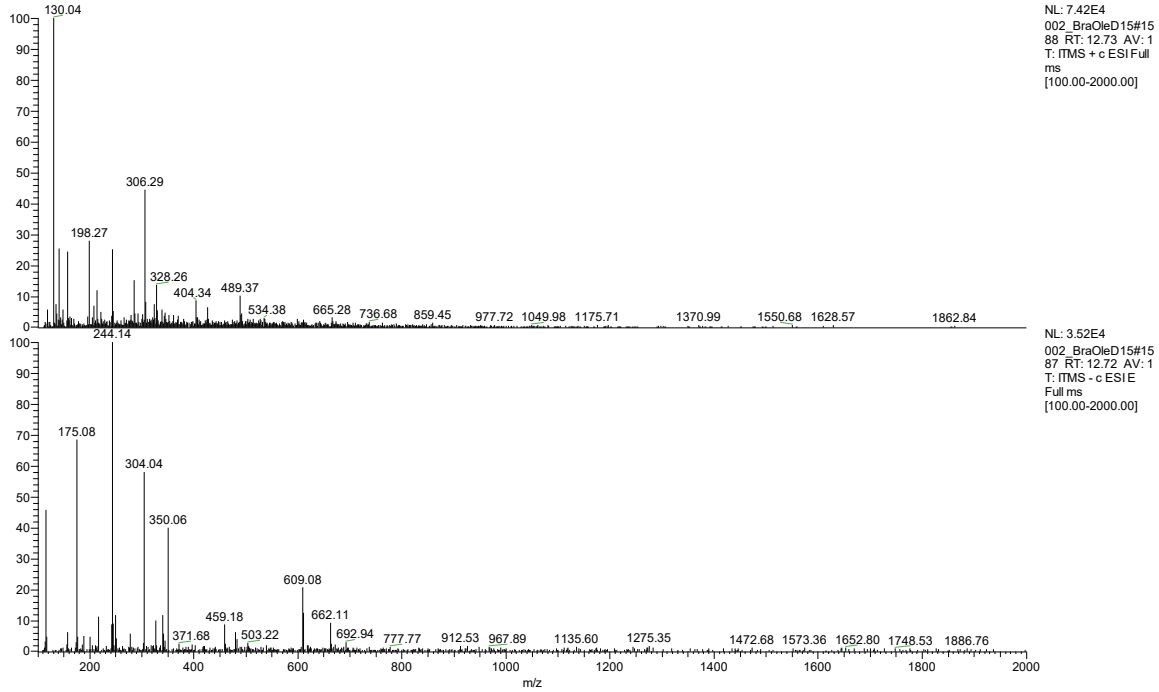

Figure A 41: MS spectra from BraOleD15 (see chapter 3.1.2, p5) corresponding to peak 3 (see Figure 21, p24). Top: positive ion mode (RT 12.73 min); bottom: negative ion mode (RT 12.72 min).

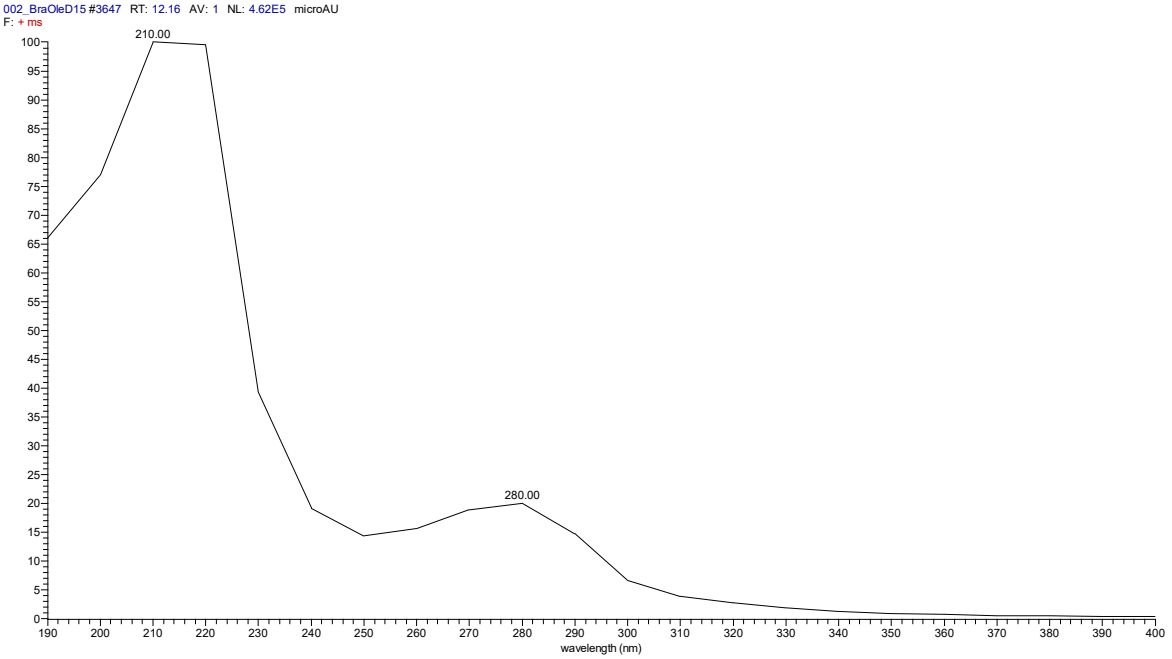

Figure A 42: UV spectrum from BraOleD15 (see chapter 3.1.2, p5) corresponding to peak 3 (see Figure 21, p24).

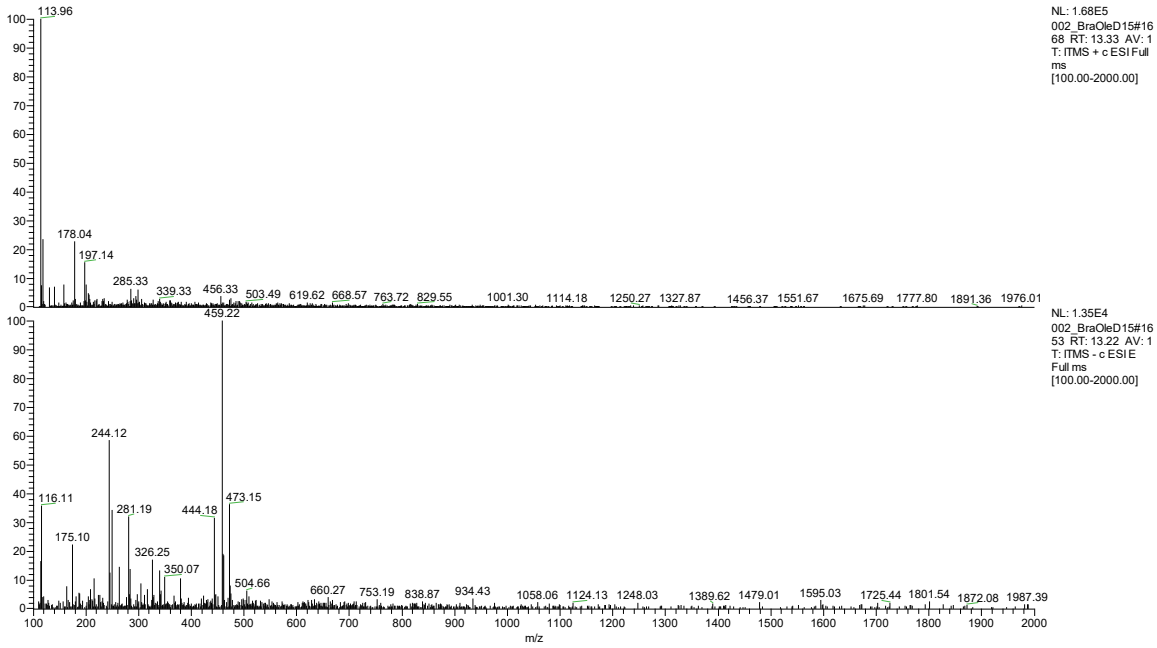

Figure A 43: MS spectra from BraOleD15 (see chapter 3.1.2, p5) corresponding to peak 4 (see Figure 21, p24). Top: positive ion mode (RT 13.33 min); bottom: negative ion mode (RT 13.22 min).

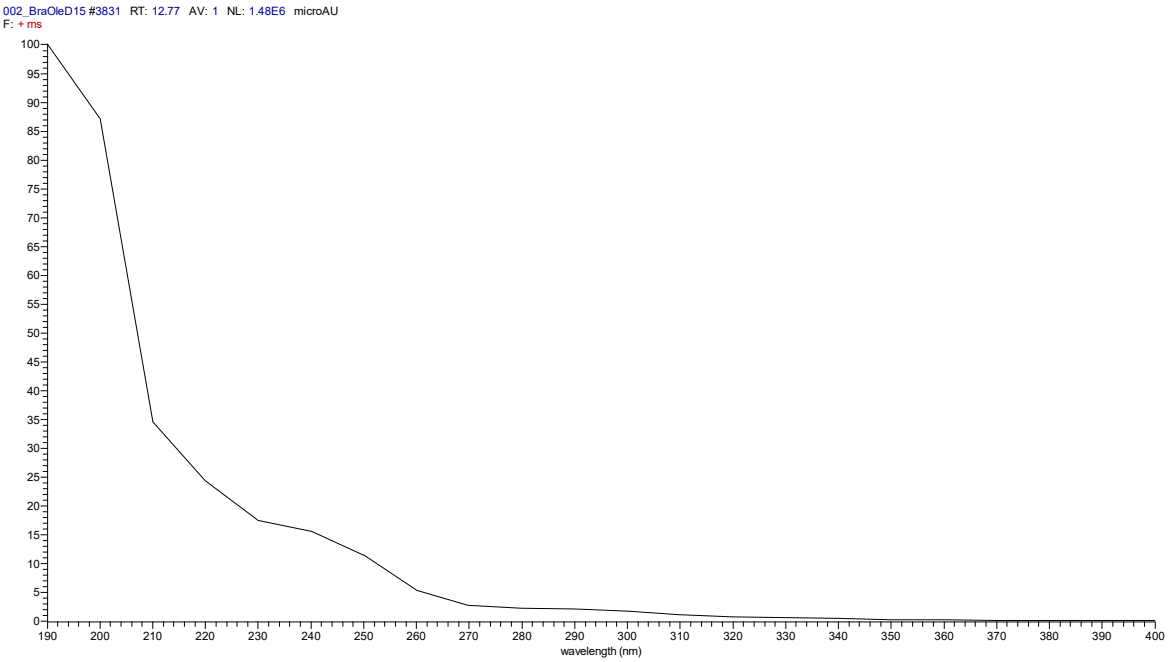

Figure A 44: UV spectrum from BraOleD15 (see chapter 3.1.2, p5) corresponding to peak 4 (see Figure 21, p24).

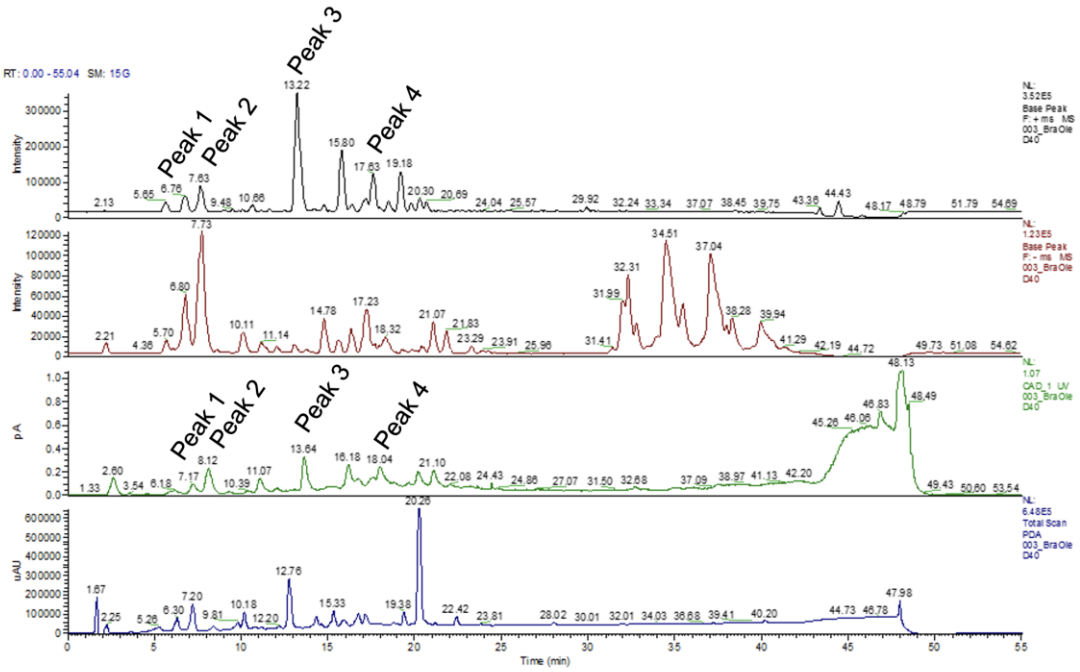

Figure A 45: Representative chromatograms obtained from BraOleD40 by HPLC coupled with mass spectrometry (MS), positive ion mode and negative ion mode, charged aerosol detection (CAD), and photodiode array detection (PDA) (see chapter 3.1.2, p5). 4 peaks were selected for further analysis. Positive mass (black), negative mass (brown), CAD signal (green) and PDA signal (blue).

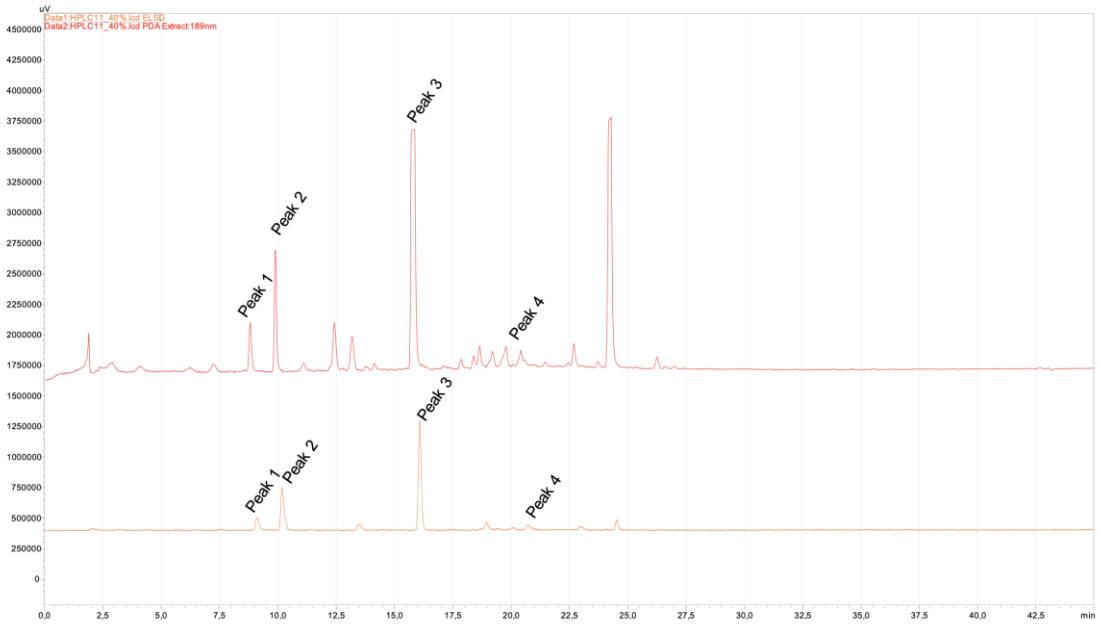

Figure A 46: HPLC data from BraOleD40 (see chapter 3.1.2, p5). 4 peaks were selected for further analysis. HPLC run 1 (see Table 5, p9). ELSD signal (orange) and PDA signal (red)

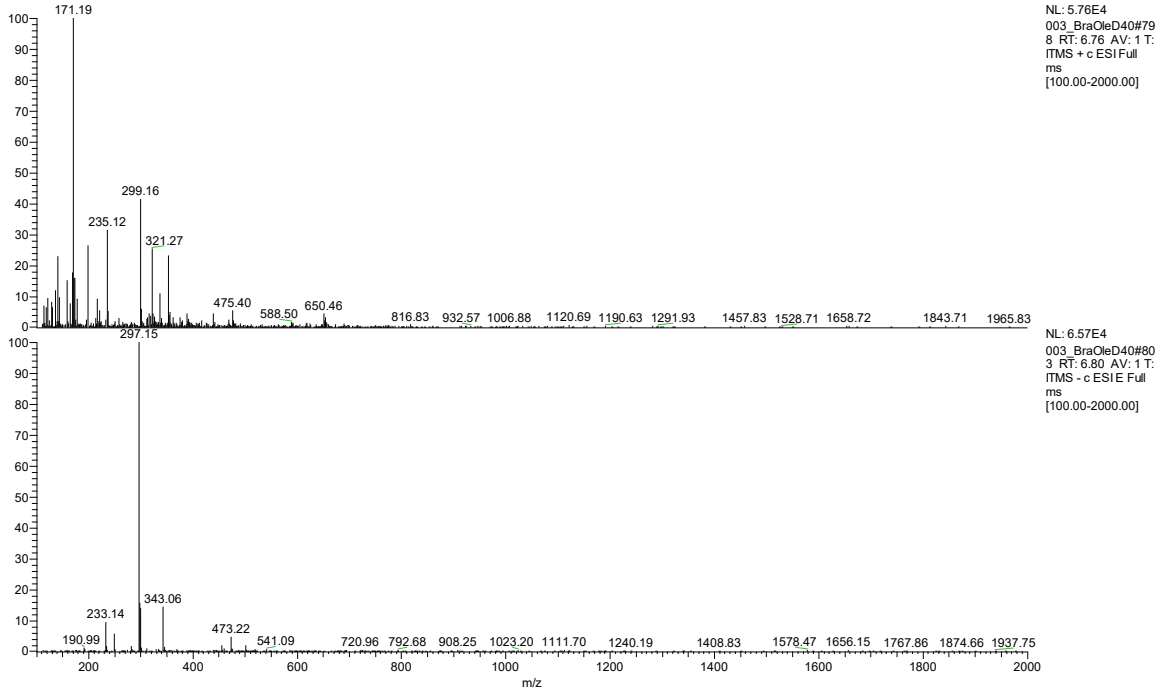

Figure A 47: MS spectra from BraOleD40 (see chapter 3.1.2, p5) corresponding to peak 1 (see Figure 29, p27). Top: positive ion mode (RT 6.76 min); bottom: negative ion mode (RT 6.80 min).

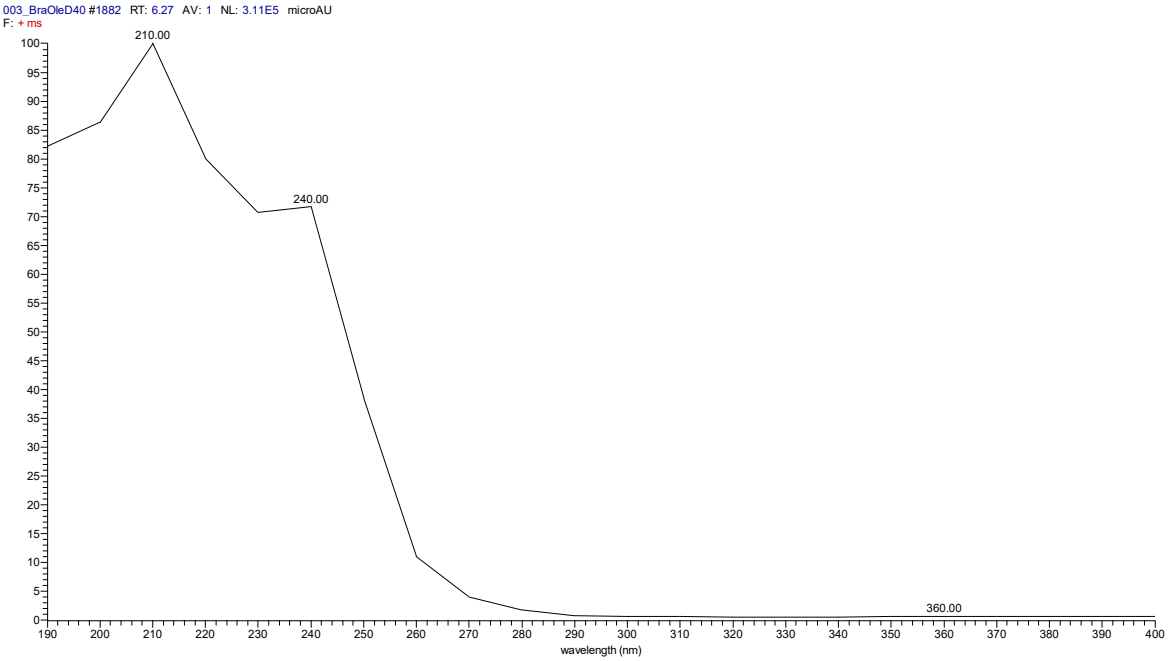

Figure A 48: UV spectrum from BraOleD40 (see chapter 3.1.2, p5) corresponding to peak 1 (see Figure 29, p27).

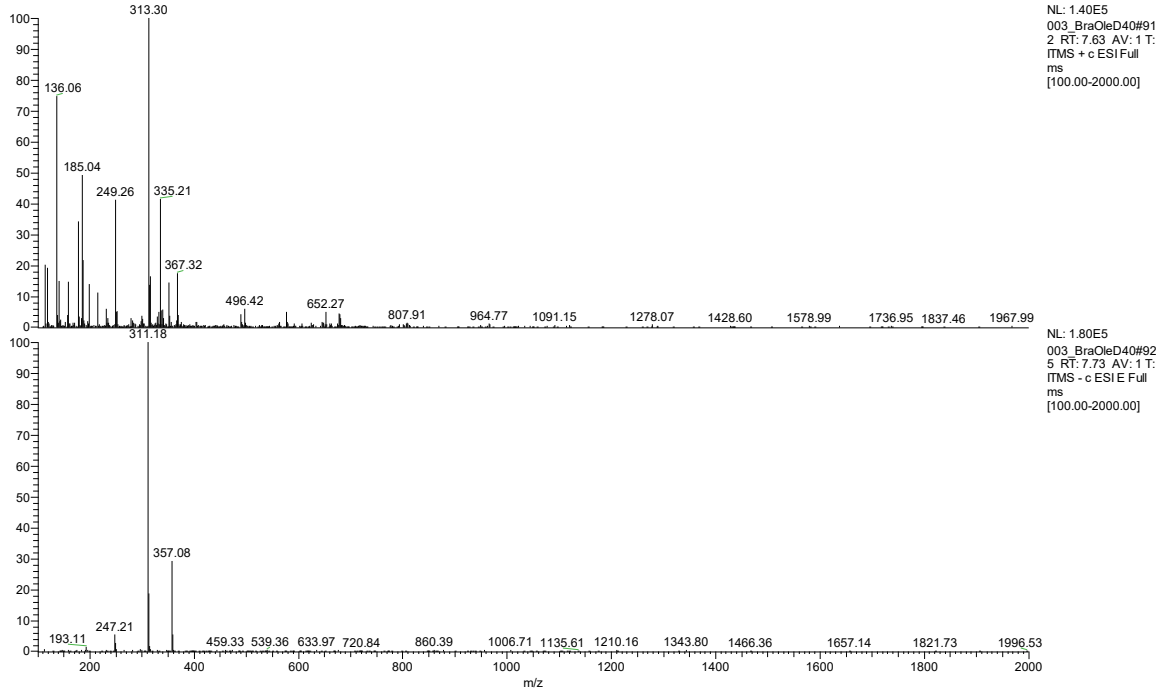

Figure A 49: MS spectra from BraOleD40 (see chapter 3.1.2, p5) corresponding to peak 2 (see Figure 29, p27). Top: positive ion mode (RT 7.63 min); bottom: negative ion mode (RT 7.73 min).

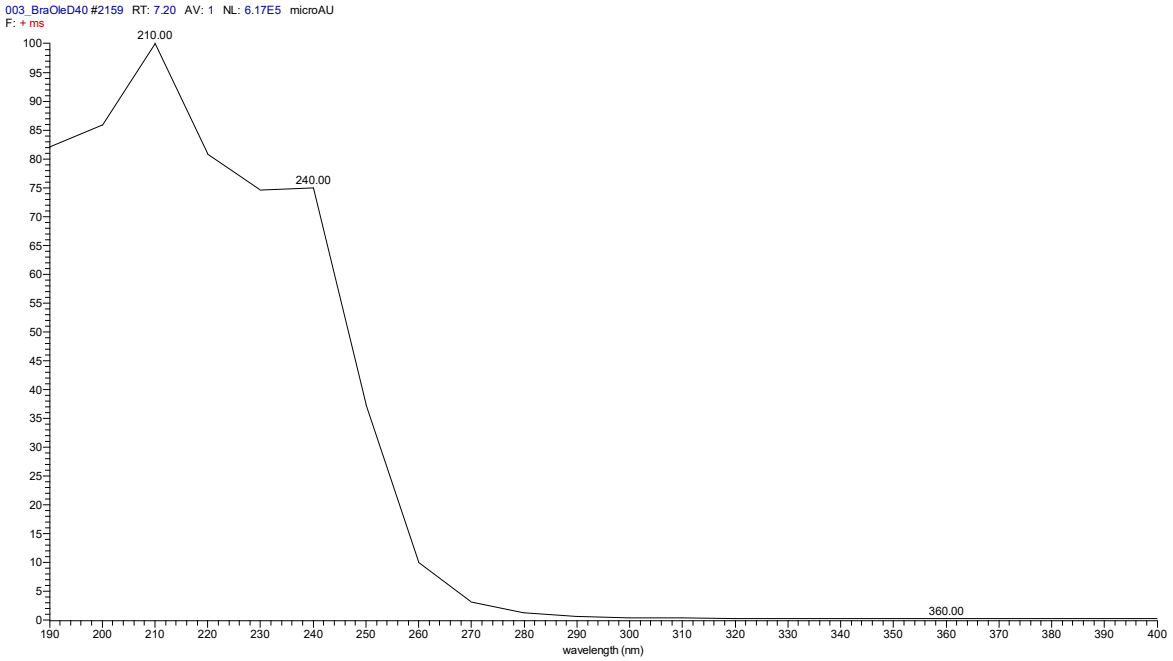

Figure A 50: UV spectrum from BraOleD40 (see chapter 3.1.2, p5) corresponding to peak 2 (see Figure 29, p27).

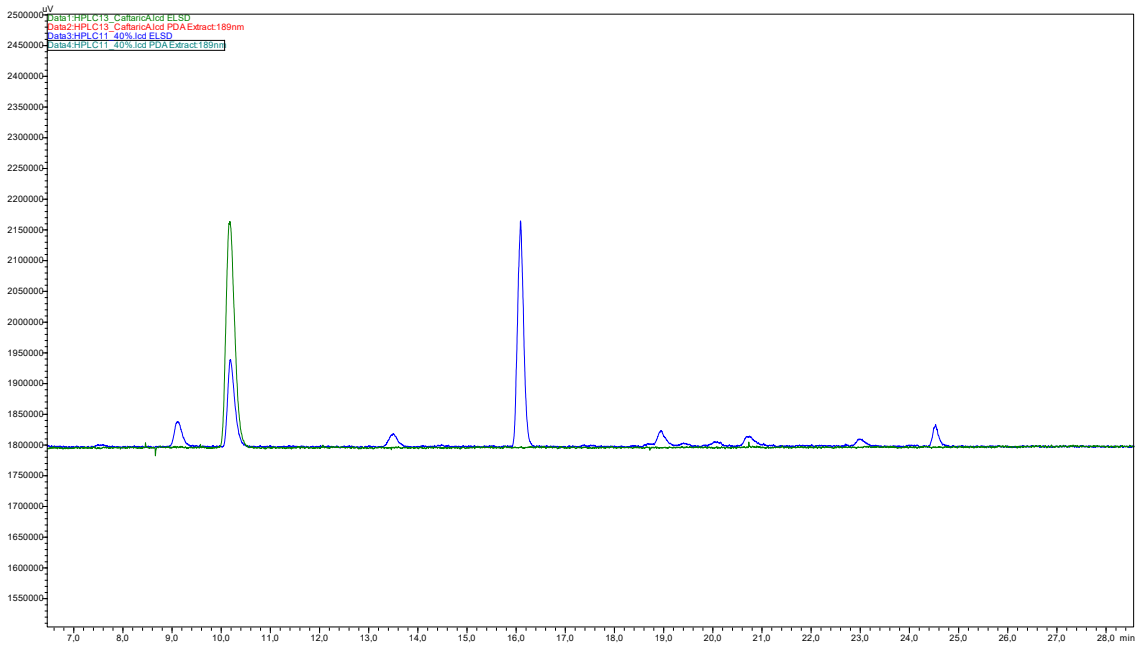

Figure A 51: ELSD peaks of caftaric acid pure substance (green) and the BraOleD40 (blue) (see chapter 3.1.2, p5). HPLC run 3 (see Table 5, p9). Based on the HPLC chromatogram, the caftaric acid reference compound (RT 10 min) was tentatively identified in BraOleD40 (see chapter 4.2.3, p27)

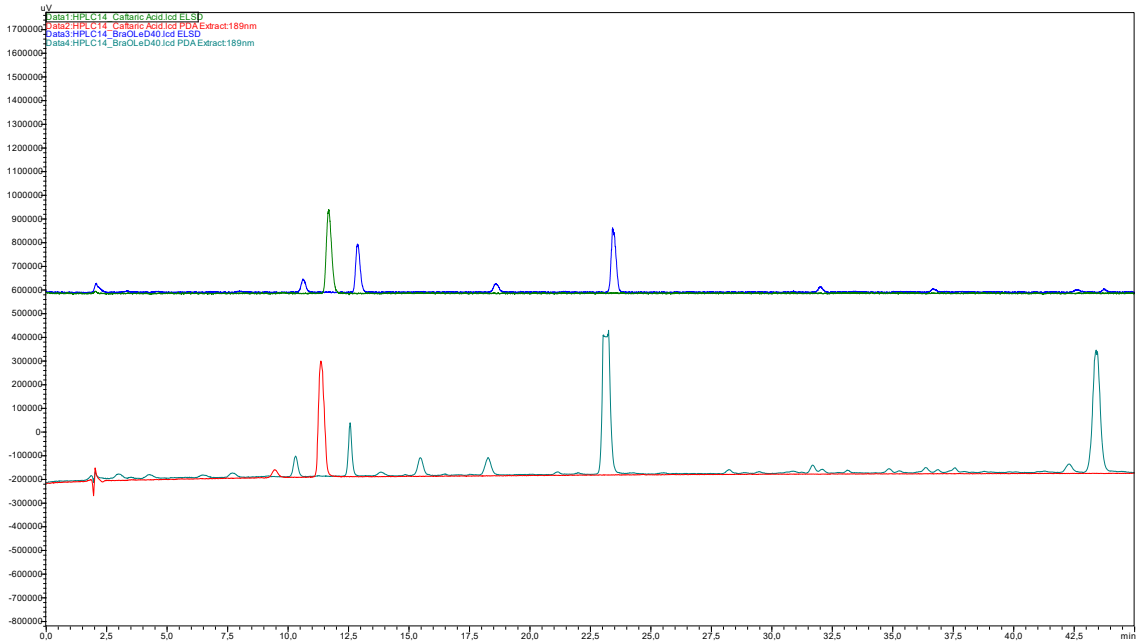

Figure A 52: ELSD peaks of caftaric acid pure substance (green) and the BraOleD40 (blue) (see chapter 3.1.2, p5). PDA peaks of caftaric acid pure substance (red) and the BraOleD40 (grey) (see chapter 3.1.2, p5). HPLC run 4 (see Table 5, p9). Based on the HPLC chromatogram, the caftaric acid reference compound (RT 11 min) and the BraOleD40 peak (RT 12.5 min) no longer aligned after the solvent gradient was changed (see chapter 4.2.3, p27).

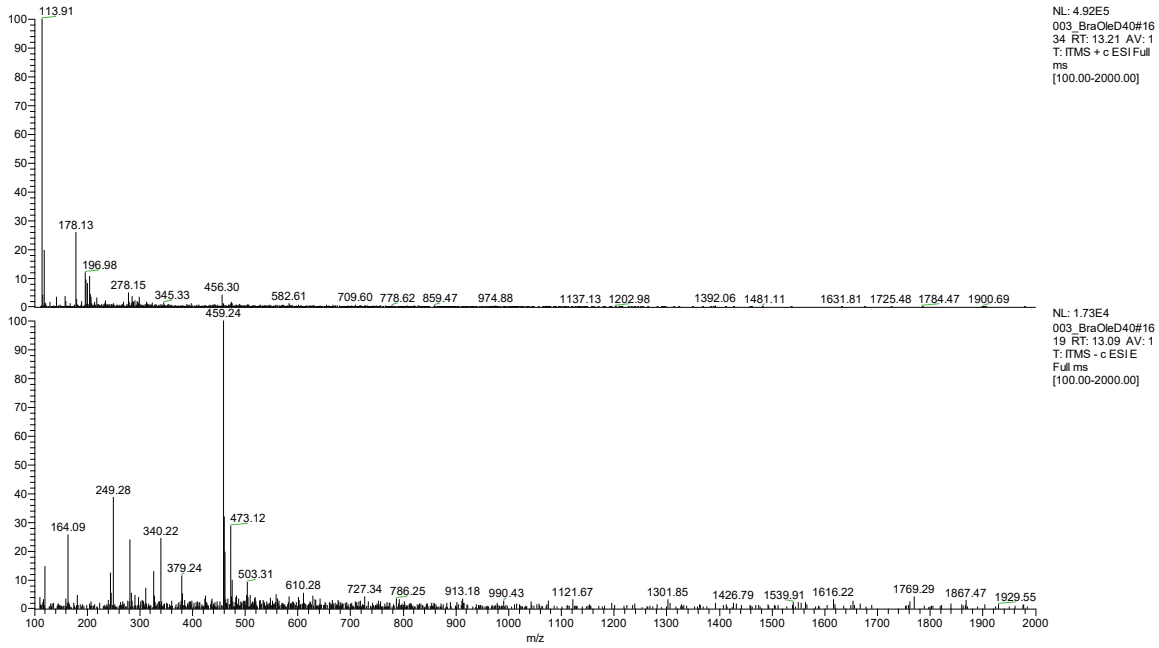

Figure A 53: MS spectra from BraOleD40 (see chapter 3.1.2, p5) corresponding to peak 3 (see Figure 29, p27). Top: positive ion mode (RT 13.21 min); bottom: negative ion mode (RT 13.09 min).

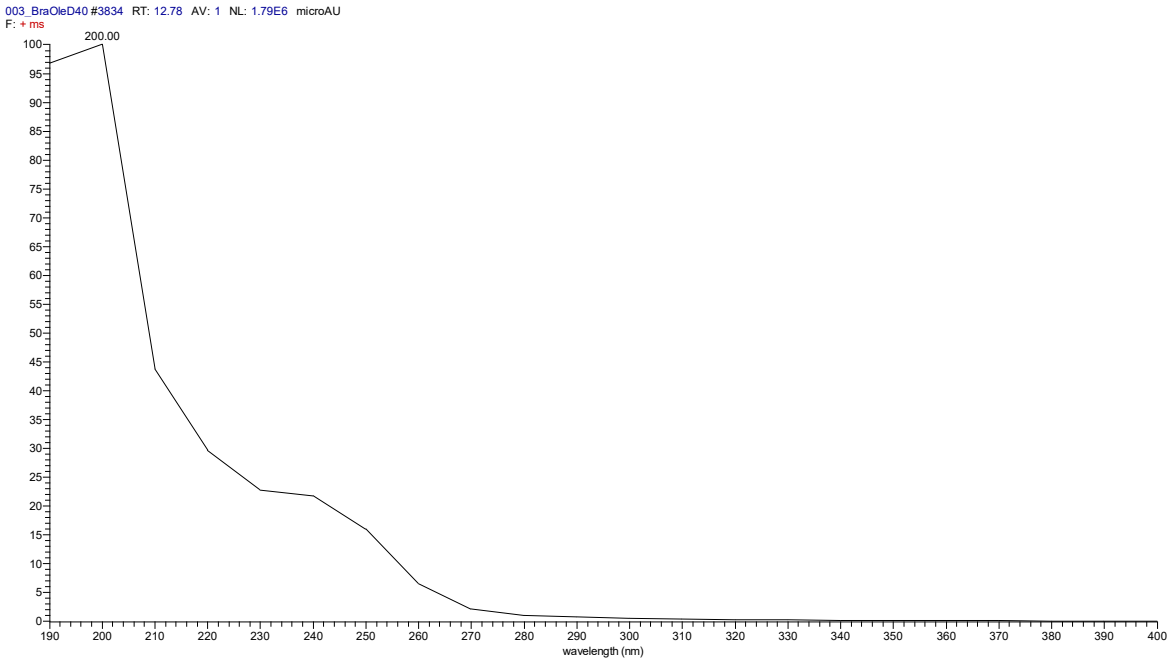

Figure A 54: UV spectrum from BraOleD40 (see chapter 3.1.2, p5) corresponding to peak 3 (see Figure 29, p27).

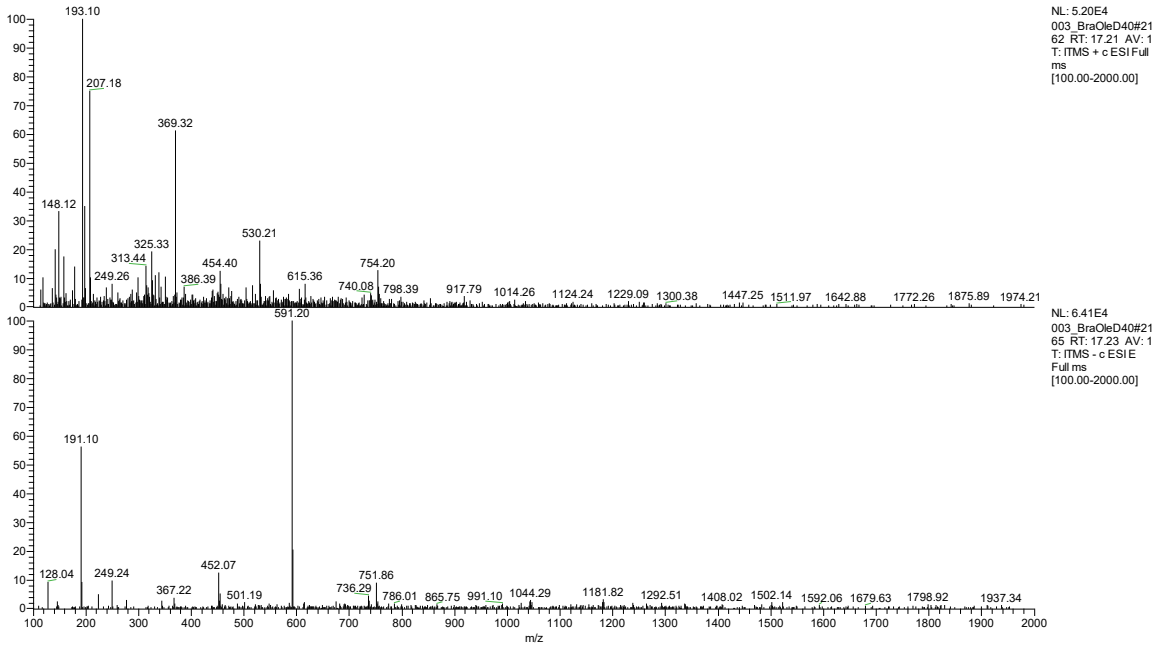

Figure A 55: MS spectra from BraOleD40 (see chapter 3.1.2, p5) corresponding to peak 4 (see Figure 29, p27). Top: positive ion mode (RT 17.21 min); bottom: negative ion mode (RT 17.23 min).

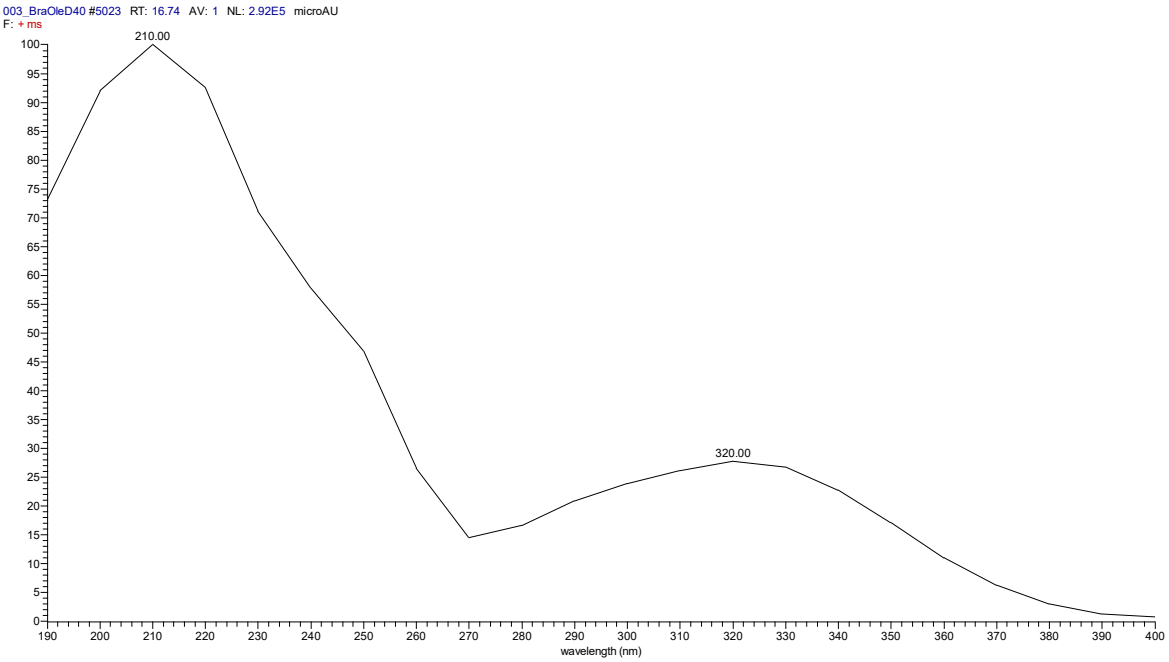

Figure A 56: UV spectrum from BraOleD40 (see chapter 3.1.2, p5) corresponding to peak 4 (see Figure 29, p27).

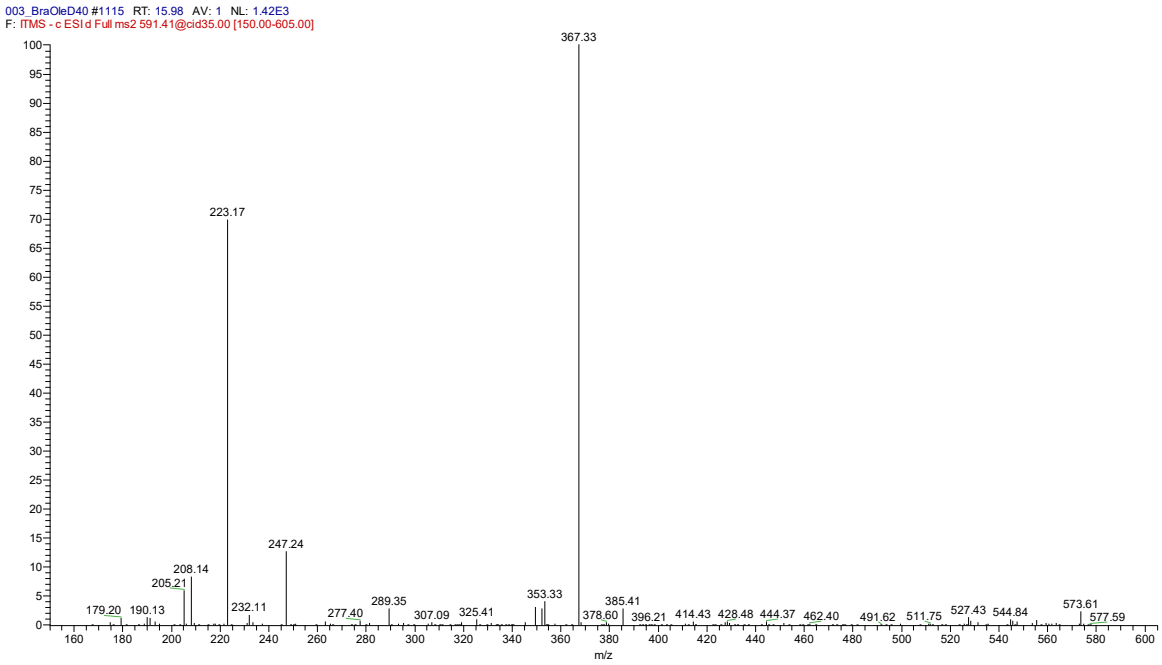

Figure A 57: MS2 spectra from BraOleD40 (see chapter 3.1.2, p5) corresponding to peak 4 (see Figure 29, p27). Negative ion mode (RT 15.98 min).

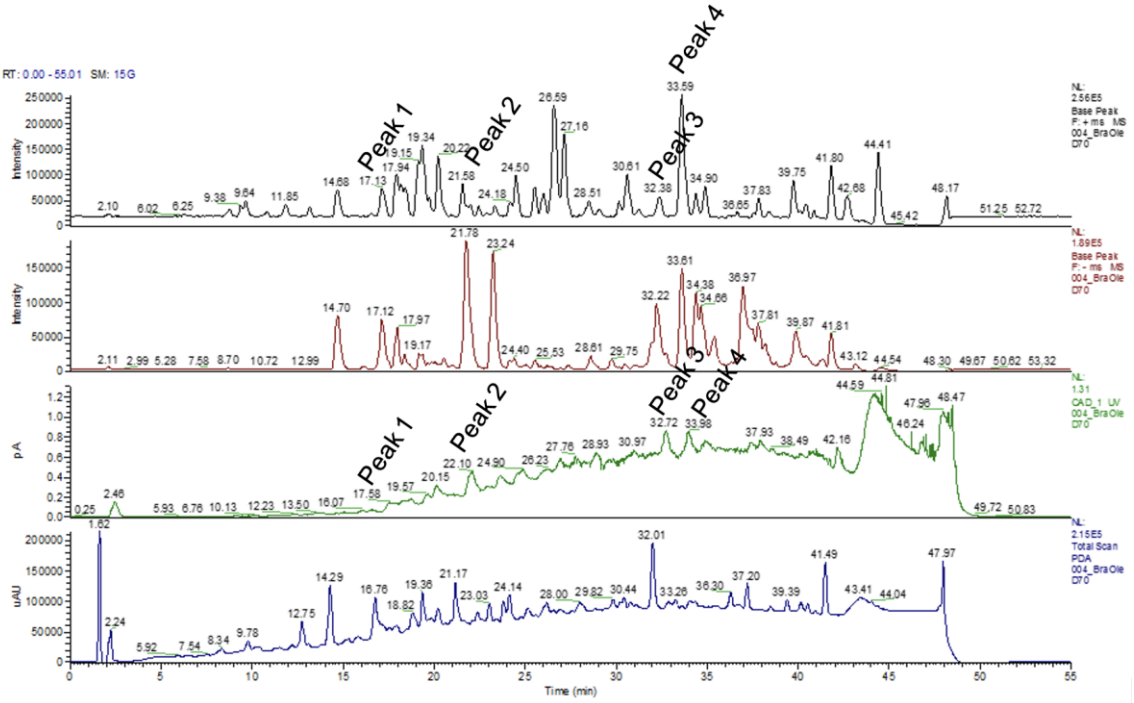

Figure A 58: Representative chromatograms obtained from BraOleD70 by HPLC coupled with mass spectrometry (MS), positive ion mode and negative ion mode, charged aerosol detection (CAD), and photodiode array detection (PDA) (see chapter 3.1.2, p5). 4 peaks were selected for further analysis. Positive mass (black), negative mass (brown), CAD signal (green) and PDA signal (blue).

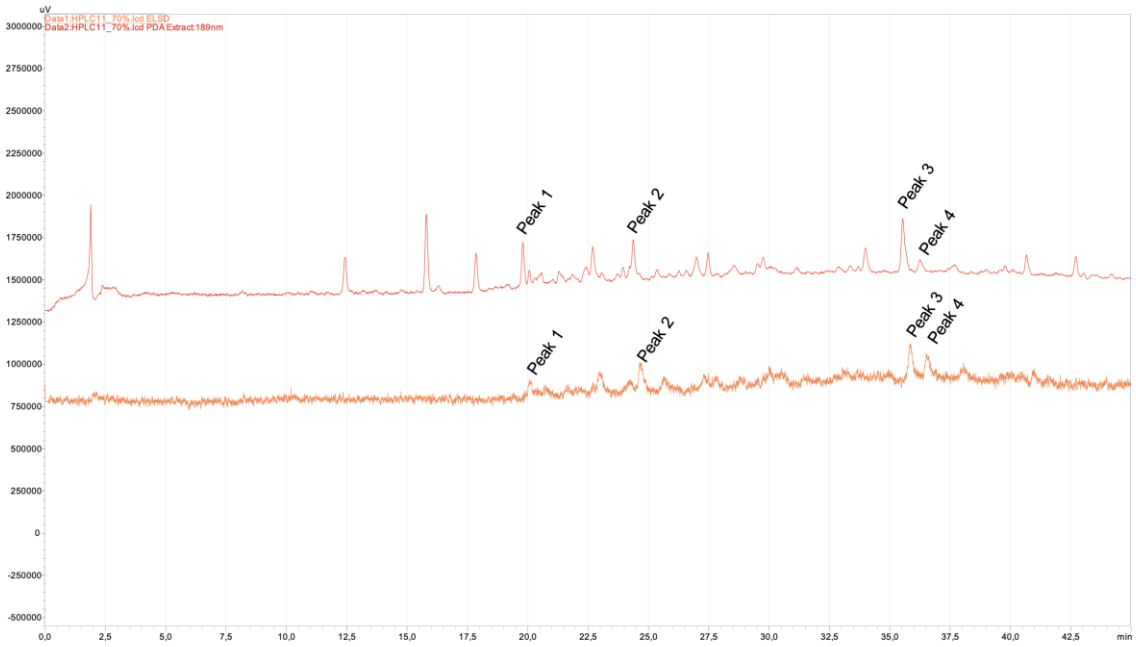

Figure A 59: HPLC data from BraOleD70 (see chapter 3.1.2, p5). 4 peaks were selected for further analysis. HPLC run 1 (see Table 5, p9). ELSD signal (orange) and PDA signal (red)

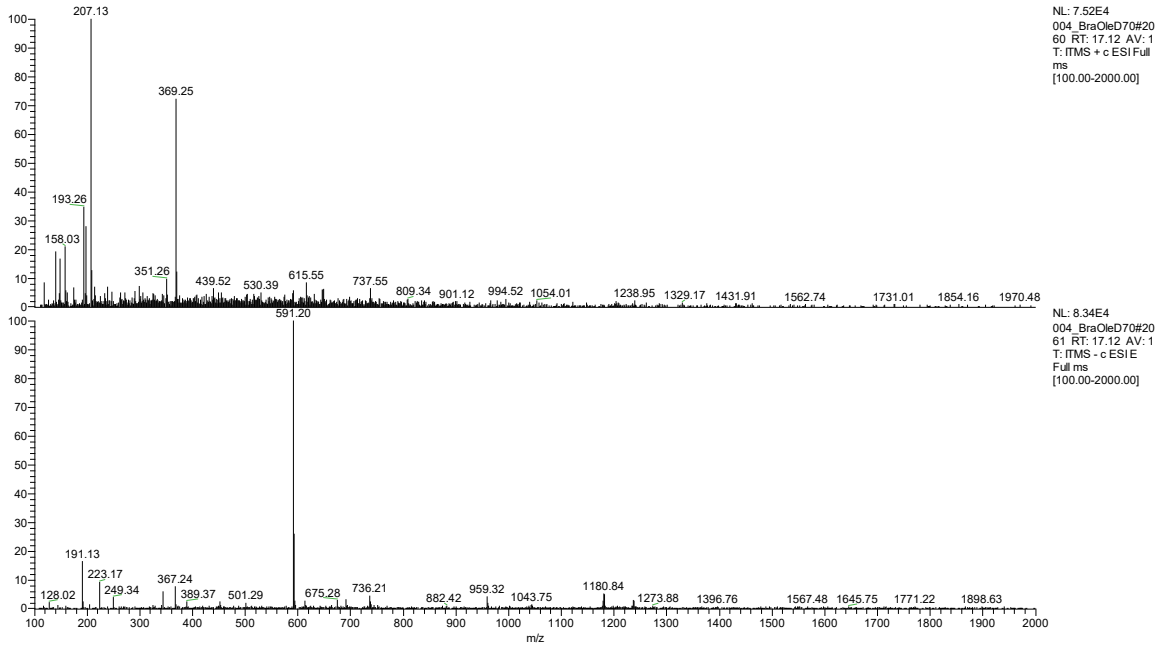

Figure A 60: MS spectra from BraOleD70 (see chapter 3.1.2, p5) corresponding to peak 1 (see Figure 32, p30). Top: positive ion mode (RT 17.12 min); bottom: negative ion mode (RT 17.12 min).

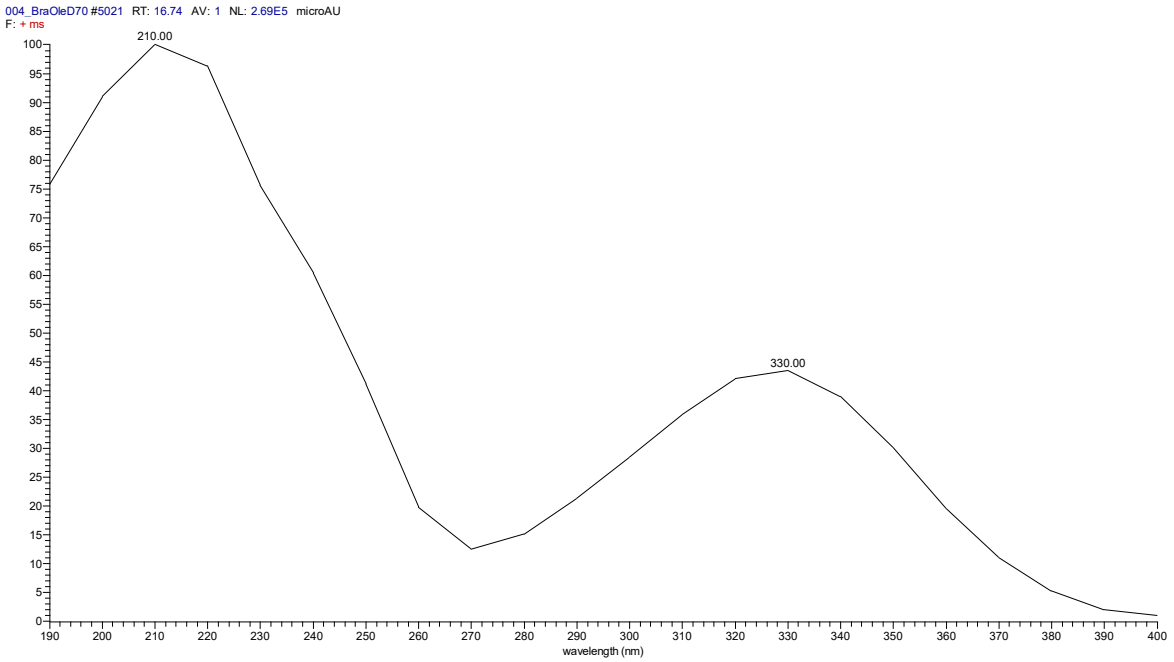

Figure A 61: UV spectrum from BraOleD70 (see chapter 3.1.2, p5) corresponding to peak 1 (see Figure 32, p30).

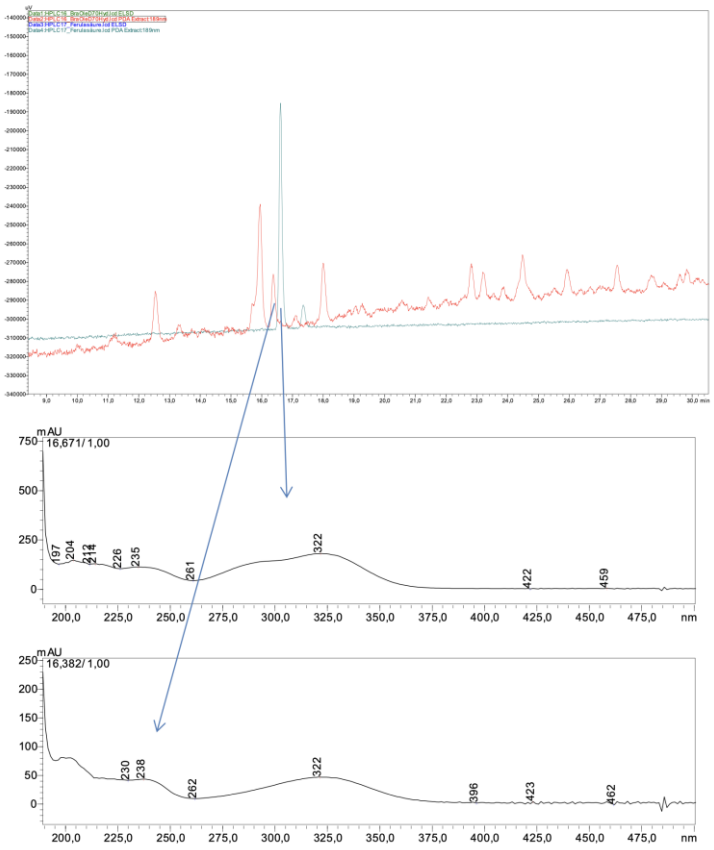

Figure A 62: PDA peaks of ferulic acid pure substance (grey) and the BraOleD70 (see chapter 3.1.2, p5) after hydrolysis (orange). HPLC run 5 (see Table 5, p9). The corresponding UV spectra can be seen below. Based on the HPLC chromatogram and the matching UV spectra, caftaric acid reference compound was tentatively identified in BraOleD70 (see chapter 4.2.4, p30).

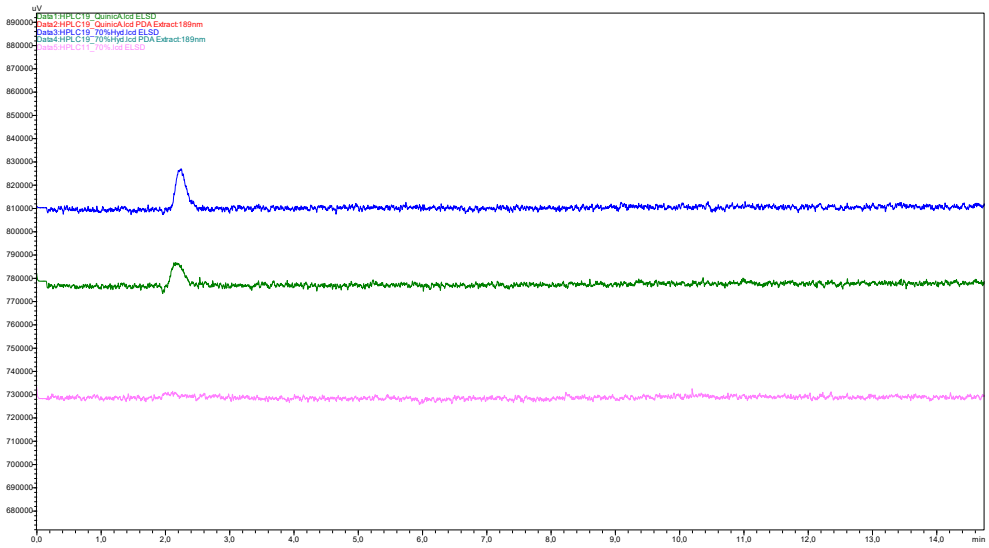

Figure A 63: HPLC run 5 (see Table 5, p9). Comparison of the quinic acid pure substance peak (green) with the peak from BraOleD70 (see chapter 3.1.2, p5) after hydrolysis (blue). Based on the HPLC chromatogram quinic acid reference compound was tentatively identified in BraOleD70 (see chapter 4.2.4, p30). Importantly, quinic acid was not detected in BraOleD70 before hydrolysis (pink, see HPLC run 1, Table 5, p8), indicating that quinic acid was released by the acid hydrolysis (see chapter 4.2.4, p30).

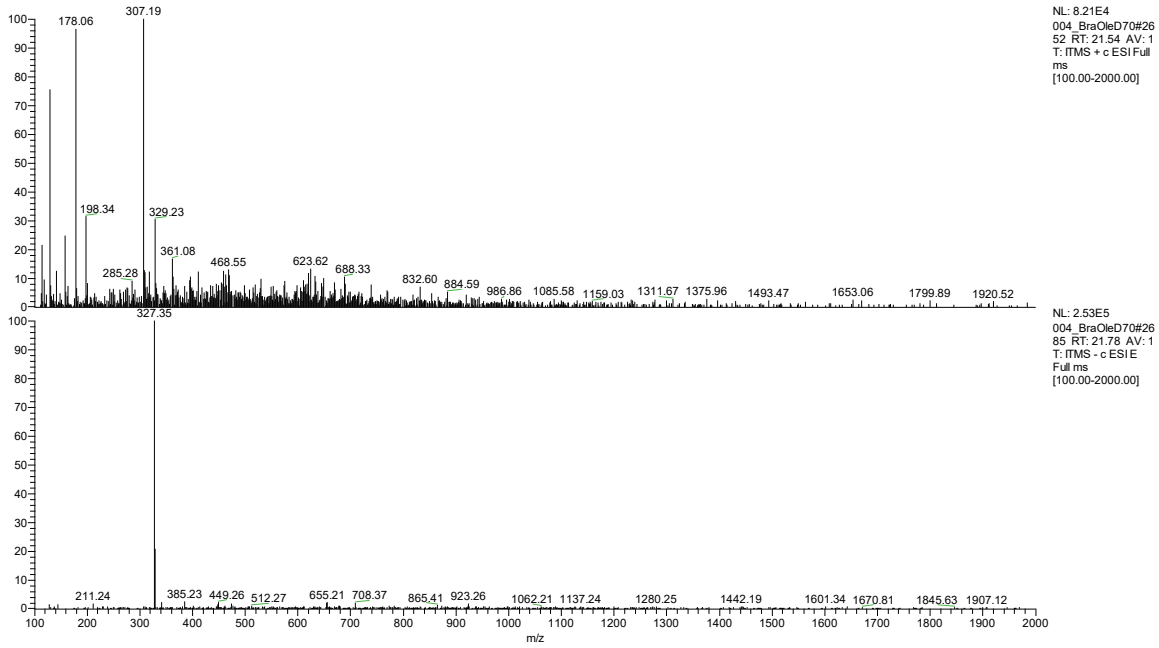

Figure A 64: MS spectra from BraOleD70 (see chapter 3.1.2, p5) corresponding to peak 2 (see Figure 32, p30). Top: positive ion mode (RT 21.54 min); bottom: negative ion mode (RT 21.78 min).

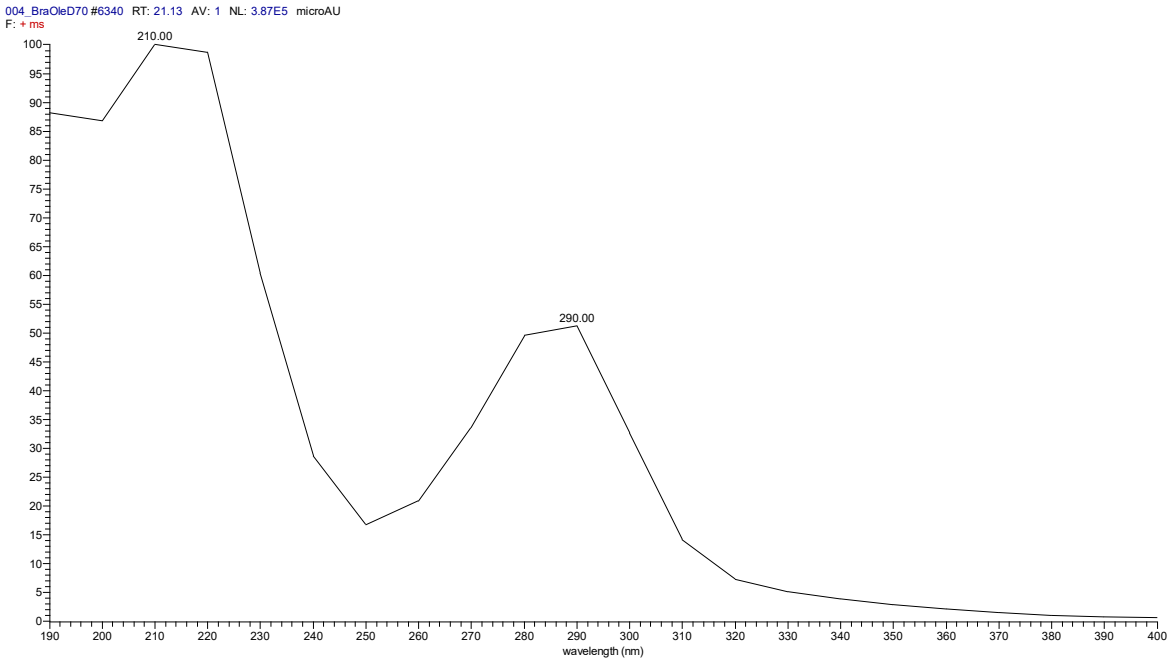

Figure A 65: UV spectrum from BraOleD70 (see chapter 3.1.2, p5) corresponding to peak 2 (see Figure 32, p30).

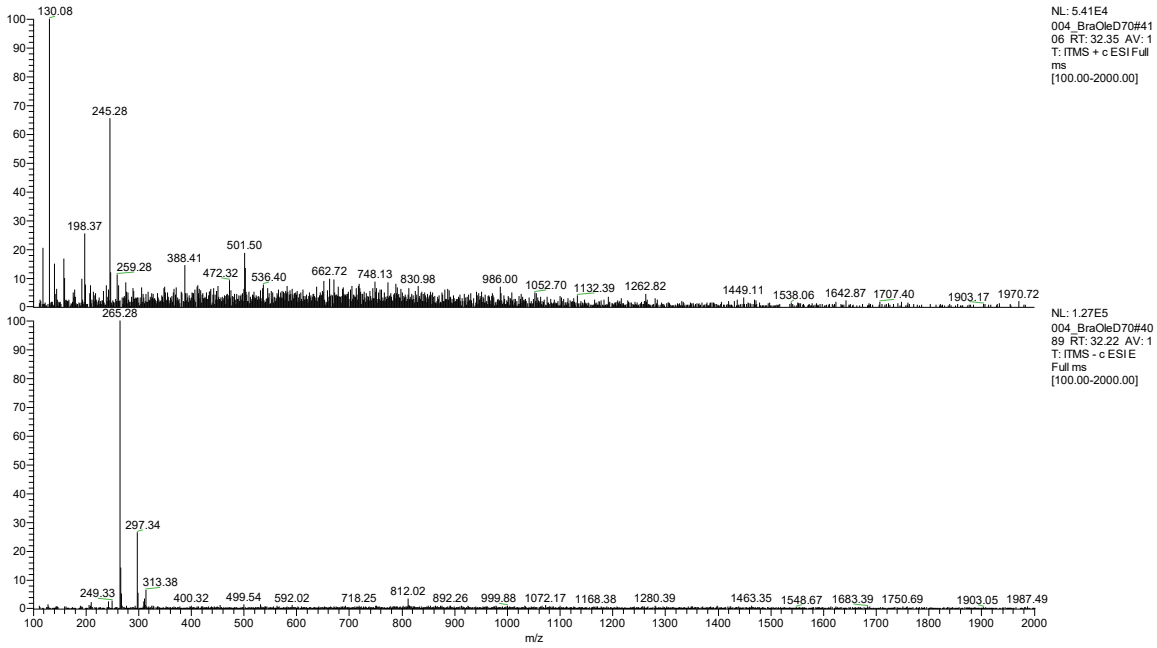

Figure A 66: MS spectra from BraOleD70 (see chapter 3.1.2, p5) corresponding to peak 3 (see Figure 32, p30). Top: positive ion mode (RT 32.35 min); bottom: negative ion mode (RT 32.22 min).

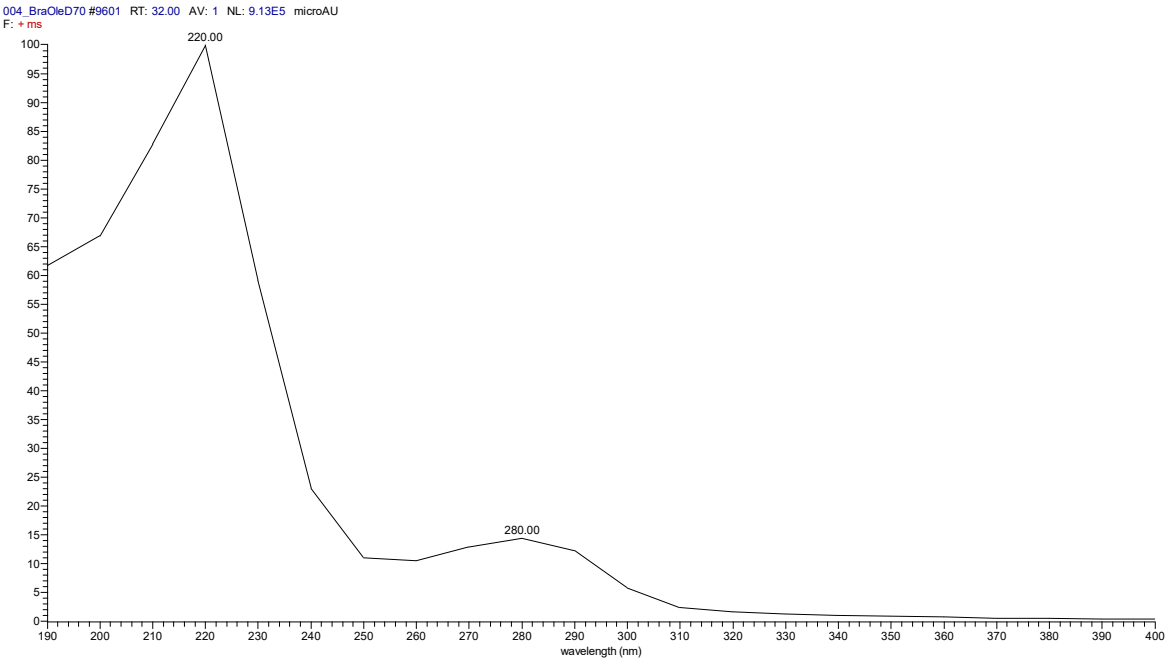

Figure A 67: UV spectrum from BraOleD70 (see chapter 3.1.2, p5) corresponding to peak 3 (see Figure 32, p30).

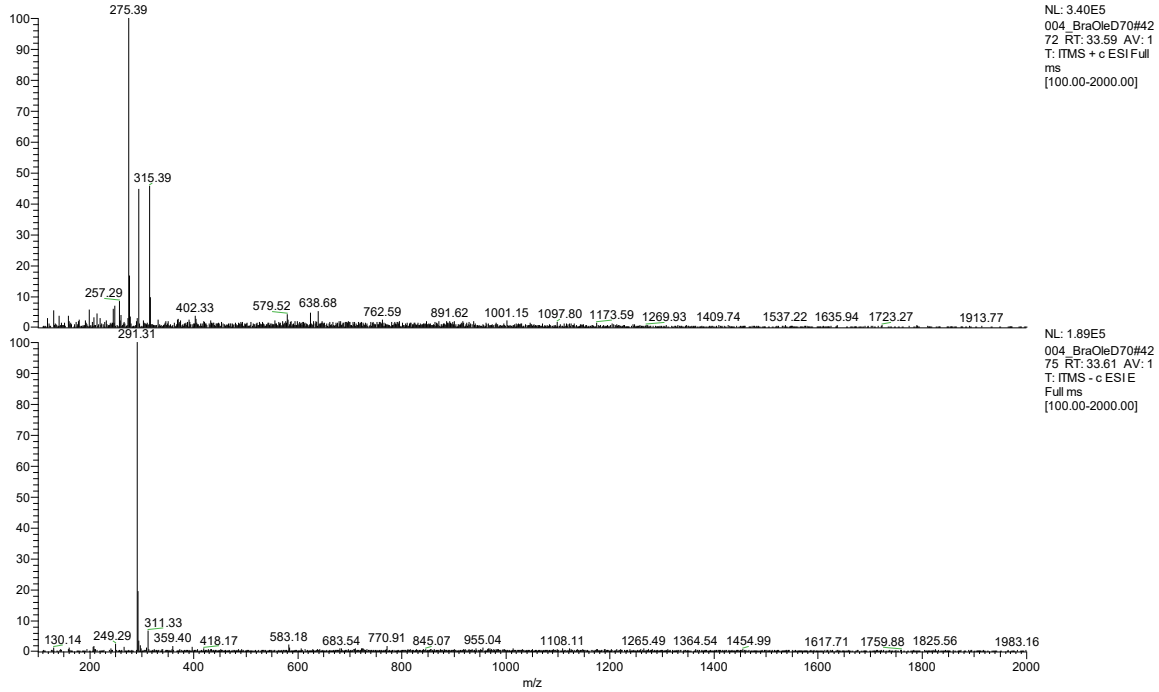

Figure A 68: MS spectra from BraOleD70 (see chapter 3.1.2, p5) corresponding to peak 4 (see Figure 32, p30). Top: positive ion mode (RT 33.59 min); bottom: negative ion mode (RT 33.61 min).

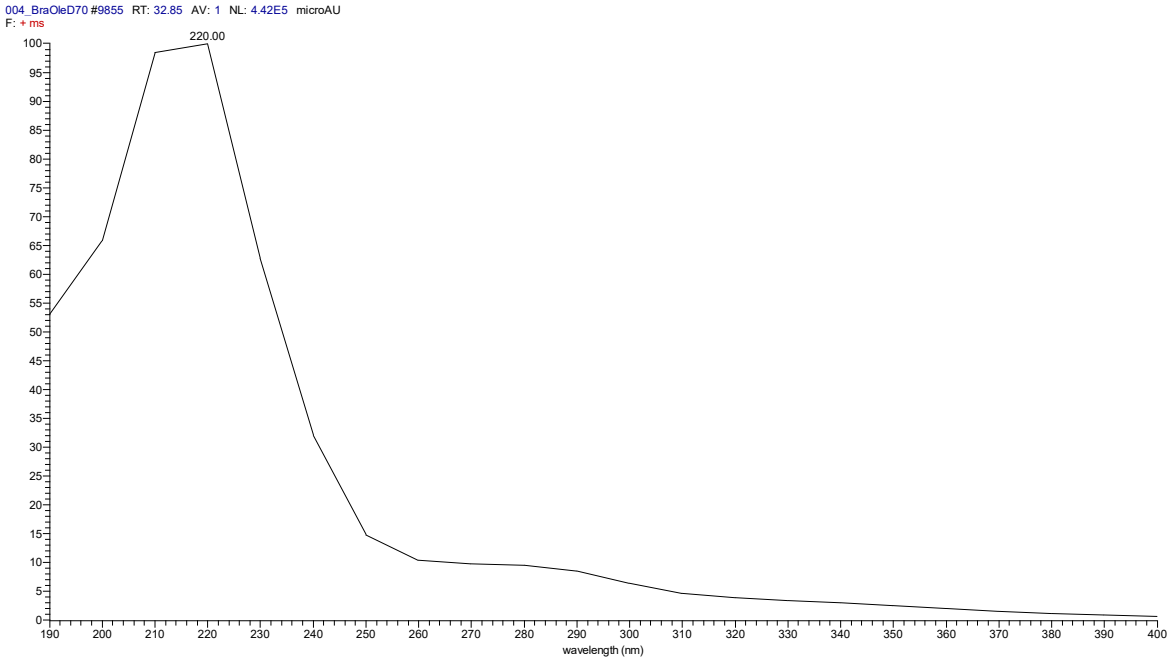

Figure A 69: UV spectrum from BraOleD70 (see chapter 3.1.2, p5) corresponding to peak 4 (see Figure 32, p30).

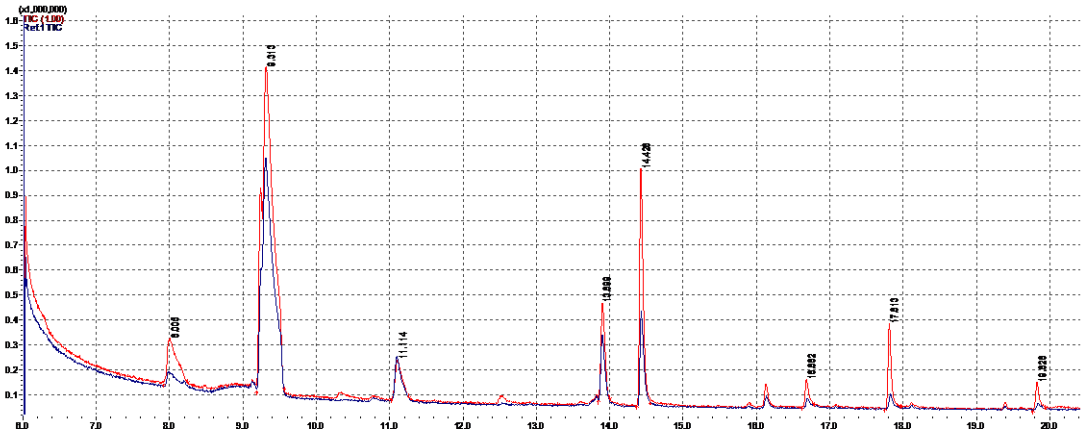

Figure A 70: Comparison of the retention times from the Austrian cabbage (GCMS run 1, red, see Table 7, p10) with the German cabbage (GCMS run 2, blue, see Table 7, p10).

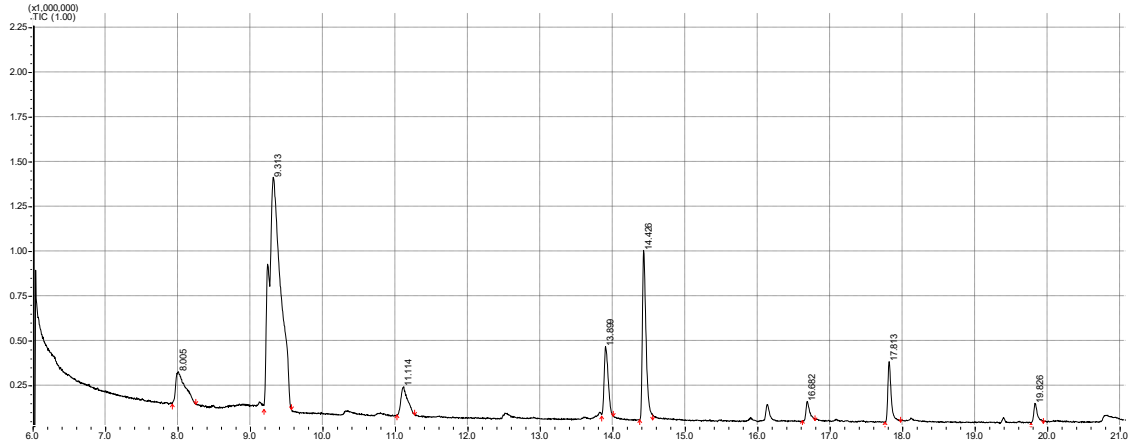

Figure A 71: Retention times of the different substances found in the Austrian cabbage (GCMS run 1, see Table 7, p10).

Peak#	Ret.Time	Start Tm	End Tm	m/z	Area	Area%	Height	Height%	A/H	Mark	Name
1	8.005	7.920	8.245	TIC	1658846	6.87	181394	5.14	9.14	MI	Dichloromethane
2	9.313	9.185	9.565	TIC	14704809	60.95	1297047	36.76	11.34	MI	Tetrachloroethylene
3	11.114	11.020	11.265	TIC	1004999	4.16	158038	4.48	6.36	MI	Allyl Isothiocyanate
4	13.899	13.845	14.005	TIC	1492939	6.19	389325	11.03	3.83	MI	3-Butenyl Isothiocyanate
5	14.426	14.370	14.550	TIC	3354287	13.90	946853	26.83	3.54	MI	Cyclopropyl Isothiocyanate
6	16.682	16.615	16.790	TIC	389453	1.61	106894	3.03	3.64	MI	4-(Methylthio)-butanenitrile
7	17.813	17.755	17.970	TIC	1105765	4.58	337830	9.57	3.27	MI	3-(Thiiran-2-yl)-propanenitrile
8	19.826	19.770	19.940	TIC	419556	1.74	111558	3.16	3.76	MI	5-(Methylthio)-pentanenitrile

Figure A 72: Substances found in the Austrian cabbage according to the NIST and WILEY library. Tetrachloroethylene serves as stabilizer in the dichloromethane (GCMS run 1, see Table 7, p10).

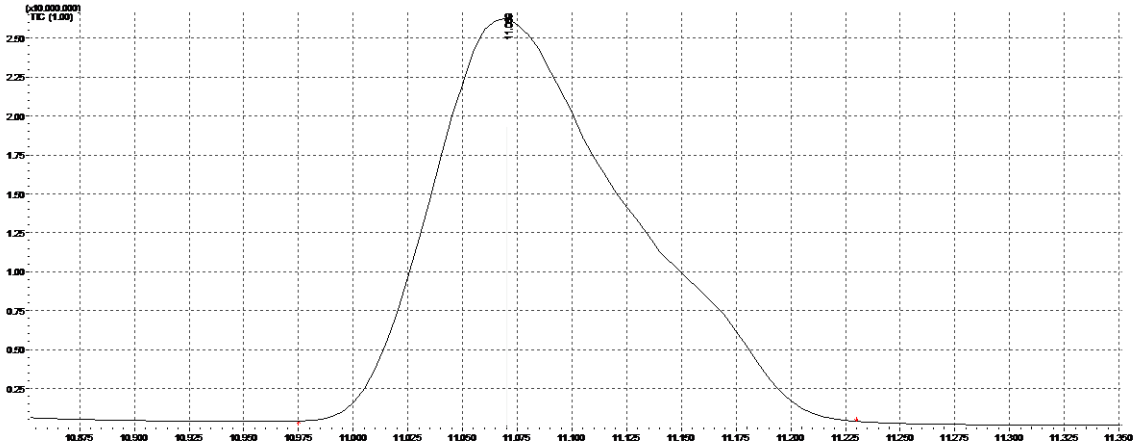

Figure A 73: AITC pure substance peak (RT = 11.069 min). GCMS run 3 (see Table 7, p10)

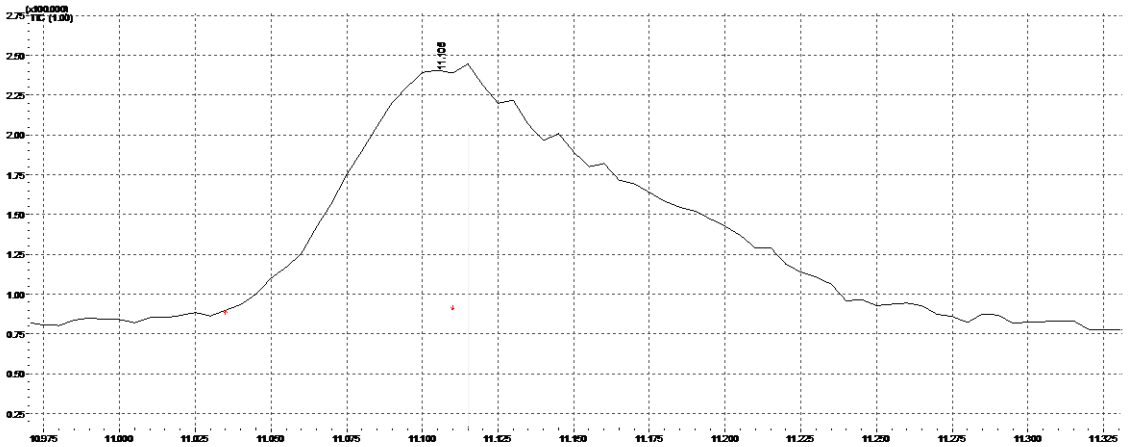

Figure A 74: AITC peak, tentatively assigned and observed in the fresh DCM extract (see chapter 3.1.2, p5) (RT = 11.105 min). GCMS run 1 (see Table 7, p10)

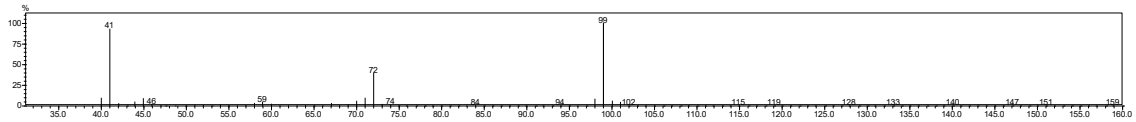

Figure A 75: AITC pure substance MS spectrum (RT = 11.069 min). GCMS run 3 (see Table 7, p10)

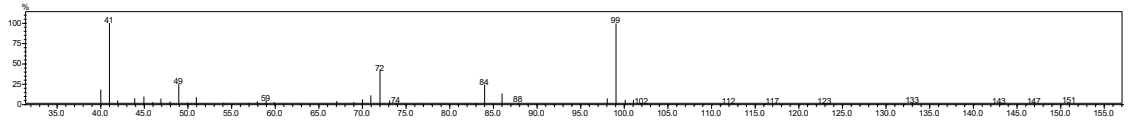

Figure A 76: Mass spectrum of tentatively assigned AITC peak in fresh DCM extract (see chapter 3.1.2, p5) (RT = 11.105 min). GCMS run 1 (see Table 7, p10)

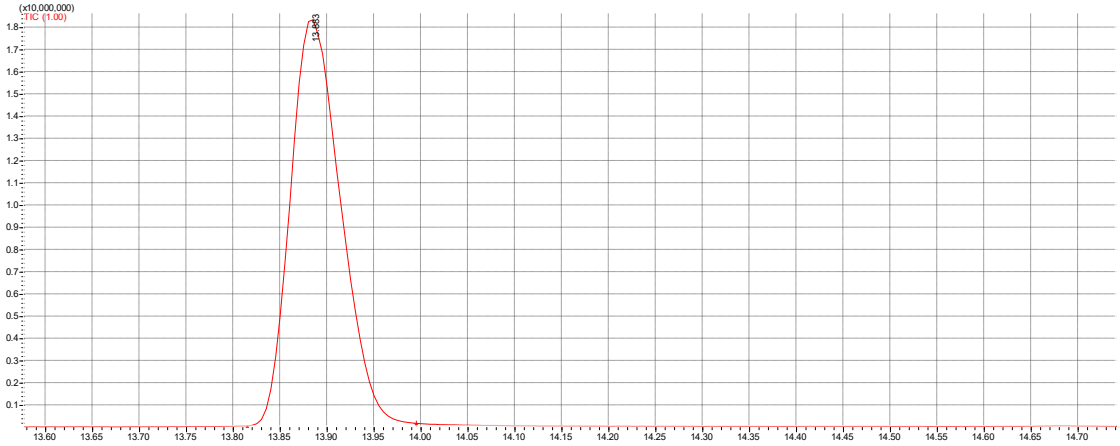

Figure A 77: 3-BITC pure substance peak (RT = 13.883 min). GCMS run 4 (see Table 7, p10)

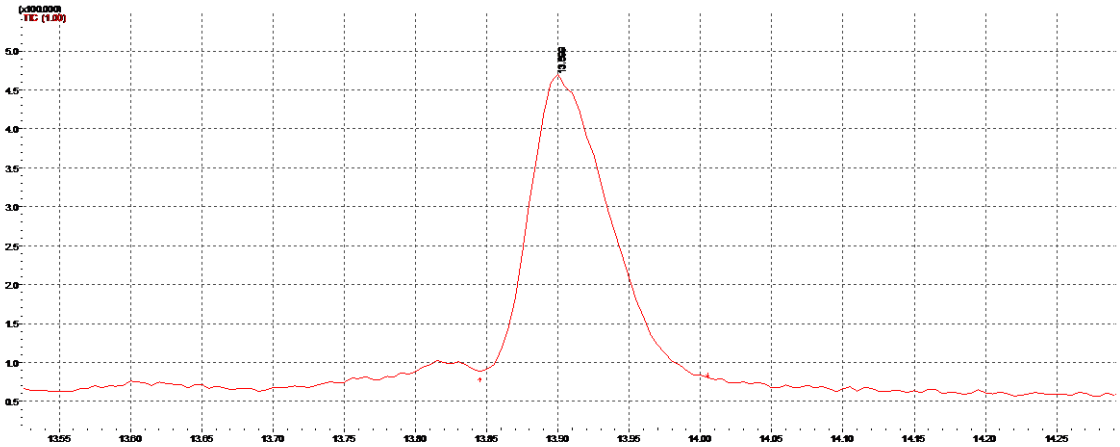

Figure A 78: 3-BITC peak, tentatively assigned and observed in the fresh DCM extract (see chapter 3.1.2, p5) (RT = 13.899 min). GCMS run 1 (see Table 7, p10)

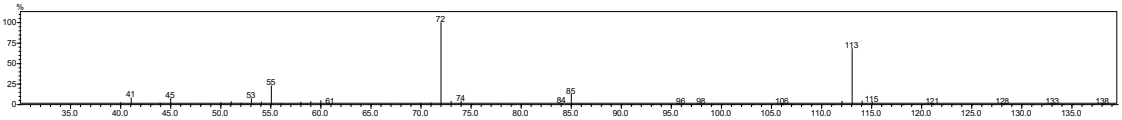

Figure A 79: 3-BITC pure substance MS spectrum (RT = 13.883 min). GCMS run 4 (see Table 7, p10)

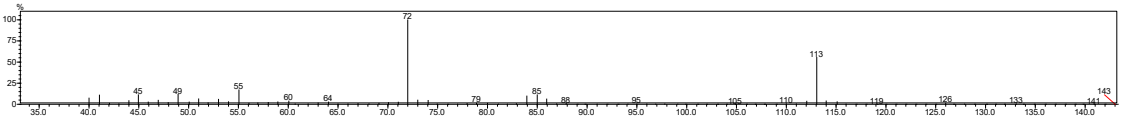

Figure A 80: Mass spectrum of tentatively assigned 3-BITC peak in fresh DCM extract (see chapter 3.1.2, p5) (RT = 13.899 min). GCMS run 1 (see Table 7, p10)

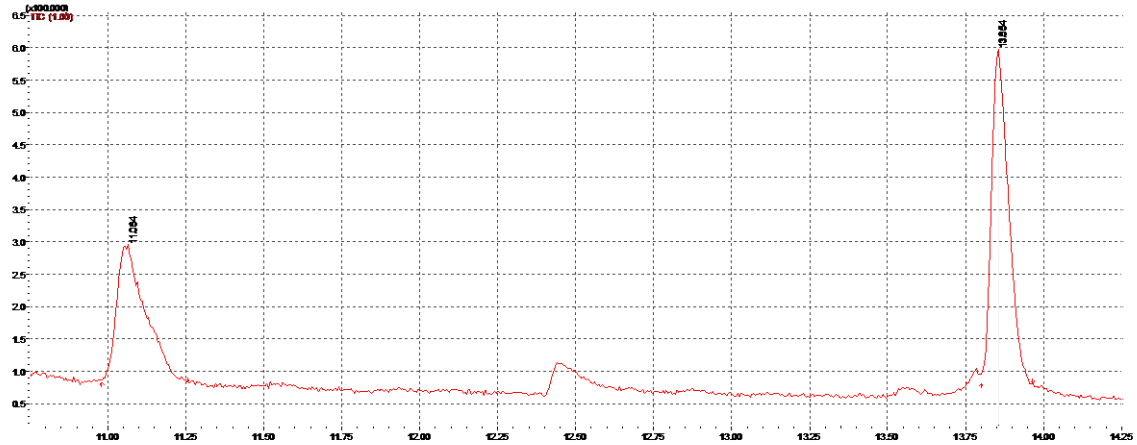

Figure A 81: Retention times of AITC (11.064 min) and 3-BITC (13.854 min) found in the Austrian cabbage (GCMS run 5, see Table 7, p10).

Print Edit View Similarity Search

Peak#	Ret.Time	Start Tm	End Tm	m/z	Area	Area%	Height	Height%	A/H	Mark	Name
1	11.064	10.980	11.255	TIC	1370883	41.26	212397	29.11	6.45	MI	AITC
2	13.854	13.800	13.965	TIC	1951877	58.74	517149	70.89	3.77	MI	3-BITC

Figure A 82: Retention times and peak areas of AITC and 3-BITC found in the Austrian cabbage (GCMS run 5, see Table 7, p10).

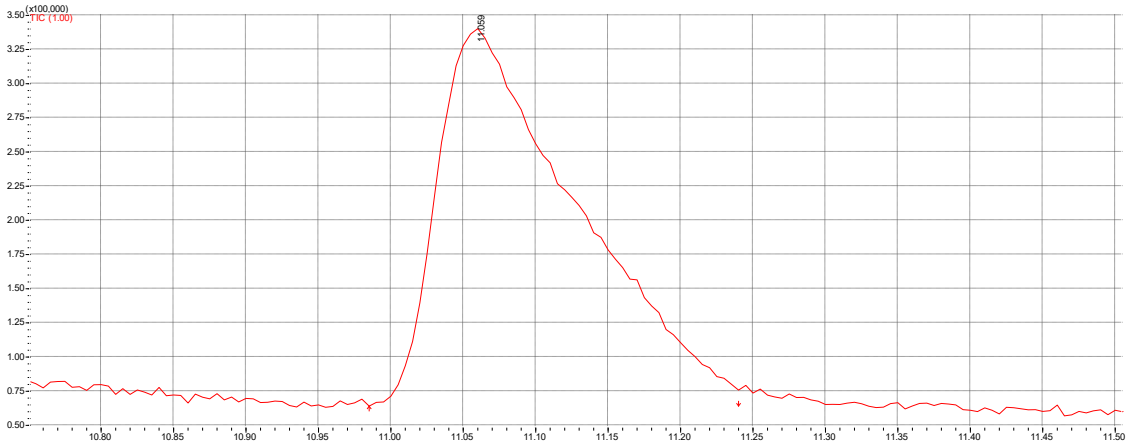

Figure A 83: AITC pure substance peak (RT = 11.059 min). GCMS run 6 (see Table 7, p10)

Print Edit View Similarity Search

Peak#	Ret.Time	Start Tm	End Tm	m/z	Area	Area%	Height	Height%	A/H	Mark	Name
1	11.059	10.985	11.240	TIC	1868083	100.00	276145	100.00	6.76	MI	AITC

Figure A 84: GCMS run 6 (see Table 7, p10), retention time and peak area of the AITC pure substance

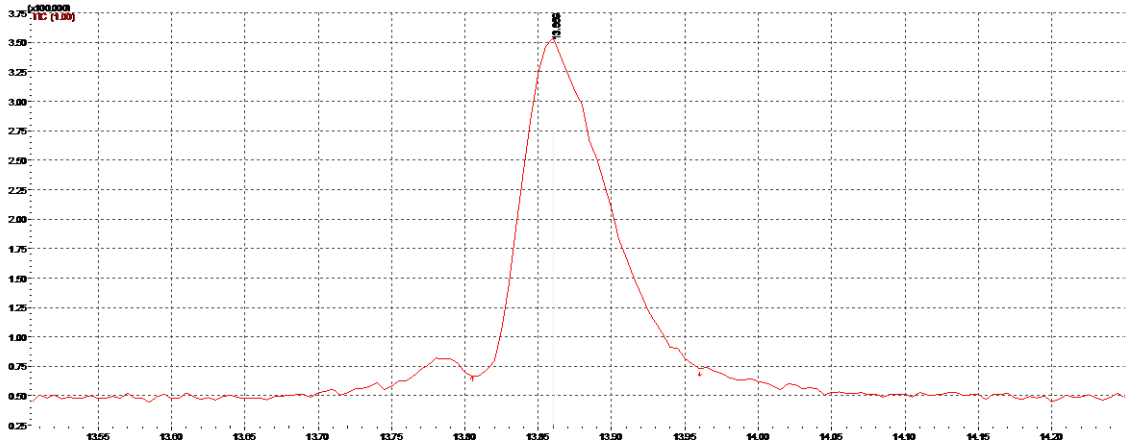

Figure A 85: 3-BITC pure substance peak (RT = 11.059 min). GCMS run 7 (see Table 7, p10)

Print Edit View Similarity Search

Peak#	Ret.Time	Start Tm	End Tm	m/z	Area	Area%	Height	Height%	A/H	Mark	Name
1	13.859	13.805	13.960	TIC	1128208	100.00	287440	100.00	3.93	MI	3-BITC

Figure A 86: GCMS run 7 (see Table 7, p10), retention time and peak area of the 3-BITC pure substance

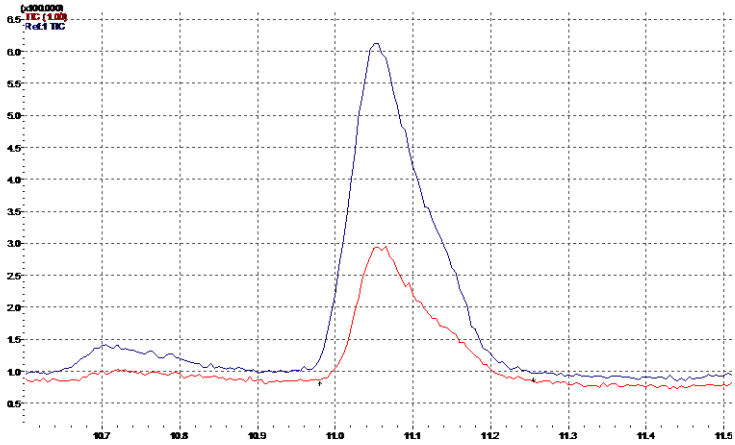

Figure A 87: red = AITC peak from the cabbage extract (see chapter 3.1.2, p5) analyzed in GCMS run 5 (see Table 7, p10). blue = AITC peak from the cabbage extract combined with the AITC pure substance analyzed in GCMS run 8 (see Table 7, p10).

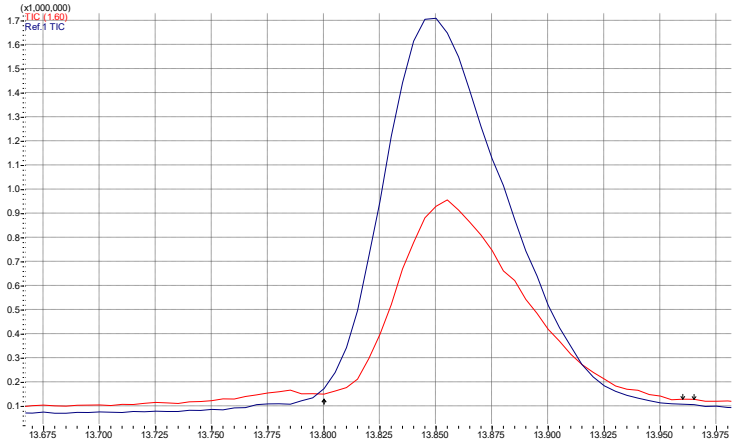

Figure A 88: red = 3-BITC peak from the cabbage extract (see chapter 3.1.2, p5) analyzed in GCMS run 5 (see Table 7, p10). blue = 3-BITC peak from the cabbage extract combined with the 3-BITC pure substance analyzed in GCMS run 8 (see Table 7, p10).

Print Edit View Similarity Search

Peak#	Ret.Time	Start Tm	End Tm	m/z	Area	Area%	Height	Height%	A/H	Mark	Name
1	13.834	13.780	13.925	TIC	3474983	100.00	921998	100.00	3.77	MI	3-BITC

Figure A 89: GCMS run 8 (see Table 7, p10), peak area from the 3-BITC peak (combined with the pure substance)

Print Edit View Similarity Search

Peak#	Ret.Time	Start Tm	End Tm	m/z	Area	Area%	Height	Height%	A/H	Mark	Name
1	11.053	10.975	11.230	TIC	3319845	100.00	509143	100.00	6.52	MI	AITC

Figure A 90: GCMS run 8 (see Table 7, p10), peak area from the AITC peak (combined with the pure substance)